

From the Leibniz-Center for Medicine and Biosciences Borstel

Director: Prof. Dr. Stefan Ehlers

Division of Biophysics

Prof. Dr. Thomas Gutschmann

**ACTIVITY AND MODE OF ACTION OF PEPTIDE NK-2 AND  
DERIVATIVES AGAINST PATIENT-DERIVED COLON CARCINOMA  
AND PROSTATE CANCER CELLS**

**Dissertation**

for Fulfillment of Requirements

for the Doctoral Degree

of the University of Lübeck

from the Department of Natural Sciences

Submitted by

Dominik Wilms

from Brühl, Erftkreis

Lübeck 2016

---

First Referee:	Prof. Dr. Thomas Gutschmann
Second Referee:	Prof. Dr. Christian Hübner
Third Referee:	Prof. Dr. Jörg Andrä
Date of Oral Examination:	February 23, 2017
Approved for Printing.	Lübeck, February 28, 2017

---

“ The most exciting phrase in science,  
the one that heralds new discoveries,  
is not ‘*Eureka!*’ but ‘*That’s funny...*’ ”

*Isaac Asimov* (1920 – 1992)

Russian-American biochemist and science fiction author

## ABSTRACT

Novel therapeutic approaches against cancer are urgently needed. Classical medication is usually compromised by detrimental effects on healthy tissues and an increasing occurrence of drug resistances. In recent years, so called host defense peptides came into focus of research as innovative anticancer agents putatively capable of overcoming these limitations. Peptide NK-2 represents the  $\alpha$ -helical, highly amphipathic core region of porcine NK-lysin and is well-reputed for its broad-spectrum activities against numerous microbial pathogens but was also found to exert basic effectiveness against cancer cells. Mechanistic details of the anti-cancer cell activities, however, still remain elusive. In the course of this study, it was aimed at optimizing peptide NK-2 in terms of its anticancer activity and identifying key structural influences, as well as at shedding light on the underlying mode of action and target specificity.

Here, for peptide NK-2 and > 30 derivatives thereof sequence- and structure-related physico-chemical peptide properties, such as charge distribution, hydrophobicity and amphipathicity, were calculated. Investigated cell types enclosed a pair of rarely considered colorectal carcinoma cells derived from individual patients, as well as a human prostate adeno-carcinoma cell line with normal keratinocytes as a non-cancerous reference. Biological data from cytotoxicity tests and fluorescence microscopic analyses were complemented by studies on artificial membranes, the lipid composition of which mimicked normal and cancer cell membranes enclosing various mixtures of zwitterionic phosphatidylcholine with anionic phosphatidylserine (PS). Details on the peptides' membrane binding, intercalation, orientation and permeabilization were addressed by dynamic light scattering, FRET spectroscopy, tryptophan fluorescence, as well as dye release and quencher uptake experiments.

Structure-function correlations enabled the identification of a set of peptide variants concomitantly improved in terms of anti-cancer cell effectiveness, selectivity and stability. Novel peptides exhibited an up to 20-fold enhanced activity against prostate cancer cells in medium, with a Cys/Ala exchange turning out to be the key substitution to sustain peptide activity under medium conditions. NK-2 and improved variants acted by a direct, physical membrane permeabilization mechanism with subsequent internalization of peptides. Remarkably, the susceptibility of cancerous cells to these peptides correlated well with the cell surface level of PS, but not with the overall surface net charge, pointing at a PS-specific target preference. As the exposure of PS is a hallmark of cancerous cells, whereas it is typically absent from the surface of healthy human cells, this finding may contribute to the desired future development of selective and effective peptide-based anticancer therapeutics.

## ZUSAMMENFASSUNG

Die Behandlung von Krebserkrankungen bedarf dringend neuartiger Ansätze, da klassische Therapiemethoden mit Schädigungen gesunder Gewebe einhergehen und durch die Zunahme von Arzneimittelresistenzen beeinträchtigt sind. Sogenannte *Host Defense Peptide* sind in den letzten Jahren als innovative Antikrebsmittel in den Fokus der Forschung gerückt, da sie derlei Nachteile potentiell überwinden können. Das Peptid NK-2 wurde ursprünglich aus der  $\alpha$ -helikalen, stark amphipathischen Kernregion des NK-Lysins des Schweins abgeleitet und ist vor allem für seine Breitbandwirkung gegen zahlreiche mikrobielle Pathogene bekannt, jedoch auch zunehmend für seine Aktivität gegen Krebszellen. Details des Antikrebstwirkmechanismus bleiben weitgehend unklar. Zentrale Ziele dieser Arbeit waren sowohl die Optimierung der Antikrebstwirkung des NK-2 und die Identifizierung entscheidender Strukturelemente als auch die Untersuchung der zugrundeliegenden Wirkweise und Zielspezifität.

Vor diesem Hintergrund wurden Sequenz- und Struktur-bedingte physikochemische Eigenschaften, wie Ladungsverteilung, Hydrophobizität oder Amphipathizität, für das Leitpeptid NK-2 und > 30 Derivate berechnet. Verwendete Zelltypen umfassten zwei jeweils aus Patientenmaterial gewonnene Kolonkarzinom-Zelllinien sowie Standardzelllinien für ein humanes Prostata-Adenokarzinom und für normale Keratinozyten als nicht-maligne Referenz. Biologische Daten aus Zytotoxizitätstests und Fluoreszenzmikroskopie wurden durch Studien an künstlichen Membranen ergänzt. Deren Lipidzusammensetzung basierte auf verschiedenen Mischungen von Phosphatidylcholin und Phosphatidylserin (PS), um Mimikry-Systeme für gesunde und kanzeröse Zellmembranen darzustellen. Membranbindung, Interkalation, Orientierung und Permeabilisierung der Peptide wurden mittels Dynamischer Lichtstreuung, FRET-Spektroskopie sowie Tryptophan-Fluoreszenz-, Calcein-Freisetzungs- und Quencher-Aufnahme-Experimenten untersucht.

Struktur-Funktions-Korrelationen ermöglichten die Identifizierung von Peptidvarianten mit gleichsam verbesserter Effektivität, Stabilität sowie Krebszellelektivität. Die neuen Peptide zeigten eine bis zu 20-fach höhere Aktivität gegen Prostatakrebszellen in Medium, wobei sich ein Cys/Ala-Aminosäureaustausch als entscheidend für die Aktivitätserhaltung in Medium herausstellte. NK-2 und seine verbesserten Varianten wirkten durch eine direkte, physikalische Permeabilisierung der Zielmembran mit anschließender Internalisierung des Peptids. Bemerkenswerterweise korrelierte die Suszeptibilität untersuchter Krebszellen gegenüber verbesserten NK-2-Peptiden mit dem PS-Gehalt auf der Zelloberfläche, nicht aber mit der zellulären Nettoladung, was auf PS als eine spezifische Zielstruktur der Peptide hinweist. Da das anionische Phospholipid PS typischerweise auf malignen nicht aber auf gesunden Zellen exponiert ist, könnten die hier erzielten Ergebnisse dazu beitragen, zukünftig verbesserte, d.h. selektive und effektive, Peptid-basierte Antikrebstherapeutika zu entwickeln.

**TABLE OF CONTENTS**

Abstract.....	IV
List of Figures.....	VIII
List of Tables .....	IX
List of Abbreviations.....	X
1 Introduction.....	1
2 Theoretical Background.....	3
2.1 Host Defense Peptides .....	3
2.1.1 Classical Mechanisms of Action .....	4
2.1.2 Anti-Cancer Cell Activities of Host Defense Peptides .....	7
2.1.2.1 Particular Mechanisms of Actions against Cancer Cells.....	7
2.1.2.2 Altered Membrane Properties of Cancer Cells.....	9
2.1.2.3 Phosphatidylserine as a Cancer Cell Marker.....	11
2.1.2.4 Perspectives on Applications of Host Defense Peptides in Cancer Therapy .	13
2.1.3 Sequence-Related Implications on Anti-Cancer Cell Peptide Activities .....	15
2.2 Peptides Employed in this Study .....	17
2.2.1 Peptide NK-2 and Derivatives thereof .....	17
2.2.2 Melittin.....	21
2.3 Human Cancer Cell Models Used in this Study .....	22
2.3.1 Patient-Derived Human Colon Cancer Cells.....	22
2.3.2 Human Prostate Cancer Cells and Non-Tumorigenic Keratinocytes .....	23
3 Materials .....	24
3.1 Peptides.....	24
3.2 Lipids.....	25
3.3 Cell Cultures.....	26
3.4 Chemicals and Reagents.....	28
3.5 Laboratory Equipment and Software .....	29
3.6 Disposables and Consumables .....	31
3.7 Buffers and Stock Solutions .....	32
3.7.1 Aqueous Buffers .....	32
3.7.2 Cell Culture Medium-Based Buffers.....	33
3.7.3 Stock Solutions.....	34
4 Methods .....	35
4.1 Software-Based Assessment of Peptide Properties .....	35
4.2 Cellular Test Systems.....	37
4.2.1 Cell Cultivation Procedures .....	37

## Table of Contents

---

4.2.2	Flow Cytometric Analysis .....	37
4.2.3	The MTT Metabolic Activity Assay .....	40
4.2.4	Fluorescence Microscopy Analysis of Colorectal Cancer Cells .....	41
4.2.5	Cell Surface Zeta Potential Measurements .....	43
4.3	Liposome-Based Test Systems.....	46
4.3.1	Liposome Preparation Procedure.....	46
4.3.2	Particle Size and Surface Zeta Potential Determination .....	46
4.3.3	Probe Dilution Förster Resonance Energy Transfer Experiments .....	47
4.3.4	Measurement of Intrinsic Tryptophan Fluorescence.....	49
4.3.5	Potassium Iodide Fluorescence Quenching.....	51
4.3.6	Dye Release Test .....	53
5	Results.....	55
5.1	Peptide Characterization .....	55
5.1.1	Peptide Design .....	55
5.1.2	Sequence- and Structure-Inherent Peptide Properties .....	57
5.2	Cell Type-Specific Membrane Surface Characteristics.....	63
5.3	Peptide Cytotoxicity.....	65
5.3.1	Cytotoxicity of NK-2-Derived Peptides against PC-3 and HaCaT Cells .....	66
5.3.2	Cytotoxicity of Selected Peptides against Colorectal Cancer Cells .....	69
5.3.3	Influences of Buffer Components on the Potency of Selected Peptides .....	71
5.4	Visualization of Peptide-Induced Effects on Colorectal Cancer Cells .....	73
5.5	Changes of Surface Zeta Potentials of CRC Cells upon Peptide Interaction .	76
5.6	Changes in Liposomal Size and Zeta Potential upon Peptide Interaction ....	79
5.7	Membrane Intercalation of NK-2 Peptides .....	83
5.8	Peptide Orientation upon Membrane Intercalation .....	86
5.9	Peptide-Induced Permeabilization of PS-Comprising Membranes .....	88
5.10	Structure-Function Analyses.....	90
5.11	Cumulated Selectivities as a Measure of a Peptide's Anticancer Potency .....	94
6	Discussion.....	96
6.1	Anticancer Activities of Peptide NK-2 and Structural Derivatives.....	96
6.2	Peptides' Mode of Action and Impacts of Membrane Phosphatidylserine .	102
6.2.1	Cellular Selectivity.....	103
6.2.2	Membrane Interaction Mechanisms .....	107
6.2.3	Concatenated Mechanistic Information .....	111
6.3	Conclusion.....	113
	Bibliography.....	115
	Appendix .....	133

**LIST OF FIGURES**

Figure 2.1: Classical modes of action of host defense peptides .....	5
Figure 2.2: Schematic overview on anti-cancer cell activities of host defense peptides.....	8
Figure 2.3: Scheme of PS-related changes in the plasma membrane in cancer evolvement ...	13
Figure 2.4: Region of natural NK-lysin corresponding to peptide NK-2 .....	18
Figure 2.5: Helical wheel projection of peptide NK-2 .....	19
Figure 3.1: Predominant constituents of employed natural phospholipids.....	25
Figure 4.1: Zeta potential of a charged particle .....	44
Figure 4.2: Exemplary representation of a blue shift phenomenon .....	49
Figure 4.3: Three distinct single-Trp variants of parent peptide NK-2.....	50
Figure 5.1: Helical wheel plots of peptide NK-2 and exemplified structural modifications ...	56
Figure 5.2: Value distribution of calculated peptide properties .....	58
Figure 5.3: Interdependency of hydrophobicity ( $H$ ) and charge per residue ( $Q/n$ ) .....	59
Figure 5.4: Representative results of flow cytometric assessments of cell surface PS levels ...	63
Figure 5.5: Surface PS exposure on various cell lines assessed by flow cytometry analysis ...	64
Figure 5.6: Surface Zeta potentials of investigated cell lines.....	64
Figure 5.7: MTT results of the cytotoxicity of selected NK-2 variants against PC-3 cells.....	66
Figure 5.8: Representative results of cytotoxicity tests with patient-derived CRC cells.....	71
Figure 5.9: Impact of buffer components on the cytotoxicity of selected peptides .....	72
Figure 5.10: Fluorescence microscopy analysis of high- and low-PS CRC cell types .....	74
Figure 5.11: Control treatment of high- and low-PS CRC cells.....	75
Figure 5.12: Changes in the surface Zeta potential of CRC cells upon peptide treatment.....	77
Figure 5.13: Average size and Zeta potential of liposomes composed of PC and PS .....	79
Figure 5.14: Changes in Zeta potential and size of liposomes upon peptide treatment .....	81
Figure 5.15: Membrane intercalation of selected peptides probed by FRET spectroscopy ....	83
Figure 5.16: Peptide intercalation into liposomal phospholipid membranes .....	85
Figure 5.17: Tryptophan fluorescence blue shift after incubation of liposomes with peptide	87
Figure 5.18: Peptide-induced permeabilization of phospholipid liposomes .....	89
Figure 5.19: Correlation of the anti-cancer cell activity and membrane intercalation properties of NK-2 derivatives with the peptide sequence length .....	90
Figure 5.20: Correlation of functional data with net charge and mean hydrophobicity .....	91
Figure 5.21: Interdependencies between functional data and the peptide amphipathicity ...	93
Figure 5.22: Peptide-specific anti-cancer cell potency and selectivity .....	95
Figure 6.1: Proposed mechanism of action of peptide NK-2 against cancer cells.....	112
Figure A.1: Pre-evaluation processing of flow cytometry data .....	133
Figure A.2: Matlab code for determining blue shifts from tryptophan fluorescence data ....	135

**LIST OF TABLES**

Table 3.1: Origins and supplier details on deployed phospholipids .....	25
Table 3.2: Overview on patient-derived human colorectal cancer cell lines.....	26
Table 3.3: Overview on commercially available human model cell lines .....	27
Table 3.4: Chemicals and reagents .....	28
Table 3.5: Instruments and laboratory equipment.....	29
Table 3.6: Software and tools .....	30
Table 3.7: Disposable labware and consumables.....	31
Table 3.8: Buffer variants I-III .....	33
Table 3.9: Buffer variants IV-VII.....	33
Table 4.1: Settings for flow cytometry experiments on a BD FACSCalibur™ platform.....	39
Table 4.2: Adjusted settings for the fluorescence microscopy imaging of CRC cells .....	43
Table 4.3: Input parameters of the Zetasizer Nano for determining Zeta potentials at 25°C..	45
Table 5.1: Overview on peptide sequences and structure-related peptide properties .....	61
Table 5.2: Average hydrophobic moment ( $\mu H_{\text{mean}}$ ) per 7-residue calculation window.....	62
Table 5.3: Cytotoxicity of NK-2-derived peptides against PC-3 and HaCaT cells .....	68
Table 5.4: Cytotoxicity of NK-2-derived peptides against human colorectal cancer cells .....	70
Table 6.1: Hemolytic activities of selected NK-2-related peptides and melittin .....	104
Table A.1: Hydrophobicity scales .....	132
Table A.2: Sequences and structure-related properties of N- and C-terminal segments.....	134

**LIST OF ABBREVIATIONS**

A-CSV	Activity-weighted cumulative selectivity value
ATP	Adenosine triphosphate
BS	Blue shift
CRC	Colorectal carcinoma
CSV	Cumulative selectivity value
DLS	Dynamic light scattering
DMEM	Dulbecco's modified Eagle's medium
DNA	Deoxyribonucleic acid
EDTA	Ethylenediaminetetraacetic acid
FACS	Fluorescence-activated cell sorting
FBS	Fetal bovine serum
FITC	Fluorescein isothiocyanate
FRET	Förster resonance energy transfer
FSC	Forward-scattered light
GAG	Glycosaminoglycan
HEPES	4-(2-hydroxyethyl)-1-piperazineethanesulfonic acid
HDP	Host defense peptide
LPS	Lipopolysaccharide
M3-PALS	Mixed-mode measurement phase analysis light scattering
MDR	Multi-drug resistance / resistant
MTT	3-[4,5-dimethylthiazol-2-yl]-2,5-diphenyltetrazolium bromide
NADH	Nicotinamide adenine dinucleotide (reduced)
NBD-	N-(7-nitrobenz-2-oxa-1,3-diazole-4-yl)-
NC	Hydrophobicity scale: Normalized Consensus
NK	Natural killer
NMR	Nuclear magnetic resonance
Rh-	N-(Lissamine-Rhodamine-B-sulfonyl)-
RI	Refractory index
RP-HPLC	Reversed-phase high-performance liquid chromatography
PBS	Phosphate-buffered saline
PC	Phosphatidylcholine
PDI	Polydispersity index
PE	Phosphatidylethanolamine
PFA	Paraformaldehyde
PI	Propidium Iodide
PS	Phosphatidylserine
SSC	Side-scattered light
spMMR-D	Sporadic mismatch repair deficiency
TFA	Trifluoroacetic acid
WIF	Hydrophobicity scale: Whole-Residue Interface

# 1 INTRODUCTION

Cancer ranks high among the most persistent threats of human health. By 2010, neoplastic diseases were reported to still be the third leading cause of death among mankind (Thun et al. 2010). Meanwhile, the world health organization estimates a tremendous increase of new cases of cancer per year from 14 million in 2012 to 22 million within the succeeding twenty years. Most state-of-the-art cancer treatments follow a so called combinational approach enclosing surgery as well as radiation, immuno- and chemotherapy. Major drawbacks comprise commonly observed low therapeutic indices, high recurrences, and severe dose-dependent toxicities against healthy host cells and tissues. Moreover, the growing burden of (multidrug) resistant cancer cells underpins the urgent need for innovative therapeutic approaches with combined potent and selective anticancer activity (Hanahan and Weinberg 2011).

Antimicrobial or Host Defense Peptides (HDPs) were originally discovered as being part of the first line of defense of almost every living organism. In general, HDPs are rather small amphipathic peptides, and provide their respective host with a fast-acting and effective armory against pathogenic microbial invaders. Due to their unique, yet, still not completely understood mode of action, HDPs have persistently attracted the attention of researchers and clinicians worldwide. For the last decades, they have been predominantly under investigation as promising future alternative antibiotics, putatively being able to overcome known and prevent the emergence of new resistances (Guani-Guerra et al. 2010; Hancock and Sahl 2006; Yeaman and Yount 2003). However, findings made in recent years extended the focus of research on another possible field of application: Several representatives of HDPs were found to exhibit effective activity against cancer cells and tumorous tissues, making them highly interesting as potent novel anticancer drug candidates (Raucher and Ryu 2015; Gaspar et al. 2013; Harris et al. 2011; Riedl et al. 2011a).

NK-2 is an HDP originally derived from the cationic core region of porcine NK-lysin (Andrä and Leippe 1999), and possesses demonstrable activities against numerous pro- and eukaryotic microbial targets, as well as against several types of cancer cells (Maletzki et al. 2014; Bankovic et al. 2013; Gross et al. 2013; Schröder-Borm et al. 2005).

This work generally aimed at shedding light on crucial aspects of the anti-cancer cell activity of peptide NK-2. Specifically, major objectives addressed in the scope of this thesis could be outlined as follows:

- To assess the activities of peptide NK-2 with respect to its basic effectiveness against and selectivity for cancerous over healthy human cells, as well as in consideration of the overall peptide stability. Of note, besides well-established standard cell lines of human prostate cancer and non-malignant normal keratinocytes the use of two patient-derived colorectal carcinoma (CRC) cell lines provided an advanced cellular test system.
- To scrutinize the effects of particular structural modifications on NK-2's anti-cancer cell performance. What changes in the amino acid sequence are favorable in order to optimize the peptide's level of activity against cancer cells, and thus, its therapeutic use? A set of more than 30 variants of the parent peptide NK-2 was included in in-depth investigations. Software-assisted calculation of peptide-specific physicochemical properties as well as detailed assessments of individual peptide-membrane interactions were performed in order to enable comprehensive structure-function correlations.
- To gain deeper insight into how the activity and target specificity of NK-2-derived peptides is influenced by the membrane surface exposure of the anionic phospholipid phosphatidylserine (PS). As a key hypothesis underlying this work, it is assumed that PS – frequently found at elevated levels on the surface of cancerous but not on healthy human cells – plays a decisive role for the selective targeting of pathologically modified cells by NK-2-derived peptides.
- To contribute to the general understanding of the peptide's anticancer mode of action.

With respect to these overarching objectives, biological data were complemented with studies on artificial membrane systems designed to mimic both cancerous as well as healthy cell membranes.

## 2 THEORETICAL BACKGROUND

### 2.1 Host Defense Peptides

In general, HDPs evolved in a broad variety of organisms, acting as an energy-effective instantaneous armory against pathogenic invaders. As such, they belong to the innate immunity of their respective hosts. Naturally occurring HDPs were discovered in virtually every life form including bacteria, insects, reptiles, amphibians, fish, plants, birds, and mammals. Up to now, the number of naturally occurring host defense peptides exceeds 2,400 (Wang et al. 2015a). Moreover, synthetic peptides expand the arsenal of HDPs and are typically either developed as variants of existing natural peptides, or designed from scratch by *de novo* rational approaches (Chu et al. 2015; Zhu et al. 2014; Sharma et al. 2013; Tyagi et al. 2013; Huang et al. 2010).

Apart from their diverse origins, HDPs also share some common features. Characteristically, they cluster hydrophilic and hydrophobic amino acid residues along their structure to adapt an overall amphiphilic conformation. Normally, a high ratio of basic over acidic amino acid residues leads to a pronounced (poly-) cationic net charge, and contributes, in coincidence with a high proportion of hydrophobic residues, to the amphipathicity. Most HDPs typically possess a limited sequence length of less than 50 amino acid residues. In general,  $\alpha$ -helical conformations as well as  $\beta$ -sheets are prevalent in nature, yet other secondary structures occur, such as loops or extended peptides. The establishment of a structured folding state is frequently not induced until interaction with a hydrophobic interface, such as a biomembrane, takes place. However, some peptides stabilize their fold *a priori*, either with or without the aid of disulfide bridges. (Mookherjee and Hancock 2007; Dennison et al. 2006; Zelezetsky and Tossi 2006; Papo and Shai 2005)

As a consequence of their particular structural properties, HDPs are capable of exhibiting a range of unique activity mechanisms exerted in host defense, which will be addressed hereafter.

### 2.1.1 Classical Mechanisms of Action

HDPs have been reported to target a wide range of potential pathogens such as bacteria, archaea, protozoa, parasites, fungi and enveloped viruses (Yeung et al. 2011; Marr et al. 2006; Boman 2003), as well as cancer cells (Chu et al. 2015; Raucher and Ryu 2015; Hoskin and Ramamoorthy 2008). Although numerous HDPs have been discovered, and even more synthesized so far, the exact mode of action is still subject of extensive research.

A vast majority of HDPs is capable of exhibiting activity through direct physical disruption of the respective target cell membrane. Various superordinate mechanistic models have been postulated to describe and classify frequently observed impacts of HDPs on target cell membranes (see figure 2.1). All of these models anticipate a multi-step cooperative mechanism basically enclosing (i) peptide binding to the membrane surface, (ii) partitioning of peptides into the lipid bilayer, and (iii) membrane permeabilization.

In a bit more detail, the initial step of spatial approximation between usually still randomly coiled cationic peptides and the cell surface is primarily driven by electrostatic attraction. Apparently, negatively charged membrane surfaces are likely to play a crucial role as principle interaction partners of cationic amphipathic HDPs. With respect to classical microbial targets, these negative surface charges can be predominantly attributed to the abundance of acidic membrane phospholipids and phosphoglycolipids, as well as, optionally, components of an enveloping cell wall and/or glycocalyx (Hammer et al. 2010; Andrä et al. 2007; Schröder-Born et al. 2003; Matsuzaki et al. 1995).

By getting in close vicinity to the hydrophobic membrane interface, previously unstructured peptides fold to secondary structures characterized by an amphipathic clustering of amino acid residues. This, in turn, promotes peptide partitioning into the membrane lipid bilayer. At lower (local) concentrations, i.e. peptide/lipid ratios, the linear peptide molecules tend to orientate in parallel to the surface plane. On this occasion, hydrophobic peptide sections strive towards the hydrocarbon core of the lipid bilayer, while hydrophilic sections align facing the aqueous environment. Typically, progressive perpendicular insertion of peptide molecules into the lipid bilayer is promoted after reaching a certain threshold concentration. (Melo et al. 2009; Bechinger and Lohner 2006)

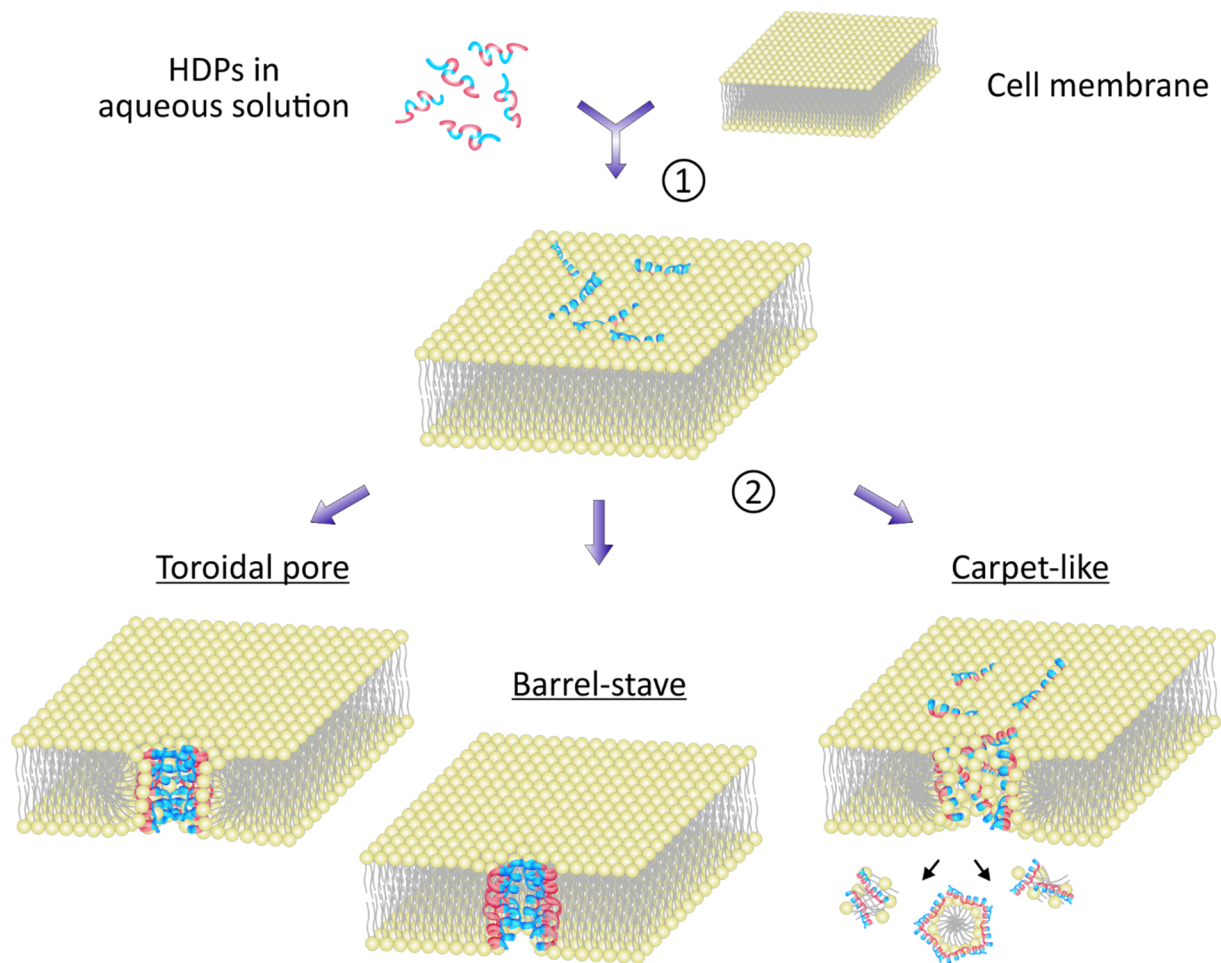


**Figure 2.1: Classical modes of action of host defense peptides.** Most HDPs are rather unstructured in aqueous solution but shape into ordered structures upon interaction with a hydrophobic interface like a plasma membrane (①). Its amphipathic amino acid distribution causes a peptide molecule to partially seek contact with both the hydrophobic acyl chains of the bilayer core as well as the hydrophilic lipid headgroups and the solvent surrounding. After exceeding a certain (local) threshold concentration, membrane impairment can occur by different mechanisms (②). An insertion of peptides perpendicular to the surface plane is established to form a toroidal pore. The pore lumen is framed partially by peptide molecules and partially by lipid headgroups, which introduces local membrane curvature strain. Instead, for a barrel-stave pore, perpendicularly inserted peptides align in parallel to the hydrocarbon bilayer core to form a continuous pore lumen from tightly associated peptide molecules only. The carpet-like mechanism suggests that highly concentrated peptides can disrupt the target membrane in a detergent-like fashion. Modified after Bahar and Ren (2013).

For the subsequent step of actual membrane impairment different mechanisms have been postulated. In general, pore formation mechanisms suggest transient or stable transmembrane aqueous channels to be established, which is delineated by the so called “barrel-stave” as well as the “toroidal pore” model. The former expects pore assembly from laterally oligomerized peptide helices, where the hydrophobic clusters associate with the membrane lipids’ hydrocarbon cores and constitute a transmembrane lumen bordered by the hydrophilic

peptide faces. Alamethicin, for instance, was repeatedly attributed to exert activity through such a barrel-stave-like mechanism (Yang et al. 2001; Beven et al. 1999; He et al. 1996; Sansom 1991). Instead, the toroidal pore formation induces local curvature strain as well as thinning in the membrane bilayer with amphipathic peptides providing alternative interaction surfaces for both polar lipid headgroups as well as non-polar acyl chains. Magainins (Hallock et al. 2003; Matsuzaki et al. 1996) as well as melittin (Yang et al. 2001) were shown to induce such a type of transmembrane pores. The carpet-like mechanism proposes peptide accumulation at the membrane in parallel to the surface plane, eventually resulting in a coverage reminiscent of a carpet. Upon exceedance of a critical concentration, the amphipathic peptides are believed to disrupt the target membrane in a detergent-like manner, eventually with micellization of peptide-lipid complexes impeding the membrane integrity (Bahar and Ren 2013; Jenssen et al. 2006). Typical representatives for this mode of action would be the cathelicidin-like peptide ovipirin (Yamaguchi et al. 2001) as well as dermaseptin (Pouny et al. 1992).

Irrespective of the particular model considered to describe the mode of action, as a final consequence, a peptide-induced loss of the cell membrane's barrier function is achieved, accompanied by the collapse of pH and ion gradients as well as the osmotic balance (Melo et al. 2009; Bechinger and Lohner 2006; Tossi 2005; Yeaman and Yount 2003; Shai 2002). Of note, HDP-mediated membrane impairments are not necessarily succeeded by immediate cell death *per se*. Yet, in the vast majority of studies, peptides were found to rapidly provoke lethality, typically within the range of just a few minutes (Boman 1995).

The afore-described models have been originally developed to characterize explicitly the diverse interactions of HDPs with microbial targets. Nevertheless, the underlying physicochemical principles of peptide-membrane interactions are most probably valid likewise as the basis for potential activities against cancer cells.

In addition to these classical scenarios of HDP action, several mechanisms were described to be unique to the interaction with cancer cells, and related concepts will be addressed in the succeeding sections.

## 2.1.2 Anti-Cancer Cell Activities of Host Defense Peptides

Among discovered naturally occurring HDPs, so far, more than 185 were found to exhibit activities against cancerous cells (Wang et al. 2015b). Many representative studies have already been vividly reviewed in the past (Gaspar et al. 2013; Schweizer 2009; Hoskin and Ramamoorthy 2008; Papo and Shai 2005; Zasloff 2002). Recent examples stressed the great diversity of human cancer types, which have been successfully targeted by anticancer HDPs, ranging from hepatoma (An et al. 2014) and colorectal cancer cells (Kuroda et al. 2015; Maletzki et al. 2014) to acute T cell leukemia (Lemeshko 2013) as well as oral squamous cell carcinoma (Chu et al. 2015), to name just a few.

In the following, an overview on the current knowledge about the underlying principles of anti-cancer cell activities of HDPs will be presented.

### 2.1.2.1 Particular Mechanisms of Actions against Cancer Cells

The exact mode of action and the key factors determining a selective cancer cell targeting by HDPs are still elusive. In close resemblance to antimicrobial mechanisms, peptide-induced oncolytic effects can be generally attributed to membrane-related or non-membrane-related mechanisms (Liu et al. 2015; Harris et al. 2011; Hoskin and Ramamoorthy 2008).

In principle, initially attracted by a net negative surface charge, a direct physical attack of the target cell membrane by amphipathic HDPs can lead to the induction of cancer cell necrosis through destabilization and disintegration of their plasma membrane (Schweizer 2009; Hoskin and Ramamoorthy 2008). However, when compared to the understanding of antimicrobial mechanisms of HDPs, little appears to be known about the exact principles underlying any direct membrane impairment of cancer cells. One relatively well-studied example is that of cecropin B, an  $\alpha$ -helical antimicrobial peptide originally isolated from insects. Patch clamp investigations using the A549 human stomach carcinoma cell line revealed that cecropin B exerted activity through the formation of transient channel-like pores (Ye et al. 2004). Besides, similar membranolytic anti-cancer cell mechanisms have also been proposed for magainins (Cruciani et al. 1991) as well as for the synthetic SVS-1  $\beta$ -hairpin peptide (Sinthuvanich et al. 2012).

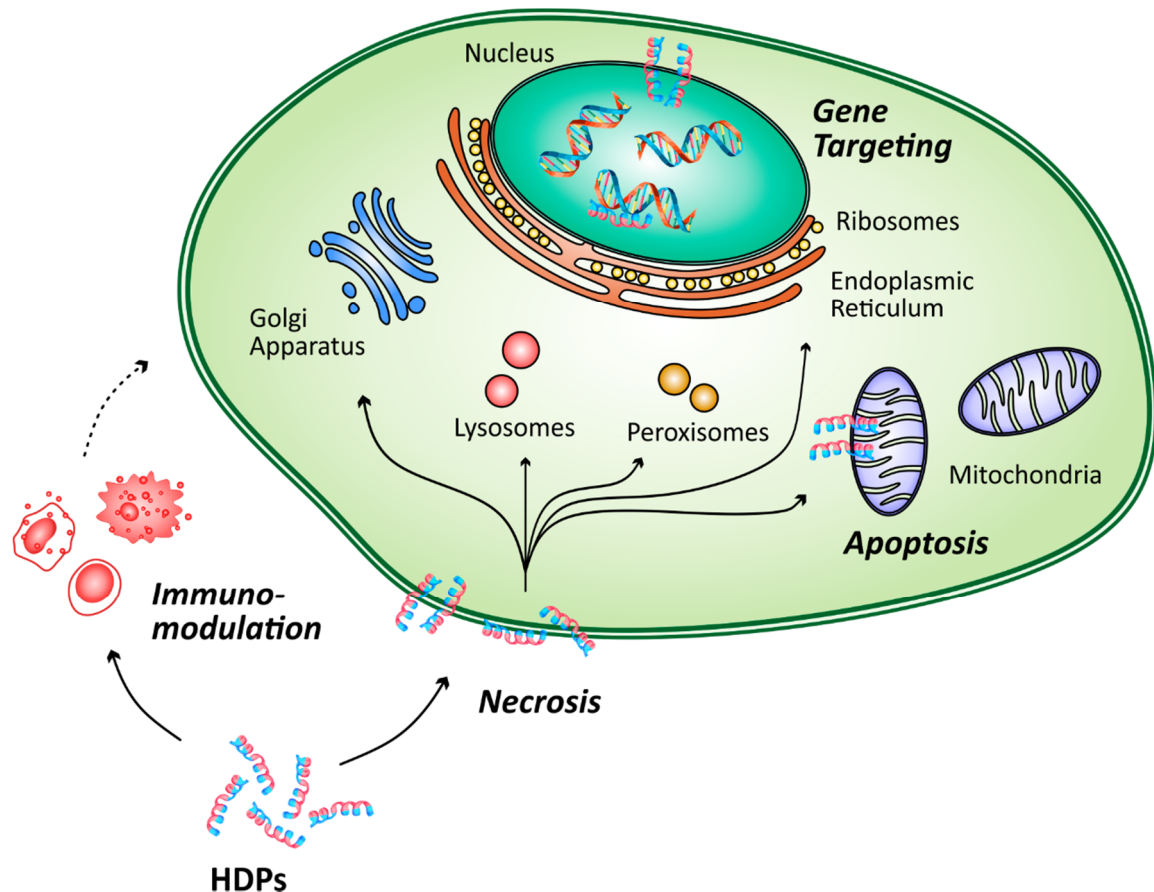


**Figure 2.2: Schematic overview on anti-cancer cell activities of host defense peptides.** Exemplarily, an arbitrary  $\alpha$ -helical amphipathic peptide was chosen to illustrate typical cellular and subcellular HDP targets. Predominantly, the cell membrane of a cancer cell is likely to be directly compromised by cationic amphipathic HDPs. Moreover, after successful translocation of peptides to the cytoplasm, various intracellular targets – especially membrane-enclosed organelles – are potentially susceptible to peptide attacks. Cell killing can finally be induced by necrosis or an apoptotic cascade, or by DNA interference with peptides entering the nucleus. HDP-induced immunomodulatory stimuli can present an alternative indirect route of peptide-mediated cancer cell attacking.

As an indirect route of cancer cell killing, specialized non-membrane-related mechanisms of action have been reported for some anticancer HDPs. These can enclose the affection of cancer cell proliferation as observed with microtubule-perturbing HDP-like dolastatins (Simmons et al. 2005), as well as the targeting of distinct intracellular destinations. Regarding the latter, for instance, mitochondria, DNA-related targets, vital enzymatic pathways, lysosomes or peroxisomes were identified as potential sites of HDP activity after peptide internalization (Yeung et al. 2011; Giuliani et al. 2007; Brogden 2005). The promotion of immunomodulatory effects in higher organisms presents another important pathway through which particular HDPs have been shown to exert activity (Hancock et al. 2016; Gaspar et al. 2013). Such routes can comprise but are not restricted to NK cell stimulation and interferon synthesis induction

as observed with alloferons (Bae et al. 2013; Chernysh et al. 2012), or the activation of complement cascades by the antitumor peptide tachyplesin (Chen et al. 2005).

In consequence, besides necrosis, the final oncolytic effect may alternatively be related to the induction of apoptosis or modified responses of the host immune system. Nevertheless, to enable interactions with internal targets, the initial translocation of peptides to the cytoplasm, either with or without permeabilization of the membrane, remains mandatory. The major targets of HDPs for exerting anti-cancer cell activity were summarized in figure 2.2.

Of note, the type and degree of potentially exerted HDP activities are believed to be strongly dependent on multiple conditions. These can include, but are not limited to, the targeted cell type and its particular membrane composition, the peptide concentration, as well as environmental influences. The latter especially considers properties of the ambient liquid phase. As well, multiple modes of action can apply for a single type of peptide either consecutively or even simultaneously. Furthermore, with respect to higher organisms bearing a diverse repertoire of endogenous HDPs, synergistic mechanisms of different peptides, as well as the interplay with other immune response-related factors are to be expected. (Huang et al. 2015; Liu et al. 2015)

#### **2.1.2.2 Altered Membrane Properties of Cancer Cells**

The transformation of healthy to neoplastic mammalian cells generally manifests in a complex variety of alterations in the cell physiology. Although *cancer* is a generic term for an utmost heterogeneous and pleiotropic disease, some common hallmarks have been identified. Cancer cells provide self-supply with growth signals and manage to ignore growth inhibitory signals. They can trigger angiogenesis and show unlimited proliferative potential. Furthermore, cancerous cells are able to avoid apoptosis induction and exhibit metastatic tissue invasion through barriers like membranes and capillary walls. Finally, successful immunosuppression is mediated by tumor cells as well as by tumor-infiltrating non-cancerous host cells. (Hanahan and Weinberg 2011)

Apparently, the overall membrane constitution plays a decisive role for the potential effective and selective interaction of cancer cells with HDPs. In comparison of healthy and cancerous cells, three major distinctions should be outlined. Without claiming universal applicability, it can be stated that the majority of cancer cells possesses (i) an extensive negative surface charge

due to the abnormal abundance of anionic (macro)molecules in the outer leaflet of their plasma membrane (Riedl et al. 2011a), (ii) an enlarged cellular surface area owed to an elevated number of microvilli (Ren et al. 1990; Kolata 1975), and (iii) an increased overall membrane fluidity attributed to changes in the cholesterol profiles (Sood and Kinnunen 2008; Sok et al. 1999). In principle, all three distinctions can be potentially favorable in terms of cancer cell susceptibility towards HDPs as they (i) provide an electrostatic “recruiting platform” for cationic peptides, (ii) increase the attackable contact surface, and (iii) facilitate peptide integration into the lipid bilayer, respectively (Alves et al. 2015; Huang et al. 2015; Harris et al. 2011; Riedl et al. 2011a; Hoskin and Ramamoorthy 2008). Both, (ii) and (iii), are cancer cell-related features with a high-potential impact on the membrane insertion and permeabilization by HDPs. Nevertheless, the cellular surface net charge is considered to be the crucial factor for the selectivity of peptide targeting due to the direct impact on the mandatory initial step of peptide approximation to the membrane (Hoskin and Ramamoorthy 2008).

Looking one step closer, a range of membrane constituents may contribute to the intensified net negative surface charge of cancer cells. Sulfated glycosaminoglycans (GAGs) as well as hypersialylated glycoproteins and glycolipids are usually anionic at physiological pH, and their cell surface occurrence was shown to be increased for various malignancies. (Han et al. 2013; Kannagi et al. 2008; Fuster and Esko 2005; Sanderson et al. 2004; Dennis et al. 1999; Kleeff et al. 1998)

Increased quantities of sialic acids as terminal carbohydrates of glycosylated membrane proteins and lipids were shown for many cancer cell types. Hypersialylation might be mainly attributed to a cancer-related upregulation of the expression of certain glycosyltransferases (Pearce and Läubli 2015; Dennis et al. 1999; Kim and Varki 1997). Several studies observed interactions of some HDPs with cell surface-associated sialic acids (Weghuber et al. 2011; Bucki et al. 2008; Risso et al. 1998). Nevertheless, previous work of Gross et al. could provide strong evidence for excluding cell surface-bound sialic acids as primary targets of peptide NK-2, which clearly favored sulfated polysaccharide structures (Gross and Andrä 2012).

In fact, the role of elevated levels of such surface-exposed sulfated glycans on cancer cells is rather controversially discussed. Several HDPs, such as magainin, melittin, LL-37, and  $\alpha$ -defensin, were found to basically interact with different GAGs (Schmidtchen et al. 2002; Schmidtchen et al. 2001; James et al. 1994). However, for a set of bovine lactoferricin-derived peptides, the presence of heparan sulfate and chondroitin sulfate on different cancer cell lines

had no or only minor effects on the anti-cancer cell activity, or even had an inhibitory impact (Fadnes et al. 2011; Fadnes et al. 2009). Adding to this, considerable amounts of sulfated glycans are often present also on the membrane surface of healthy cells (Khoo and Yu 2010), and their upregulated exposure can be restricted to particular phases in cancer evolution (Fernandez-Vega et al. 2015; Garcia-Suarez et al. 2014; Sanderson et al. 2004). Overall, these ambivalent characteristics make sulfated glycans rather non-ideal candidates as selectivity-determinant HDP target structures.

Finally, and of special note, the surface exposure of the anionic phospholipid phosphatidylserine (PS) is considered to be a highly important marker for many types of cancer cells. In the scope of this work, special emphasis lies on PS as a putative key surface factor on cancer cells for the initial targeting of the here-deployed peptide NK-2 and structural variants thereof to cancerous cells.

### **2.1.2.3 Phosphatidylserine as a Cancer Cell Marker**

Overall, besides phosphatidylcholine (PC), phosphatidylethanolamine (PE) and sphingomyelin, the anionic phospholipid phosphatidylserine (PS) is one of the most abundant phospholipids in mammalian cell membranes (Schutters and Reutelingsperger 2010; Vance and Steenbergen 2005). In general, each cell type and even its subcellular membrane-enveloped structures can feature an individual lipid constitution and organization. Yet, the plasma membrane of healthy cells is typically characterized by an asymmetric distribution of its lipid components. Zwitterionic choline-based phospholipids (PC, sphingomyelin) are predominantly located on the lipid bilayer's outward facing leaflet. In despite, aminophospholipids like zwitterionic PE and anionic PS are usually sequestered to the cytoplasmic side of the lipid bilayer (Verkleij et al. 1973; Bretscher 1972). Explicitly, the exoplasmic membrane leaflet is found to be virtually void of PS and other, though less abundant, negatively charged constituents like phosphatidylinositol phosphates or phosphatidic acid (Bruckheimer and Schroit 1996). This asymmetry is basically maintained by the outbalanced interplay of membrane-spanning enzymes classified as ATP-dependent flippases and floppases, as well as calcium-dependent scramblases (Kay et al. 2012; Zwaal et al. 2005). The translocation of PS to the outer membrane surface is typically found on aged or pathologically modified cells and has various physiological implications. It serves as a marker

for early stage apoptosis and triggers the engulfment of aberrant cells by macrophages. Moreover, surface-exposed PS participates in the suppression of inadvertent immune and inflammatory responses, and promotes initiation of blood clotting at sites of injury. (Birge et al. 2016; Vance and Tasseva 2013; Zwaal et al. 2005)

Apart from these regulatory tasks of PS in homeostasis, the multiple pathological modifications taking place during cancer evolution can induce a similar loss of the plasma membrane's asymmetric constitution. The disturbance of the underlying enzymatic pathways can result in the exposure of elevated levels of PS on the exoplasmic membrane leaflet of cancer cells (Riedl et al. 2011b; Kirszberg et al. 2009; Schröder-Borm et al. 2005; Utsugi et al. 1991). Increased PS-exposure was also shown for MDR cells of human non-small cell lung (Bankovic et al. 2013) as well as gastric carcinoma (Pohl et al. 2002), where the transport of PS was shown to be related to the activity of MDR cell-specific P-glycoprotein. It is generally assumed that PS can make up to 10 % of the total membrane lipid content (Schutters and Reutelingsperger 2010). Nevertheless, very little appears to be known about this in detail, e.g. about a potential disease-related upregulation of the PS synthesis, or to what extent the total membrane PS actually translocates to the outer bilayer leaflet.

However, affected cancer cells possess a markedly enhanced number of negatively charged cell surface factors, which distinguishes them from their non-pathogenic counterparts. In this context, it is suggested that PS translocation plays an essential role in rendering cancerous cells highly susceptible for selective interactions with cationic anticancer HDPs (see figure 2.3). Explicitly, some HDPs, including NK-2 (Schröder-Borm et al. 2005), were shown to preferentially target cells with increased surface-bound PS levels. Iwasaki et al. (2009) obtained a positive correlation of the surface levels of PS on several cancer cell lines with the susceptibility of these cells to enantiomeric peptide analogs of beetle defensins, while Riedl et al. (2015) characterized cancer cell-specific membranous PS as a key target for certain derivatives of human lactoferricin. In another study, the colocalization of the synthetic host defense-like peptide, D-K<sub>6</sub>L<sub>9</sub>, with surface-bound PS was identified as being crucial to a selective interaction of the peptide with cancer cells after intratumoral injection into human breast and prostate cancer xenografts (Papo et al. 2006). Most recently, for PPS1, a so called peptide-peptoid hybrid, Desai and co-workers (2016) claimed PS-selective cancer cell targeting and toxicity.

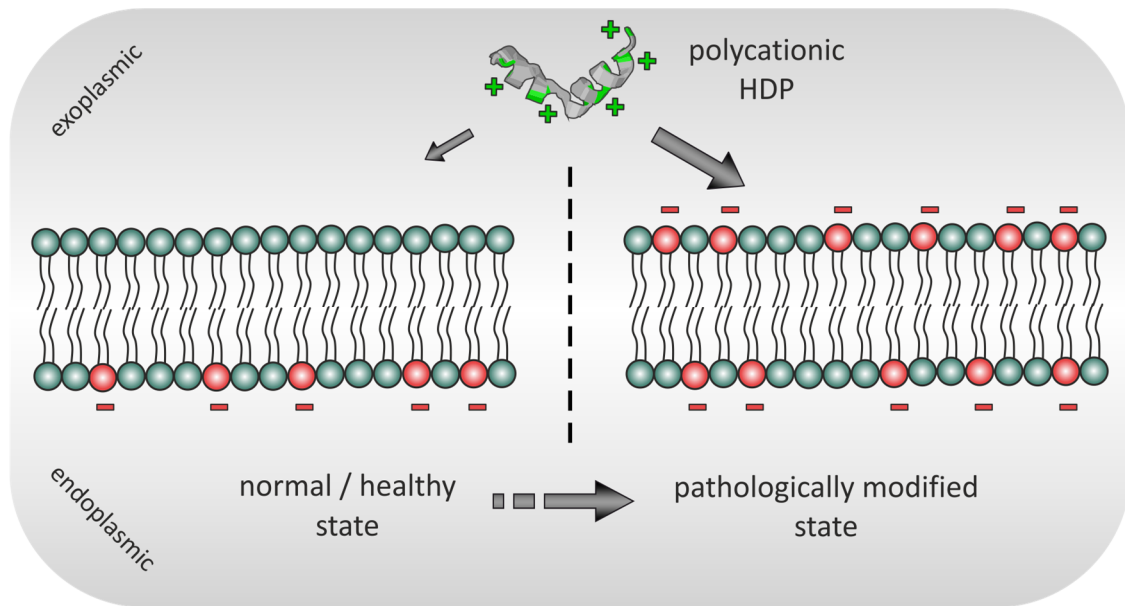


**Figure 2.3: Schematic depiction of PS-related changes in the human plasma membrane upon cancer evolution.** The increased abundance of PS on the outer leaflet of the lipid bilayer is connected to the disturbance of connected regulatory enzymatic pathways during the transformation of healthy to pathologically modified cells. This is usually believed to contribute to an enhanced electrostatic attraction of cationic HDPs, thus, putatively renders cancerous cells susceptible to peptide-induced lysis.

#### 2.1.2.4 Perspectives on Applications of Host Defense Peptides in Cancer Therapy

Chemotherapeutic treatment still is the principle approach in fighting progressed and metastatic stages of cancerous diseases (Siegel et al. 2014). However, severe adverse effects on healthy cells, and ineffectiveness towards dormant or slow-growing cancer cells are major drawbacks to this therapy. Moreover, the emergence of multi-drug resistant (MDR) cancer cells, e.g. via active drug efflux pumps or adapted expression of drug-specific cellular receptors, has become an increasing problem for common chemotherapeutic strategies (Chen and Sikic 2012). With a completely different novel mechanism of action, anticancer HDPs can provide a powerful treatment option. The direct physical disruption of targeted cancer cells minimizes the risk of emerging resistances and is capable of circumventing existing resistance mechanisms. As stated before, this includes explicitly an HDP effectiveness against MDR cells. (Huang et al. 2015; Raucher and Ryu 2015; Douglas et al. 2014; Bankovic et al. 2013; Gaspar et al. 2013; Yeung et al. 2011; Schweizer 2009; Hoskin and Ramamoorthy 2008)

Based on their respective target specificity, anticancer HDPs can roughly be classified into two main categories: Peptides exerting potent activity against cancerous but not healthy

mammalian cells on the one hand, and peptides which are about equally toxic towards neoplastic and normal cells on the other hand (Papo and Shai 2005). The first group of anticancer HDPs provides a promising opportunity for innovative cancer therapy with the potency to overcome the limitations of conventional treatment approaches.

However, apart from the variety of distinct HDPs showing effective anti-cancer cell toxicity *in vitro*, so far, only a limited number of peptides made it through to clinical trials, not to mention actual drug approval (Hu et al. 2011). Predominantly, this was attributed to the significant inactivation of many HDPs in blood serum, where the association of charged but amphipathic peptides to high- and low-density lipoproteins as well as to albumins and other plasma abundant proteins seem to be determining factors (Sivertsen et al. 2014; Vij et al. 2010; Maisetta et al. 2008; Svenson et al. 2007; Peck-Miller et al. 1993). Beyond that, proteolytic degradation constitutes another obstacle putatively contributing to reduced pharmacokinetics (Yeung et al. 2011), and for several HDPs a diminished activity in the presence of elevated concentrations of salts as well as mono- and bivalent metal ions, mainly speaking of  $\text{Ca}^{2+}$  and  $\text{Mg}^{2+}$ , has been reported (Wei et al. 2007; Minahk and Morero 2003; Pink et al. 2003; Brewer and Lajoie 2000; Lehrer and Ganz 1999; Scane and Hawkins 1986). The risks of undesired immunogenicity and unspecific toxicity underpin the need for HDPs of high selectivity (Mader and Hoskin 2006). From an economic point of view, also the high manufacturing expenses of peptide synthesis procedures can become critical in the drug development process.

Nevertheless, much effort is put into solving each of these issues in order to pave a way for anticancer HDPs to fully unfold their therapeutic potential. Firstly, the advent and ongoing advancement in recombinant biotechnological production strategies can provide alternatives with reduced costs of goods (Fan et al. 2014; Wang et al. 2014; Bommarius et al. 2010). Moreover, through the design of HDP-like peptidomimetics (Kim et al. 2011), or the incorporation of non-natural (Chu et al. 2015) or D-enantiomeric amino acids (Iwasaki et al. 2009; Papo et al. 2006), proteolytic cleavage could be alleviated, ideally without compromising the anti-cancer cell activity (Rodrigues et al. 2008; Papo and Shai 2005). Specifically adapted formulations, ranging from prodrug creation (Forde and Devocelle 2015; Desgranges et al. 2012) over peptide conjugation with tumor-homing substrates (Kondo et al. 2012; Colombo et al. 2002) to the incorporation into nanoparticulate carriers (Medeiros et al. 2014; Urban et al. 2012) can improve HDP selectivity, serum half-life and stability, and reduce peptide-related

immunogenicity and unintended toxicity. Yet, assessing the usefulness and applicability of each measure remains a case-by-case developmental task.

For already established antimicrobial HDPs, topical or local administration forms are prevailing for approved indications (Wang et al. 2015a; Yount and Yeaman 2012). This circumvents the above-described pitfalls of systemic application and is probably the preferred initial strategy also for potential anticancer drug development. Exemplarily, the human HDP LL37, from the group of cathelicidins, is currently under investigation in a phase II trial on the effectiveness of its intratumoral injection into human melanoma (M.D. Anderson Cancer Center and National Cancer Institute (NCI) 2015).

It is furthermore suggestive that the local administration of multifunctional HDPs, e.g. at the site of surgical tumor resections, could entail the benefit of combined anticancer and antimicrobial peptide activities, including inflammation inhibition (Wei et al. 2015; Björn et al. 2012) as well as endotoxin neutralization (Schadich et al. 2013; Kaconis et al. 2011). Besides, also anti-angiogenic activities have been reported for several HDPs (Hou et al. 2013; Steinstraesser et al. 2011; Mader and Hoskin 2006; Ran et al. 2002), which seem to be able to inactivate tumor-associated vascular endothelial cells (Rodrigues et al. 2008; Mader et al. 2006). This provides an opportunity to additionally target solid tumors by diminishing their nutrient supply.

Additive or synergistic effects can arise from a combinational cancer treatment comprising classical chemotherapeutics as well as anticancer HDPs. Putatively, this can also enable a dose reduction of both therapeutic compounds, which, in turn, would concomitantly lessen any dose-dependent toxic side effects. Cecropin A, for example, was shown to synergize with the common chemotherapeutics 5-fluorouracil as well as cytarabine in the treatment of lymphoblastic leukemia cells (Hui et al. 2002), whereas modification of doxorubicin-carrying gold nanoparticles with a cell-penetrating peptide enhanced the cytotoxicity towards brain metastatic breast cancer cells (Morshed et al. 2016).

### **2.1.3 Sequence-Related Implications on Anti-Cancer Cell Peptide Activities**

The number of studies on HDPs with anti-cancer cell activity is still quite limited as compared to the originating class of antimicrobial peptides (Wang et al. 2015a; Wang et al. 2009a). Nevertheless, various authors consistently concluded from statistical analyses and reviews of

experimental efforts that there could not be identified a unifying single factor determining the selectivity and/or effectiveness of anticancer HDPs in general (Liu et al. 2015; Harris et al. 2011; Hoskin and Ramamoorthy 2008).

However, for the fundamentally required ability of HDPs to partition into biological membranes, the establishment of a stable amphipathic secondary structure is essential at some point. This is basically achieved by a certain composition and arrangement of hydrophilic and hydrophobic amino acid residues. Thus, the amino acid composition, i.e. types, frequencies, and relative positions of particular amino acid residues, is highly important. (Huang et al. 2010; Dennison et al. 2006; Zelezetsky and Tossi 2006)

With pKa values of  $\geq 11$ , Lysine (K) and Arginine (R) residues are both readily positively charged at physiological pH values (Nozaki and Tanford 1967). Hence, their abundance is a major determinant for the overall cationic character of natural HDPs. Besides, just like the peptides used in this study, many anticancer HDPs possess an amidated carboxy-terminus (Wang et al. 2009a). This can further contribute to a positive net charge, but the influence of this feature on the toxicity and selectivity of HDPs is ambiguous (Harris et al. 2011). On the contrary, negatively charged Glutamic acid (E) and Aspartic acid (D) residues appear at only very low frequencies in the sequence of HDPs in general (Wang et al. 2009a).

Typically, more than one third of all residues is constituted by hydrophobic amino acids (Liberio et al. 2013). Within this group, Alanine (A) and Leucine (L) seem to be of elevated importance for many  $\alpha$ -helical HDPs, which might be owed to these residues' combined high hydrophobicity and helix-formation propensity (Harris et al. 2011; Pace and Scholtz 1998). Nonetheless, other residues of pronounced hydrophobicity, such as Isoleucine (I), Phenylalanine, and Valine (V) substantially contribute to the nonpolar portion of amphipathic HDPs.

Of note, all of these "building blocks" must be kept well-balanced with respect to the overall sequence length, net charge and charge distribution, as well as the mean hydrophobicity and distinct hydrophobic moment(s). At the same time, these parameters must be adjusted so that an effective but highly selective interaction with respective target cancer cells is accomplished. Moreover, also peptide stability under physiological conditions as well as at its target site of activity must be accounted for.

Any modification of the amino acid composition of an HDP, i.e. the substitution, addition, or deletion of at least one residue, can have an impact on one or more of the afore-mentioned

characteristics (Du et al. 2014; Huang et al. 2014; Schmidtchen et al. 2014; Yin et al. 2012; Huang et al. 2011).

To sum up, no generally applicable unifying concepts were established so far to systematically designate defined structural peptide properties to a predictable functional outcome. Instead, it appears that the specific features of a given HDP's sequence and structure allow for an effective and selective interaction with a particular membrane composition and constitution. Regarding anticancer HDPs, it is conceivable that a particular peptide will rather be active against a certain kind of than against all types of cancerous cells, taking additionally into account the enormously variable phenotypes and specificities of neoplastic cells.

## 2.2 Peptides Employed in this Study

As a general remark, in the following, the one-letter-code will be applied to denote amino acid residues as part of peptide names or sequences, and to assign substitutions. Three-letter-coding with suffixed sequence position number will be used to address specific single residues, e.g. as substitution sites. In all other cases, amino acid names will be spelled out. Anticipatory, for example, I2W is the name of an NK-2 derivative where an isoleucine (I) at position 2 (Ile-2) was substituted by tryptophan (W).

### 2.2.1 Peptide NK-2 and Derivatives thereof

The peptide NK-2 was originally derived as the key functional fragment of NK-lysin (Andrä and Leippe 1999), which is an antimicrobial effector molecule produced by porcine cytolytic T and NK immune cells (Andersson et al. 1995). NK-lysin belongs to the saposin-related protein family (Stenger et al. 1999), and possesses a rather limited range of antimicrobial activities, e.g. against *Escherichia coli*, *Bacillus megaterium* and *Candida albicans* (Andersson et al. 1996). Andersson et al. (1996) were the first to demonstrate a cytolytic effect of NK-lysin against NK-sensitive cancer cells of mice. Also recently, NK-lysin was observed to exhibit lytic activity against YAC-1 mouse T-lymphoma cells, and the human analog, granulysin, showed potent *in vitro* and *in vivo* tumor cell killing abilities (Martinez-Lostao et al. 2015; Al-Wasaby et al. 2015).

NK-2 comprises a total of 27 amino acid residues referring to NK-lysin's cationic core region of residues 39-65 (Andrä and Leippe 1999). The sequence encompasses NK-lysin's helices 3 and 4 with adjacent (mostly positively charged) residues (see figure 2.4), and the two helices are tightly connected by a flexible hinge region. The possession of demonstrable bactericidal (Hammer et al. 2010; Andrä et al. 2007), LPS-neutralizing (Brandenburg et al. 2010; Andrä et al. 2004), anti-protozoa (Jacobs et al. 2003), anti-plasmodial (Gelhaus et al. 2008) as well as anti-fungal activities, along with low hemolytic potential and poor toxicity towards healthy human cells (Andrä and Leippe 1999), drew attention to NK-2 as a promising therapeutic candidate for various indications.

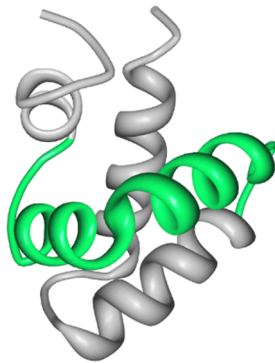


**Figure 2.4: Region of natural NK-lysin corresponding to peptide NK-2.** The three-dimensional depiction illustrates the originating NK-lysin structure solved by NMR and refers to the Protein Database record 1NKL (Liepinsh et al. 1997). The given ribbon model was created and modified using the Protein Workshop tool (Moreland et al. 2005). Highlighted in green is NK-lysin's core region of residues 39 to 65, which is the sequence segment representing peptide NK-2.

Moreover, anticancer activity of NK-2 was comprehensibly shown against a range of cell lines of human origin, including neuroblastoma, leukemia, lymphoma, prostate cancer, and colorectal adenocarcinoma cells, as well as even against MDR non-small cell lung cancer and colon cancer cells (Bankovic et al. 2013; Gross and Andrä 2012; Drechsler and Andrä 2011; Schröder-Borm et al. 2005). In addition, colorectal adenocarcinoma tumors, grown as xenografts subcutaneously in immunocompromised nude mice, responded with necrotic and apoptotic growth inhibition to the treatment with NK-2 and some of its structural variants stressing the remarkable *in vivo* potential (Maletzki et al. 2014). By contrast, human glioblastoma cells seemed to be somehow protected against NK-2-related cytotoxicity (Jacobs et al. 2003).

In line with its biological activities, NK-2 was found to be capable of binding to, insertion into and permeabilization of artificial membrane systems mimicking the lipid constitution of distinct microbial (Andrä et al. 2007; Willumeit et al. 2005; Andrä et al. 2004; Schröder-Borm et al. 2003) as well as pathologically modified mammalian cells (Gross et al. 2013; Gross and Andrä 2012; Schröder-Borm et al. 2005). Of special note, it was repeatedly suggested that the



along the linear sequence of 27 residues in total. This can be substantiated by the complete absence of a consecutive stretch of more than four non-charged residues, while the average distance between two non-adjacent charged amino acids is about 3.6 residues, which is exactly the number of residues per helical turn in an ideal  $\alpha$ -helix. Consequently, 9 of 10 positively charged residues are clustered on the upper-right face of the helical wheel. By contrast, this clustered abundance of charges is complemented by an increased frequency of hydrophobic amino acid residues on the opposing face of the cross section. Considering phenylalanine, isoleucine, leucine, methionine, and valine to be the hydrophobic residues present in peptide NK-2, the average distance between non-neighboring hydrophobic amino acids is about 3.4 residues, again closely matching the size of one helical turn.

Nonetheless, both the predominantly charged/hydrophilic moiety as well as the mostly hydrophobic face are occasionally interfused by single residues of opposite polarity. Yet, with respect to the longitudinal amino acid distribution, the presence of such interfering residues seems to be mainly restricted to the C-terminal sequence moiety (positions > 14). This is well exemplified by amino acids Arg-17 and Asp-21 being the only charged residues interrupting the hydrophobic helical face, while two hydrophobic leucine residues at positions 15 and 23 can be found in the predominantly hydrophilic face.

Here, besides NK-2, a total of 33 structural variants thereof were subject to detailed investigations on their respective interactions with different (cancer) cells as well as artificial membrane systems. The design of most of these modified variants was explicitly motivated by rational considerations (Andrä et al. 2007) rather than by e.g. iterative or randomized amino acid residue alterations. Selected variants have already been included in studies regarding structural and functional features with respect to microbial as well as cancer cells (Ciobanasu et al. 2015; Maletzki et al. 2014; Gross et al. 2013; Gross and Andrä 2012; Andrä et al. 2011; Drechsler and Andrä 2011; Andrä et al. 2008; Andrä et al. 2007). Notably, the extensively shortened derivative NK11 was shown to be unable to adopt a helical conformation and was repeatedly proven to be virtually void of membrane-activity. Furthermore, variants C7A, C7A-D21K, as well as C7A- $\Delta$  tended to exhibit enhanced stability and anti-cancer cell activity. For the lead structure of peptide NK-2 as well as for each of the here-involved derivatives, software-assisted calculations of distinct physicochemical properties yielded detailed structure-related information and will be delineated in the results section.

### 2.2.2 Melittin

Melittin is a principle toxic component in the venom of honey bees (*Apis mellifera*). Its highly potent lytic interactions with cell membranes of diverse kind have been studied extensively since the 1950s (Hanulova et al. 2009; Dempsey 1990; Habermann 1954). In total, melittin comprises 26 amino acid residues organized in strongly amphipathic  $\alpha$ -helical conformation. An extended hydrophobic section spans over 19 residues, followed by a highly basic tetrapeptide stretch (KRKR) in close-to-C-terminal position. Depending on features of the targeted membrane, pH and salt conditions, and, especially, the melittin concentration, different conformations can be found, with either monomers or tetrameric aggregates in aqueous surrounding (John and Jähnig 1988).

The peptide was found to act by diverse mechanisms of action against microbial as well as eukaryotic cells (Dempsey 1990). Besides the direct physical membrane impairment generally prevalent with cationic amphipathic peptides (see above), melittin is capable of exhibiting secondary cytotoxic effects, also in the scope of cancer cell targeting (Son et al. 2007). For example, a selective activation of phospholipase A<sub>2</sub> was observed in Ras-overexpressing cancer cells, inducing calcium influx and rapid cell death (Sharma 1993). However, melittin's extensive membrane destruction properties were found to be accompanied by pronounced hemolytic activity (Gross et al. 2013; Dempsey 1990; Tosteson et al. 1985; Habermann 1972) and overall poor membrane selectivity (Sommer et al. 2012; Hanulova et al. 2009; Maher and McClean 2008). Hence, in the course of this work, melittin was deployed as an effective but non-specific positive control peptide in cell- and artificial membrane-based experiments.

## 2.3 Human Cancer Cell Models Used in this Study

### 2.3.1 Patient-Derived Human Colon Cancer Cells

Globally, colorectal cancer ranks third among the most prevalent cancers, diagnosed with incidences in about 10 % of the population, and about equally distributed among women and men (Torre et al. 2015).

Several attempts have been made worldwide to characterize the activities of HDPs against various CRC cell lines (Chen et al. 2015; Kuroda et al. 2015; Niemirowicz et al. 2015; Ren et al. 2015; Nie et al. 2013). Exemplarily, Kuroda et al. (2015) determined a dose-dependent apoptosis induction in HCT116 cells by a structural derivative of the human HDP LL-37, namely FF/CAP18. KL15, a synthetic variant of bacteriocins from *Lactobacillus casei*, was shown to exhibit necrosis-related activity against SW480 colon adenocarcinoma cells and to adopt an  $\alpha$ -helical conformation in the presence of unilamellar lipid vesicles. This clearly points at the profound ubiquitous relevance of this field of research and, explicitly, of HDP-based treatment strategies.

For the assessment of a given compound's general interactions with cancer cells, most studies rely on well-characterized, long-cultivated standard cancer cell lines. Along with those named above, in case of colon cancers, common CRC models encompass CaCo-, HCT-, or COLO-cells, to name just a few. Here, of special note, advantage was taken of two cancer cell cultures, which were established by Linnebacher and co-workers at the University of Rostock, Germany, from colon cancer tissue of individual patients after surgical resection. To be more precise, the actual cell lines, HROC24 and HROC107, were derived from primary adenocarcinoma material subsequent to a successful engrafting and growth in immune-compromised mice (Maletzki et al. 2012; Linnebacher et al. 2010).

In general, such cells are considered advantageous over standard model cell lines in terms of information on and characterization of closer-to-reality applicability and effectiveness of therapeutic strategies (Ince et al. 2015; Maletzki et al. 2015; Whittle et al. 2015; Maletzki et al. 2012; Linnebacher et al. 2010). Both cell types were originally derived from the ascending colon of the respective patient, and share further commonalities down to the oncological molecular type of the so called sporadic mismatch repair deficiency (spMMR-D). Apart from these common features, HROC24 and HROC107 cells show particular distinctions, e.g. in their growth kinetics and morphologies. Noticeably, a study by Maletzki et al. (2014) indicated a

marked difference of both cell types in their surface-exposure of PS, with HROC107 and HROC24 cells attributably expressing low and high surface-PS levels, respectively.

Under consideration of these promising initial data, here, a more in-depth analysis of these cell types was conducted, including alternative cell characterization techniques as well as further studies on their interactions with NK-2-derived peptides. In addition, the HCT116 human colon cancer model cell line was included as a commercially available colorectal adenocarcinoma reference.

### **2.3.2 Human Prostate Cancer Cells and Non-Tumorigenic Keratinocytes**

Prostate cancer approximately accounted for one third of all new cancer cases in US American males in 2014, representing the most prevalent type of cancer in total (Siegel et al. 2014). The adenocarcinoma of the prostate gland is the most common subtype, and the PC-3 human prostate adenocarcinoma cell line is a commercially available, well-characterized standard cell line established in the late 1970s from disease grade IV epithelial tissue of a bone metastatic site (Kaighn et al. 1979). Here, this easy-to-handle cancer cell model was predominantly applied to study structure-activity relationships upon interaction with peptides. As a reference, HaCaT human keratinocytes were included in these investigations to represent non-cancerous, healthy human cells. They grow adherently as monolayers and have originally been characterized as *in vitro* spontaneously transformed cells from histologically normal human dermal tissue (Boukamp et al. 1988).

## 3 MATERIALS

### 3.1 Peptides

In total, a set of 35 peptides including NK-2 and 33 structural derivatives thereof, as well as melittin as a reference, have been deployed in the course of this study. With the exception of peptide C7S-OH, all peptides had been synthesized with an amidated carboxy-terminus on a peptide synthesizer (ASP 222; Intavis, Bioanalytical Instruments, Cologne, Germany) by Rainer Bartels and Volker Grote from the division of Structural Biochemistry at the Leibniz-Center for Medicine and Biosciences (Borstel, Germany). The synthesis was done according to a standardized Fmoc solid-phase technique, and peptides were provided in RP-HPLC-purified and lyophilized form. Peptide stock solutions at a molar concentration of 1 mM were prepared by dissolving the peptides in 0.01 % trifluoroacetic acid (TFA; Sigma-Aldrich, Steinheim, Germany). The stocks were stored at -20°C, thawed for usage and refrozen again immediately afterwards. A detailed overview on individual peptide sequences and properties will be given in result section 5.1.

## 3.2 Lipids

Natural phospholipids L- $\alpha$ -phosphatidylcholine (PC) from hen egg and L- $\alpha$ -phosphatidylserine (PS) from porcine brain were purchased from Avanti Polar Lipids (Alabaster, AL, USA). Their respective predominant hydrocarbon species, as referred to supplier information (see table 3.1), are depicted in figure 3.1.

**Table 3.1: Origins and supplier details on deployed phospholipids.**

Product	Manufacturer / supplier	Product no.
L- $\alpha$ -phosphatidylcholine (PC), from chicken egg, powder	Avanti Polar Lipids, Alabaster, AL, USA	840051P
L- $\alpha$ -phosphatidylserine (PS), from porcine brain, powder	Avanti Polar Lipids, Alabaster, AL, USA	840032P
N-(7-nitrobenz-2-oxa-1,3-diazol-4-yl)-phosphatidylethanolamine	Molecular Probes, Eugene, OR, USA	N360
N-(Lissamine-Rhodamine-B-sulfonyl)-phosphatidylethanolamine	Molecular Probes, Eugene, OR, USA	L1392

In resemblance to conditions found on the surface of healthy human cells, liposomes solely made of zwitterionic PC lipids remain about non-charged at physiological pH values. Instead, PS is an anionic phospholipid with a negative net charge at physiological pH. The charges within the lipid headgroup are distributed to a more or less zwitterionic terminal serine and a primarily anionic phosphate anchor.

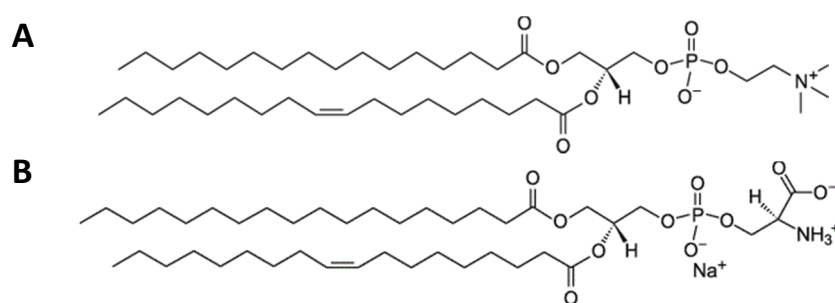


**Figure 3.1: Predominant constituents of employed natural phospholipids.** Depicted are skeletal formulas of L- $\alpha$ -phosphatidylcholine from hen egg (A) (fatty acid carbons:double bonds = 16:0, 18:1) and L- $\alpha$ -phosphatidyl-serine from porcine brain (B) (18:0, 18:1). Structural representations were modified from Avanti Polar Lipids (web source, Avanti Polar Lipids Inc. homepage).

In addition, fluorescently labeled phospholipids were utilized in FRET spectroscopy experiments. Phosphatidylethanolamine (PE) is also considered zwitterionic, hence, shows negligible influence on the net charge of phospholipid membranes. Pre-conjugated, lyophilized N-(7-nitrobenz-2-oxa-1,3-diazol-4-yl)-phosphatidylethanolamine (NBD-PE) and N-(Lissamine-Rhodamine-B-sulfonyl)-phosphatidylethanolamine (Rh-PE) were purchased from Molecular Probes (Eugene, OR, USA).

### 3.3 Cell Cultures

The following tables summarize information on key features and origins of all cell lines deployed in the course of this work.

**Table 3.2: Overview on patient-derived human colorectal cancer cell lines.**

---

<b>HROC24</b>	<i>Patient-derived low-passage colorectal cancer (CRC) cells</i>
Organism:	Homo sapiens, human
Ethnicity:	Caucasian
Age:	98 years
Gender:	Male
Tissue:	Colon ascendens
Morphology:	Epithelial
Growth Properties:	Monolayer, adherent
Supplier / depositor:	PD Dr. M. Linnebacher / University clinic of Rostock, Germany
Generated by:	Linnebacher et al. (2010)

---

<b>HROC107</b>	<i>Patient-derived low-passage colorectal cancer (CRC) cells</i>
Organism:	Homo sapiens, human
Ethnicity:	Caucasian
Age:	81 years
Gender:	Female
Tissue:	Colon ascendens
Morphology:	Epithelial
Growth Properties:	Monolayer, adherent
Supplier / depositor:	PD Dr. M. Linnebacher / University clinic of Rostock, Germany
Generated by:	Linnebacher et al. (2010)

**Table 3.3: Overview on commercially available human model cell lines.**

<b>PC-3</b>	<i>Prostate adenocarcinoma cells</i>	
	Organism:	Homo sapiens, human
	Ethnicity:	Caucasian
	Age:	62 years
	Gender:	Male
	Tissue:	Prostate
	Morphology:	Epithelial
	Growth properties:	Monolayer, adherent. Cells form clusters in soft agar and can be adapted to suspension growth.
	Supplier / depositor:	ATCC® No. CRL-1435™
Generated by:	Kaighn et al. (1979)	
<b>HCT116</b>	<i>Colorectal adenocarcinoma cells</i>	
	Organism:	Homo sapiens, human
	Ethnicity:	Caucasian
	Age:	not available
	Gender:	Male
	Tissue:	Colon
	Morphology:	Epithelial
	Growth properties:	Monolayer, adherent
	Supplier / depositor:	ATCC® No. CCL-247™
Generated by:	Brattain et al. (1981)	
<b>HaCaT</b>	<i>Normal skin cells</i>	
	Organism:	Homo sapiens, human
	Ethnicity:	Caucasian
	Age:	62 years
	Gender:	Male
	Tissue:	Skin
	Morphology:	Keratinocyte
	Growth Properties:	Monolayer, adherent
	Supplier/depositor:	CLS Cell Line Service No. 300493 / DKFZ, Heidelberg, Germany
Generated by:	Fusenig, Boukamp (Boukamp et al. 1988)	

### 3.4 Chemicals and Reagents

**Table 3.4: Chemicals and reagents.**

Product	Quality	Manufacturer / supplier	Product no.
2-Propanol	≥ 99.95 %, Rotisolv®	Roth, Karlsruhe, Germany	AE73.2
3-[4,5-dimethylthiazol-2-yl]-2,5-diphenyltetrazolium bromide (MTT) tested	≥ 97.5 % TLC, cell culture	Sigma Aldrich, Steinheim, Germany	M5655
Accutase	Cell dissociation buffer	Capricorn Scientific, Ebsdorfergrund, Germany	ACC-1B
Ammonium chloride	≥ 99.5 % for analysis, ACS, ISO	Roth, Karlsruhe, Germany	K298.1
Binding buffer (2x)	ApoDETECT™ kit (reagent 2)	Life Technologies, Darmstadt, Germany	331200
Calcein	Powder, mixed isomers	Sigma Aldrich, Steinheim, Germany	C0875
Calcium chloride (CaCl <sub>2</sub> )	≥ 94 %, dehydrated	Roth, Karlsruhe, Germany	A119.1
Chloroform (CHCl <sub>3</sub> )	pro analysis	Merck, Darmstadt, Germany	1.024.452.2500
D(+)-Glucose	≥ 99.5 %, Cellpure®	Roth, Karlsruhe, Germany	HN06.3
Dulbecco's modified eagle medium (DMEM)	incl. stable Na-glutamine	Biochrom, Berlin, Germany	FG 0445
Ethanol	≥ 96 %, with ca. 1 % MEK	Roth, Karlsruhe, Germany	T171.4
Fetal bovine serum (FBS)	EU-approved origin	Biochrom, Berlin, Germany	S 0115
FITC-annexin V	ApoDETECT™ kit (reagent 1)	Life Technologies, Darmstadt, Germany	331200
HEPES	≥ 99.5 %, Pufferan®	Roth, Karlsruhe, Germany	6763.2
Hydrochloric acid (HCl)	37 % pure, fuming	Roth, Karlsruhe, Germany	9277.1
Magnesium sulfate (MgSO <sub>4</sub> )	≥ 99 % heptahydrate	Roth, Karlsruhe, Germany	T888.1
Mowiol 4-88 reagent	97.8 % (lot B23468)	Merck, Darmstadt, Germany	475904
Paraformaldehyde	≥ 95 %, ReagentPlus®	Sigma Aldrich, Steinheim, Germany	P-6143
Penicillin / streptomycin	10.000 U/ml / 10.000 µg/ml	Biochrom, Berlin, Germany	A 2212
Phosphate-buffered saline (PBS)	1x, pH 7.4, w/o Ca <sup>2+</sup> and Mg <sup>2+</sup>	Biochrom, Berlin, Germany	L 1825
	Powder for 50 l, w/o Ca <sup>2+</sup> and Mg <sup>2+</sup>	Biochrom, Berlin, Germany	L 182-50
Potassium chloride (KCl)	≥ 99.995 %, Roti®metic	Roth, Karlsruhe, Germany	5346.1
Potassium iodide (KI)	≥ 99.995 %, Suprapur®	Merck, Darmstadt, Germany	1.05044.0050
Propidium iodide (PI)	ApoDETECT™ kit (reagent 3)	Life Technologies, Darmstadt, Germany	331200
Sodium chloride (NaCl)	≥ 99.5 % for analysis, ACS, ISO	Roth, Karlsruhe, Germany	9265.1
Sodium hydroxide (NaOH)	1 mol/l ± 0.2 %	Roth, Karlsruhe, Germany	K021.1
Sodium thiosulfate pentahydrate	ACS, ISO, Reag. Ph. Eur.	Merck, Darmstadt, Germany	106516
Sytox green	5 mM solution in DMSO	Life Technologies, Darmstadt, Germany	S7020
Trifluoroacetic acid (TFA)	≥ 99 %, Pufferan®	Sigma Aldrich, Steinheim, Germany	T6508
Triton X-100	Class 9 / purity grade III	AppliChem, Darmstadt, Germany	A4975
Trypsin / EDTA	0.05 % / 0.02 % (w/v)	Biochrom, Berlin, Germany	L 2143

### 3.5 Laboratory Equipment and Software

**Table 3.5: Instruments and laboratory equipment.**

<b>Instrument</b>	<b>Type</b>	<b>Manufacturer / supplier</b>
Balances	Entris 2202I-1S, max. 2200 g	Sartorius, Göttingen, Germany
	5-digit KERN analysis balance	Kern & Sohn, Balingen, Germany
Cell counter	Countess automated cell counter	Life Technologies GmbH, Darmstadt, Germany
Centrifuges	MiniSpin <i>plus</i> centrifuge	Eppendorf, Hamburg, Germany
	Multifuge 3 S-R	Thermo Fisher Scientific, Braunschweig, Germany
	Centrifuge 5415R	Eppendorf, Hamburg, Germany
CO <sub>2</sub> incubator	Binder CB, class 3.1	Binder, Tuttlingen, Germany
Electronic dispenser pipette	Multipette stream	Eppendorf, Hamburg, Germany
Extruder	Avanti Mini-Extruder	Avanti Polar Lipids, Alabaster, AL, USA
Flow cytometer	BD FACSCalibur™ platform	Becton Dickinson, Franklin Lakes, NJ, USA
Fluorescence microscope	Olympus DP71	Olympus, Hamburg, Germany
Laminar flow hood	Herasafe KS 18, class II clean bench	Thermo Fisher Scientific, Braunschweig, Germany
Magnetic stirrer	Big quid	IKA, Staufen, Germany
Multichannel pipette	Transferpette S, 10-100 µl	Brand, Wertheim, Germany
Multiwell platereader	Tecan infinite M200pro	Tecan, Crailsheim, Germany
pH meters	inoLab, WTW series, pH 720	WTW, Weilheim, Germany
	Knick calimatic	Knick, Berlin, Germany
Phase contrast microscope	Axiovert 40 CFL, inverted	Carl Zeiss, Oberkochen, Germany
Pipetting aid	accu-jet pro	Brand, Wertheim, Germany
Piston-stroke pipettes	Research plus 10 / 200 / 1000 µl	Eppendorf, Hamburg, Germany
Sonifier	Branson Sonifier 250	Branson Ultrasonics, Danbury, CT, USA
Spectrofluorometer	SPEX-III Fluorolog	SPEX Industries, Edison, NJ, USA
Thermostat	Haake F3	Thermo Fisher Scientific, Braunschweig, Germany
Tilting shaker	Rocking Platform	VWR International, Hannover, Germany
Vacuum pump	DIVAC 2.4 L	Oerlikon Leybold Vacuum, Cologne, Germany
Vortex mixer	Test tube shaker, VWR Collection	VWR International, Hannover, Germany
Water bath	GFL 1003	GFL, Burgwedel, Germany
	JB Aqua S Plus	Grant Instruments, Cambridge, United Kingdom
	Sonorex Digitec	Bandelin electronic, Berlin, Germany
Zetasizer	Zetasizer Nano ZS, ZEN3600	Malvern Instruments, Malvern, United Kingdom

**Table 3.6: Software and tools.**

<b>Software</b>	<b>Version</b>	<b>Manufacturer / supplier</b>
CellQuest Pro	6.0	Becton Dickinson, Franklin Lakes, NJ, USA
cellSens	Entry	Olympus, Hamburg, Germany
CorelDRAW X7	17.6.0.1021	Corel GmbH, Munich, Germany
Flowing Software	2.5.1	University of Turku, Turku, Finland
Helical Wheel Projections	v 1.4	Armstrong and Zidovetzki, (2015)
Magellan	7.1	Tecan, Crailsheim, Germany
MATLAB	R2014a, 8.3.0.532	MathWorks Inc., Natick, MA, USA
OriginPro 8 SR0	v8.0724 (B724)	OriginLab, Northampton, MA, USA
Photoshop CS5	12.0.2	Adobe Systems, Mountain View, CA, USA
Profilegraph	1.03	University of Cologne, Germany
Protein Workshop	4.2.0	Moreland et al. (2005)
Zetasizer Software	7.03	Malvern Instruments, Malvern, United Kingdom

### 3.6 Disposables and Consumables

**Table 3.7: Disposable labware and consumables.**

<b>Product</b>	<b>Manufacturer / supplier</b>	<b>Order no.</b>
24-well cell culture plates, transparent, flat	TPP, Trasadingen, Switzerland	92424
96-well cell culture plates, Cellstar, clear, flat	Greiner Bio-One, Frickenhausen, Germany	655180
96-well microtiter plates, Nunclon $\Delta$ , black, flat	Greiner Bio-One, Frickenhausen, Germany	137101
Cell culture flasks, 25 / 75 cm <sup>2</sup>	TPP, Trasadingen, Switzerland	90026 / 90076
Centrifuge tubes, 15 ml / 50 ml	TPP, Trasadingen, Switzerland	91015 / 91050
Combitips advanced 0.1 / 1 / 2.5 / 5 ml	Eppendorf AG, Hamburg, Germany	0300 089.405 /.430 /.448 /.456
Countess cell counting chamber slides	Thermo Fisher Scientific, Braunschweig, Germany	C10228
Eppendorf tubes, safe-lock, 1.5 / 2.0 ml	Eppendorf AG, Hamburg, Germany	0300 120.086 /.094
Glass cover slips, round, 12 mm	Roth, Karlsruhe, Germany	P231.1
Microscopy glass slide	Roth, Karlsruhe, Germany	H868.1
Nitrile gloves, rotiprotect, size L	Roth, Karlsruhe, Germany	P778.1
Parafilm M	Roth, Karlsruhe, Germany	H666.1
Pipette tips, epT.I.P.S. 20 / 200 / 1000 $\mu$ l	Eppendorf AG, Hamburg, Germany	0300 00.854 /.870 /.919
Polycarbonate membrane, 25 mm	Whatman, GE Healthcare, Uppsala, Sweden	110605
Quartz cuvettes 109.000F-QS	Hellma Analytics, Müllheim, Germany	109000F-10-40
Quartz cuvettes 101-QS	Hellma Analytics, Müllheim, Germany	111-10-40
Reagent reservoirs	VWR International, Hannover, Germany	1.800.932.5
Rotilabo glass sample vials	Roth, Karlsruhe, Germany	E159.1
Septum PTFE, 8 mm	Roth, Karlsruhe, Germany	E163.1
Serological pipettes, 2 / 5 / 10 / 25 ml	Biochrom, Berlin, Germany	940-02 /-05 /-10 /-24
Syringe filters, CME, 0.22 $\mu$ m, 33 mm	Roth, Karlsruhe, Germany	KH54.1
Syringes, Braun Injekt-F, 1 ml	Roth, Karlsruhe, Germany	T987.1
Syringes, Braun Omnifix, 20 ml	Roth, Karlsruhe, Germany	T550.1
TG 100 separation gauze, 50 mm	Whatman, GE Healthcare, Uppsala, Sweden	10423029
Zetasizer folded capillary cells DTS1070	Malvern Instruments, Malvern, United Kingdom	DTS1070

### 3.7 Buffers and Stock Solutions

As a general remark, all buffers and stock solutions were sterile-filtered through syringe filters with a pore size of 0.2  $\mu\text{m}$  (Nucleopore, GE Healthcare, Uppsala, Sweden) prior to usage. The only exceptions to this were *complete medium* as well as *PBS/medium* solutions, which were prepared from sterile solutions and strictly handled under a laminar flow hood in order to prevent contamination. All ingredients used are listed in table 3.4 together with details on concentration, purity and supplier.

#### 3.7.1 Aqueous Buffers

All of the following buffers were prepared by dissolving the ingredients in endotoxin-filtered, demineralized water (purified  $\text{H}_2\text{O}$ ), adjustment of the pH value to 7.4 using HCl or NaOH, and final storage at 4°C in the dark until usage.

##### *Buffer A*

HEPES	20 mM
NaCl	150 mM

##### *Buffer B*

HEPES	40 mM
-------	-------

##### *Buffer IN*

HEPES	10 mM
EDTA	1 mM

##### *Buffer OUT*

HEPES	10 mM
NaCl	150 mM
EDTA	1 mM

##### *Annexin V binding buffer (ApoDETECT™ kit – reagent 2)*

HEPES	10 mM
NaCl	140 mM
$\text{CaCl}_2$	2.5 mM

### 3.7.2 Cell Culture Medium-Based Buffers

#### *Complete medium*

DMEM	500 ml
Heat-inactivated FBS	50 ml
Penicillin / streptomycin	5 ml

Details on the preparation are provided in the corresponding method section 4.2.1.

#### *PBS/medium*

PBS (1x) w/o Ca <sup>2+</sup> and Mg <sup>2+</sup>	9/10 <sup>th</sup>
Complete medium	1/10 <sup>th</sup>

Stock solutions of PBS/medium were freshly prepared for each experiment.

#### *Buffer variants for cytotoxicity testing*

Several buffer variants composed of PBS/medium supplemented with distinct DMEM-related additives (see table 3.8), as well as defined mixtures of PBS, DMEM, and FBS (see table 3.9) were used during cytotoxicity testing.

**Table 3.8: Buffer variants I-III.** PBS/medium buffer was augmented with additive components at DMEM-equivalent final concentrations as indicated.

Variant name	Component	Additive
I	PBS/medium	4.5 g/l D(+)-Glucose
II	PBS/medium	200 mg/l MgSO <sub>4</sub>
III	PBS/medium	200 mg/l CaCl <sub>2</sub>

The given concentration of each additive reflect this components final mass concentration in equivalence to pure DMEM conditions. Appropriate additive stock solutions were prepared by dissolving the respective substance in PBS (1x) followed by sterile filtration.

**Table 3.9: Buffer variants IV-VII.** Given values represent each component's volumetric share (vol. %) in the final buffer variant.

Variant	Component / vol-%		
	PBS (1x)	DMEM	FBS
IV	90	10	0
V	90	0	10
VI	80	10	10
VII	0	99	1

### 3.7.3 Stock Solutions

#### *Mowiol stock*

Glycerin	6 g
Mowiol	2.49 g
Purified H <sub>2</sub> O	6 ml
Tris-HCl stock (0.2 M) at pH 8.5	12 ml

Dissolved in 6 ml purified H<sub>2</sub>O in a water bath at 53°C. After centrifugation for 20 minutes at 4,000 rpm supernatant aliquots (~0.5 ml) were stored at -20°C.

#### *Paraformaldehyde (3 % w/v) stock*

Paraformaldehyde	3 g
------------------	-----

Dissolved to clearance with ca. 80 ml pre-heated (~60°C) and stirred PBS solution under a ventilated hood. The volume of the cooled down and filtered solution is adjusted to 100 ml with PBS. The pH value was readjusted to 7.4, if necessary. Storage of aliquots (5 to 15 ml) at -20°C.

## 4 METHODS

### 4.1 Software-Based Assessment of Peptide Properties

The public-domain software Profilegraph (version 1.03, University of Cologne, Germany) introduced by Hofmann and Stoffel (1992) served as a computational tool for amino acid sequence analysis.

Presuming a physiological pH value, aspartic acid is the only negatively charged amino acid residue present in any given peptide. Basic residues lysine and arginine were considered positively charged. Moreover, all peptides, except C7S-OH, used for the experimental part of this work had been synthesized with an amidated carboxy-terminus, which, in conjunction with the amino-terminus, increases the net charge by +1. Under these prerequisites, a given peptide's net charge ( $Q$ ) was calculated by subtracting the number of aspartic acid residues from the sum of positive charges.

All calculations addressing hydrophobicity properties were based on the so called Normalized Consensus scale introduced by Eisenberg et al. (1984). This scale ranks the contribution of all 20 proteinogenic amino acids in terms of hydrophobicity in such a way that the mean over all 20 values sums up to 0, while the corresponding standard deviation equals exactly 1 (see appendix table A.1). Due to this weighting, the scale ranges asymmetrically from -2.53 for arginine, bearing a well-accessible positive charge in its side chain, to +1.38 for highly hydrophobic isoleucine.

As a first parameter, the average hydrophobicity ( $H$ ) was deduced as the arithmetic mean of all amino acid residue-specific hydrophobicities of a given sequence. Moreover, the so called hydrophobic moment ( $\mu H$ ) can serve as a measure of the amphipathicity of a defined amino acid sequence (Eisenberg et al. 1982). The Profilegraph software allows the implementation of sliding window analysis routines in order to take not only the contribution of one amino acid residue into account, but to include influences from neighboring residues.

Generally speaking, the mean value of  $\mu H$  within a segment of defined window width  $(2m+1)$  could be calculated by

$$\mu H_{2m+1}(i) = (2m + 1)^{-1} \cdot \sqrt{\left[ \sum_{j=i-m}^{i+m} H(j) \sin(\delta(j-1)) \right]^2 + \left[ \sum_{j=i-m}^{i+m} H(j) \cos(\delta(j-1)) \right]^2}, \quad (6.1)$$

where  $m$  represents the half-width of the sliding window,  $H(j)$  is the scale-related hydrophobicity value of the  $j^{\text{th}}$  residue, and  $\delta$  is the inter-residue angular frequency.

Here, an ideal continuous  $\alpha$ -helical conformation was assumed for all peptides. Accordingly, the sliding window width  $(2m+1)$ , for which  $\mu H$  values should be calculated, was set to 7 (yielding  $m = 3$ ) to span approximately the size of two helical turns (see above). Moreover, the inherent periodicity of an  $\alpha$ -helical secondary structure specifies the angle between two consecutive residues ( $\delta$ ) to be approximately  $100^\circ$ .

Considering these prerequisites, for each peptide the mean hydrophobic moment over all 7-residue segments ( $\mu H_{\text{mean}}$ ) as well as the local maximum hydrophobic moment ( $\mu H_{\text{max}}$ ) were assessed. Of note, the terminal three windows were generally neglected for further analyses due to the ambiguous definition of pre- and post-sequence residues.

Finally, in addition to the full sequence analysis, also N- and C-terminal moieties of each peptide were individually investigated. The linear amino acid sequence of each peptide bearing  $n$  residues in total was divided to yield two parts of about equal size. For even numbers of  $n$ , the residue counts of the C- and N-terminal moieties were identical, with  $n_{\text{N}} = n_{\text{C}} = \frac{n}{2}$ , while for odd numbers of  $n$ , the carboxy-terminal segment was chosen to be larger ( $n_{\text{C,odd}} = \frac{n+1}{2}$ ) than the amino-terminal part ( $n_{\text{N,odd}} = \frac{n-1}{2}$ ).

## 4.2 Cellular Test Systems

### 4.2.1 Cell Cultivation Procedures

Despite of their diverse origins, all cell types could be cultured in Dulbecco's Modified Eagle's Medium (DMEM) supplemented with 10 % heat-inactivated fetal bovine serum (FBS), and 1 % penicillin (100 U/ml)/streptomycin (100 µg/ml). Inactivation of FBS was achieved by incubation for 30 minutes at 56°C. In the following, accordingly supplemented cell culture medium is termed "complete medium".

Cells were cultured adherently in complete medium in an incubator at 37°C in a humidified atmosphere with 5 % CO<sub>2</sub> in tissue culture flasks of 25 or 75 cm<sup>2</sup>. Cell harvest and passaging was done after reaching 80-90 % confluency by treatment of PBS-washed cells with either trypsin/EDTA or accutase. The addition of 0.5 ml or 1 ml of either of these dissociation reagents, and subsequent incubation for a few minutes at 37°C was applied for cell detachment from either 25 cm<sup>2</sup> or 75 cm<sup>2</sup> tissue culture flasks, respectively.

Accutase is an enzyme-based cell dissociation reagent derived from crustaceans and allows a gentler detachment of adherently growing cells, which yields higher cell viability and improved separation of single cells. The latter is considered advantageous for flow cytometric applications.

### 4.2.2 Flow Cytometric Analysis

In general, flow cytometry enables the simultaneous light-based analysis of multiple physical properties of individual cells in a liquid stream. Distinction of cells is based on their respective optical characteristics. These comprise the relative particle size deduced from forward-scattered light (FSC), relative granularity or internal complexity deduced from side-scattered light (SSC), as well as the relative fluorescence emission intensities for typically up to four defined ranges of wavelengths (FL1 to FL4).

Cells were harvested from cell culture flasks using accutase cell dissociation reagent. Washing the cell pellet twice was accomplished by centrifugation for 1 minute at 800 rpm in a MiniSpin<sup>® plus</sup> lab centrifuge (Eppendorf AG, Hamburg, Germany), removal of the supernatant, and immediate resuspension in ice-cold PBS. Finally, the resuspended cells were filtered through a single layer of TG 100 separating gauze (100 µm pore size, Whatman,

GE Healthcare, Uppsala, Sweden). Cell density was determined by a Countess automated cell counter (Invitrogen, Life Technologies, Darmstadt, Germany) and subsequently set to  $0.5 \times 10^6$  cells/ml in 500  $\mu$ l ice-cold PBS.

Hereafter, cells were again spun down in a laboratory centrifuge (5415R, Eppendorf, Hamburg, Germany) for 1 minute at 800 rpm and, afterwards, resuspended in 490  $\mu$ l of binding buffer (ApoDETECT™ kit – reagent 2, Life Technologies GmbH, Darmstadt, Germany) at room temperature.

A minimum of four samples (S1-S4) was prepared for each cell type: (S1) Unstained control cells, (S2) cells stained with propidium iodide (PI; ApoDETECT™ kit – reagent 3) only, (S3) cells stained with FITC-annexin V (ApoDETECT™ kit – reagent 1) only, and (S4) cells stained with both FITC-annexin V as well as PI.

Annexin V possesses a very high, calcium-dependent binding specificity towards PS and is widely used for membrane PS assessment (Lee et al. 2013; Dong et al. 2009; Kenis and Reutelingsperger 2009; Cichorek et al. 2000; Rao et al. 1992; Tait and Gibson 1992). FITC-conjugation allows high emission intensity fluorescence analysis by flow cytometry or microscopic techniques. FITC can be excited over a broad range with a maximum at about 495 nm. The emission spectrum peak can be found at approximately 519 nm.

For the quantification of cell surface PS-levels, two (S3 and S4) out of four samples per cell type were stained with 10  $\mu$ l of annexin V coupled to the fluorescent dye FITC. After incubation in the dark for 15 minutes at room temperature, all samples were centrifuged again and finally taken up in 475  $\mu$ l of binding buffer. The samples were transferred to FACS tubes, stored on ice and shielded from light until used within the subsequent 2 hours.

Flow cytometry was performed on a BD FACSCalibur™ platform (Becton Dickinson, Franklin Lakes, NJ, USA) operated with the CELLQuest software for data acquisition using instrument settings as given in table 4.1. Immediately prior to sample injection, 25  $\mu$ l of PI solution were added to samples (S2) and (S4) to yield a final concentration of 1  $\mu$ g/ml. PI is an intercalating nucleic acid stain and considered as impermeant to intact cell membranes. Bound to DNA, the fluorescence emission intensity of PI is enhanced about 20- to 30-fold, and its excitation and emission spectrum peaks of about 535 and 617 nm, respectively, allow the simultaneous detection of fluorescein-derivatives such as FITC (Suzuki et al. 1997).

Both FITC as well as PI were excited by an argon-ion laser at 488 nm, and emission intensities were detected simultaneously from 500 to 560 nm and 543 to 627 nm by two distinct detection

channels FL1 and FL2, respectively. Each individual measurement comprised a total count of 10,000 events per sample. Evaluation of raw data was done by the aid of the public-domain tool Flowing Software 2.5.1 (University of Turku, Finland).

**Table 4.1: Standard instrument settings for flow cytometry experiments on a BD FACSCalibur™ platform.** Given are information on parameter-specific voltage set points, signal amplification and scaling modes formatted as requested by the CELLQuest controller software. Experiments conducted comprised analyses of unstained, FITC-annexin V- and/or PI-stained cells. Unless stated otherwise, listed settings applied to all cell lines tested.

Detection	Voltage / V	Amp Gain	Mode
FSC	E-1	6.06	Lin
SSC	260	-	Log
FL1	474	-	Log
FL2 (a)*	412	-	Log
FL2 (b)	443	-	Log
FL3	650	-	Log
FL1A	-	1.00	Lin
FL4	800	-	Log

\* The given set point of FL2 (a) was used for the analysis of HCT116 and HROC107 cells only.

In order to exclude PI-positive (dead) cells from evaluation, cell type-specific gates were set in dot plot displays of FL2 (PI) vs. FSC signals for results from cells stained with PI only (S2). These gates were set manually and kept constant for all experiments and reproductions conducted with the respective cell type.

Histograms of intensity counts from FL1 (FITC-annexin V) signals were created for the initially pre-gated population (see appendix figure A.1). The geometric mean fluorescence intensity (*MFI*) of FITC-annexin V-stained ( $MFI_{\text{FITC}}$  from S3) and unstained control ( $MFI_{\text{control}}$  from S1) cells were deduced from these histograms.

In total, three independent experiments were performed using individual cell preparations. Finally, as a quantitative marker for the cell type-specific level of surface-exposed PS, the quotient ( $Q$ ) of the average  $MFI_{\text{FITC}}$  and  $MFI_{\text{control}}$  was determined. Respective standard deviations  $s_{MFI_{\text{FITC}}}$  and  $s_{MFI_{\text{control}}}$  were considered to calculate the error propagation corrected standard deviation of the quotient ( $s_Q$ ) according to equation 6.2:

$$s_Q = \sqrt{\left(\frac{s_{MFI_{\text{FITC}}}}{MFI_{\text{FITC}}}\right)^2 + \left(\frac{s_{MFI_{\text{control}}}}{MFI_{\text{control}}}\right)^2} \cdot Q \quad (6.2)$$

### 4.2.3 The MTT Metabolic Activity Assay

The water-soluble tetrazolium salt 3-[4,5-dimethylthiazol-2-yl]-2,5-diphenyltetrazolium bromide (MTT) can be reduced, predominantly by reducing equivalents such as NADH, to yield crystalline formazan, whereby the dye undergoes a photometrically traceable color change from yellowish to purple. Hence, the intensity of the color change is a measure for the cell metabolic activity, i.e. viability (van Meerloo et al. 2011; Marshall et al. 1995; Mosmann 1983). Freshly harvested cells (accutase treatment, see above) were counted and suspended in complete medium to a density of  $5.0 \times 10^5$  cells/ml for HROC107 cells or  $2.5 \times 10^5$  cells/ml for all other cell types. Cells were seeded (100  $\mu$ l/well) in a sterile flat-bottom 96-well microtiter plate (Cellstar<sup>®</sup> cell culture plate, Greiner Bio-One, Frickenhausen, Germany) and incubated at 37°C in a humidified atmosphere with 5 % CO<sub>2</sub>. The higher seeding density for HROC107 cells was chosen to take adequate account of the comparably lower growth rate of these cells. After 24 hours, wells of each plate were visually controlled for confluency on a random basis.

Either FBS-supplemented DMEM cell culture medium (“complete medium” 4.2.1) or PBS supplemented with 10 % of complete medium (“PBS/medium”), or any of the buffer variants I-VII as outlined in section 3.7 (see tables 3.9 and 3.8) was used to dilute peptide stocks (1 mM in 0.01 % TFA) to final concentrations of 0.1, 0.3, 1, 3, 10, 30, and 100  $\mu$ M. After washing the confluent cell-covered wells twice with the respective buffer and removal of the supernatant from each cavity, peptide solutions were transferred to the microtiter plate at 100  $\mu$ l/well according to the corresponding method layout. After incubation for 4 hours at 37°C, 10  $\mu$ l of water-soluble MTT (Sigma-Aldrich, Steinheim, Germany) dissolved again in the respective buffer to 5 mg/ml were added to each well, followed by a final incubation for 2 hours at 37°C.

Dye reduction was stopped and formed formazan crystals were dissolved by the addition of 100  $\mu$ l of acidified isopropanol (Roth, Karlsruhe, Germany) containing 10 %v/v Triton X-100 (AppliChem, Darmstadt, Germany) and 0.8 %v/v concentrated hydrochloric acid (Roth, Karlsruhe, Germany) into each well. Repeated rigorous up and down pipetting is needed to quantitatively solubilize all visible crystals to homogeneity. If necessary, any residual air bubbles were removed by a heated sterile disposable steel cannula. Acidification of the solubilizing solution served to keep phenol red, the pH indicator component of DMEM cell

culture medium, in its yellow-colored state, which minimizes the risk of interference, thus, of artificially increased absorbance detection.

Extinction ( $M_{\text{Exp}}$ ) was determined on the microtiter plate reader Tecan infinite M200pro (Tecan, Crailsheim, Germany) at absorbance and reference wavelengths of 570 and 690 nm, respectively. Positive and negative controls were represented by cells incubated under the respective buffer/medium conditions alone ( $M_{100}$ ) or in buffer/medium supplemented with 5 % Triton X-100 ( $M_0$ ), respectively. Calculation of the metabolic activity of the cells (% $M$ ) was done according to equation (6.3):

$$\%M = 100 \cdot \left( \frac{M_{\text{Exp}} - M_0}{M_{100} - M_0} \right) \quad (6.3)$$

Mean  $\text{IC}_{50}$  values, representing the molar peptide concentration at half-maximal cell viability, were derived from the afore-described titration curves by sigmoidal,  $\chi^2$ -reduced Boltzmann's fitting by OriginPro 8 software (OriginLab, Northampton, MA, USA).

#### 4.2.4 Fluorescence Microscopy Analysis of Colorectal Cancer Cells

Partially anticipating the outcome of the aforementioned flow cytometry investigations, HROC24 as well as HROC107 cells treated with fluorescently labeled peptides were subjected to fluorescence microscopy analysis in order to compare peptide effects on CRC cells exposing high or low levels of surface-bound PS, respectively.

For sample preparation, cells were initially cultivated in tissue culture flasks as described above (see section 4.2.1). At a confluency of more than 80 %, the cells were harvested by Accutase treatment, counted and seeded in complete DMEM medium at densities of  $2.0 \times 10^5$  cells/well on glass cover slips (Roth, Karlsruhe, Germany) placed into the cavities of a 24-well plate (TPP, Trasadingen, Switzerland). After incubation for 24 hours at 37°C and 5 %  $\text{CO}_2$  in a humidified atmosphere, the cells were washed twice using 1 ml PBS/well for 5 minutes per step.

Subsequently, the cells were incubated with either PBS including 3  $\mu\text{M}$  Sytox green (control) or fluorescently labeled peptides Rh-NK-2, Rh-C7A-D21K, or Rh-NK11 for up to six distinct periods of time (1, 5, 10, 20, 30, or 60 minutes). Accordingly, peptides were diluted in PBS containing 3  $\mu\text{M}$  Sytox green to yield a finally applied peptide concentration of 10  $\mu\text{M}$ . Sytox

green is a fluorescent nucleic acid stain impermeable to plasma membranes of living cells. Upon impairment of the membrane, e.g. by HDPs, the stain penetrates into the cell and binds nucleic acids with high affinity. DNA-binding leads to a more than 500-fold enhancement of the fluorescence emission intensity, enabling dead cell indication in microscopic analysis.

Immediately after expiration of the respective incubation period, fixation was accomplished well-wise, after two-fold washing with 1 ml PBS, by the treatment with 0.5 ml of 3 % (w/v) paraformaldehyde (PFA; Roth, Karlsruhe, Germany) for 30 minutes. The membrane-permeable fixative PFA covalently cross-links soluble proteins to the cytoskeleton while concomitantly allowing the preservation of the chemical and structural status of each cell as close to the living state as possible (Fox et al. 1985).

Thereafter, the cells of each well were washed again for 3 x 5 minutes with 1 ml PBS per step. The PFA reactivity was quenched by the addition of 1 ml of 50 mM ammonium chloride (Roth, Karlsruhe, Germany) per well for 30 minutes. After another 3 x 5 minutes washing with PBS, each cover slip was mounted in 5 µl of Mowiol solution (Calbiochem®, Merck, Darmstadt, Germany) on a glass microscopy slide (Roth, Karlsruhe, Germany).

Well plates were kept on a tilting shaker during all incubation and washing steps. Finally, all samples were allowed to dry overnight in the dark before being stored at 4°C until analyzed.

### *Cytotoxicity of Rh-labeled peptide variants*

Notably, Rhodamine-related toxicity was checked in control experiments by comparatively treating CRC cells with either labeled or non-labeled peptide variants with concomitant PI-staining for dead cell determination. Resulting differences, if any, revealed Rh-labeled peptides to exhibit a slightly reduced cytotoxic potency.

### *Imaging procedure*

Each individual experiment was conducted independently at least twice using distinct freshly cultured cell preparations. Analysis was performed on an Olympus DP71 fluorescence microscope equipped with appropriate fluorescence and phase contrast objectives. Images were taken by means of the cellSens Entry software provided by the supplier. Of note, after a scheduled annual system maintenance procedure, the exposure times were required to be adjusted for comparability between both cell lines. Manually adjusted exposure settings are summarized by table 4.2.

Motifs were chosen manually to be representative for the conducted experiment. Phase contrast images were taken providing general information on count and morphology of the cells. Additionally, fluorescence images of the same motif were recorded either through a FITC/Cy2- or a Cy3-filter in order to visualize Sytox green- or Rh-staining, respectively. To distinguish between any peptide effects in detail, images were taken using three distinct objectives with internal magnification factors of 10x, 40x and 100x.

**Table 4.2: Adjusted exposure time settings for fluorescence microscopy imaging of distinct CRC cells.** Adjustments were required after scheduled instrument maintenance between both experimental series. Changed exposure time values are delineated by *italics*.

Objective magnification	Channel	Exposure time / ms	
		HROC24 cells	HROC107 cells
10x	Phase contrast	10	10
	FITC channel	1000	<i>500</i>
	Cy3 channel	150	<i>50</i>
40x	Phase contrast	55	55
	FITC channel	300	<i>150</i>
	Cy3 channel	70	<i>40</i>
100x	Phase contrast	350	350
	FITC channel	50	50
	Cy3 channel	10	35

#### 4.2.5 Cell Surface Zeta Potential Measurements

In electrolytic media, the surface charge of a particle in suspension is compensated by counter ions of opposite charge (see figure 4.1). An electrochemical double layer is formed by such counter ions in the outer circumference of the particle. Within a first layer of counter ions, termed Stern-layer, counter ions are associated firmly with the particle surface, while ions of the second, so called diffuse layer, are attached much looser. By this, a gradual decrease of counter ions can be observed. Upon application of an electric field, any charged particle moves towards the electrode of opposite charge to the particle's net-charge. This causes a partial removal of ions in the diffuse layer, while Stern-layer ions move with the particle. The Zeta potential reflects the electrostatic potential at the resulting surface of hydrodynamic shear (slipping plane), and can be followed by measuring the electrophoretic mobility of the moving particle. The slipping plane is defined as the interface between tightly particle-attached ions

and the surrounding medium. The particle velocity is proportionally dependent on the applied field strength and the Zeta potential (Kirby and Hasselbrink 2004).

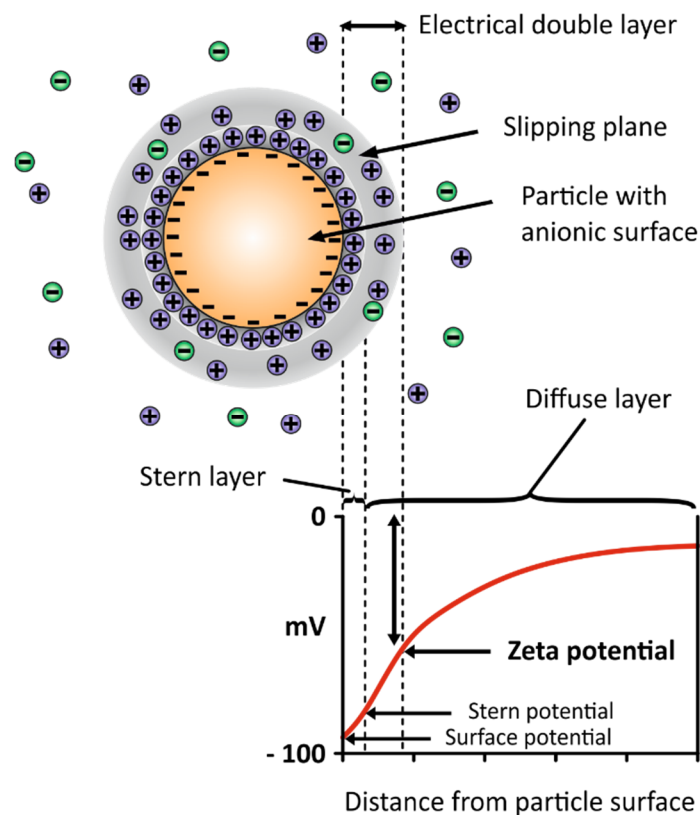


**Figure 4.1: Zeta potential of a charged particle.** Schematically depicted is a negatively charged particle with associated layers of ions in the surrounding medium. Upon particle movement, e.g. in an electrical field, ions outside of the slipping plane are sheared off by the hydrodynamic resistance. The Zeta potential is defined as the potential at the surface of hydrodynamic shear.

Here, individual cells of the distinct human cell lines represented these charged particles, and their Zeta potential was determined in a defined aqueous buffer. In a second approach, cells were sequentially titrated with NK-2-derived peptides or melittin, and the measurement was repeated to elucidate any peptide-induced changes.

For the purpose of sample preparation, cells were harvested using accutase cell detachment solution. Washing was done twice with buffer B by consecutively dissolving the cells in buffer, spinning down on a MiniSpin *plus* centrifuge (Eppendorf, Hamburg, Germany) at  $800 \times g$  for 5 minutes and discarding of the supernatant. Afterwards, the suspension was filtered through TG 100 separation gauze with a pore size of  $100 \mu\text{m}$  (Whatman, GE Healthcare, Uppsala, Sweden). Subsequently, the cells were counted by means of the Countess automated cell counter (Invitrogen, Life Technologies, Darmstadt, Germany), and finally, adjusted to a

density of  $1 \times 10^6$  cells/ml. Prior to the first Zeta potential determination, each sample was further diluted in buffer B to  $2 \times 10^5$  cells/ml.

Filtered and diluted cell samples (1000  $\mu$ l) were titrated with increasing peptide concentrations of 0.1, 0.3, 1, 3, 10, and 30  $\mu$ M and the respective cell surface Zeta potential was determined at 25°C in thoroughly pre-washed and dried folded-capillary cuvettes equipped with gold electrodes (DTS1070) on a Zetasizer Nano ZS (both from Malvern Instruments, Malvern, United Kingdom). Equivalent volumes of 0.01 % TFA served as buffer control. For the purpose of thermal equilibration, cuvette-deposited cell samples were incubated directly within the instrument for 180 or 20 seconds prior to each first or follow-up measurement of a titration series, respectively. The first measurement of each series was done using cell dilutions only, i.e. without peptide addition.

Each individual experiment of a series comprised a six-fold repeated measurement cycle of 20 runs. In accordance with equation 6.4, software-based evaluation of the Zeta potential (Zetasizer Software, Malvern Instruments, Malvern, United Kingdom) was done under the assumption of a Smoluchowski approximation of the Henry's equation; i.e.  $f(\kappa a)$  (Henry's function) = 1.5, which is considered adequate for aqueous solutions or suspensions of particles and moderate electrolyte concentrations:

$$\zeta = \frac{3 \cdot \mu_e \cdot \eta}{2 \cdot \varepsilon \cdot f(\kappa a)} \stackrel{\text{def}}{=} \frac{\mu_e \cdot \eta}{\varepsilon} \quad (6.4)$$

The electrophoretic mobility ( $\mu_e$ ) was determined by laser-Doppler velocimetry (M3-PALS technique) under consideration of input parameters as summarized in table 4.3.

**Table 4.3: Input parameters of the Zetasizer Nano ZS for determining Zeta potentials at 25°C.**

Symbol	Name	Value	Unit
$\varepsilon$	Dielectric constant	78.3	$\text{A s V}^{-1} \text{m}^{-1} = \text{F m}^{-1}$
$\eta$	Solvent viscosity	0.8417	$\text{kg m}^{-1} \text{s}^{-1} = \text{Pa s}$
$RI$	Refractory index	1.331	-

Results are given as mean Zeta potentials with range from experiments performed independently at least twice on separate days using different cell preparations. Of note, due to the marked polydispersity of the analytes, average particle sizes and size distributions could not be determined by the Zetasizer Nano ZS for any cell sample investigated.

## 4.3 Liposome-Based Test Systems

### 4.3.1 Liposome Preparation Procedure

Each lipid was dissolved to 1 mM in chloroform:methanol (3:1 to 2:1) in a flat-bottom glass vial. When required, dissolved lipids were mixed in the respective ratio. Lipid solutions were dried under nitrogen streaming of the liquid surface. The generated lipid film was desiccated overnight to remove traces of organic solvents. The film was rehydrated in appropriate volumes of aqueous buffer A, containing 20 mM HEPES and 150 mM NaCl at pH 7.4, and vortex-mixed for at least 2 minutes to yield multilamellar vesicles. Small unilamellar vesicles were obtained by sonication for 1-3 minutes to clarity on a Branson Sonifier 250 (Branson Ultrasonics, Danbury, CT, USA). To form large unilamellar vesicles the suspension was subjected to three thermocycles by alternately placing it on ice and into a heated water bath (60-65°C) for 30 minutes per step, followed by extruding the thermally treated vesicle solution 19-times through a polycarbonate filter membrane (0.1 µm pore size; Nucleopore, GE Healthcare, Uppsala, Sweden) by the aid of an Avanti® Mini-Extruder (Avanti Polar Lipids, Alabaster, AL, USA). Liposome preparations were stored at 4°C in the dark until used.

### 4.3.2 Particle Size and Surface Zeta Potential Determination

Liposome stock solutions, prepared according to the standard procedure (see section 4.3.1), were initially diluted in ultrapure water and/or buffer A to a total volume of 1000 µl in order to adjust (i) the lipid concentration to ~50 µM, and (ii) the overall sample conductivity to 1.05 to 1.45 mS/cm. Diluted liposome samples were sequentially treated with increasing peptide concentrations of 0.1, 0.3, 1, 3, 10, and 30 µM. After each titration step, a particle size measurement was performed, immediately succeeded by a Zeta potential determination. The average particle size was assessed based on dynamic light scattering (DLS). Particles in solution or suspension are persistently undergoing Brownian motion. As a consequence, time-dependent fluctuations in the intensity of scattered light occur. Analytical interpretation of these intensity fluctuations allows the determination of the diffusion coefficients of the particles and the subsequent deduction of a size distribution (Nitzsche and Simon 1997).

Here again, all experiments were carried out on a Zetasizer Nano ZS with preset input parameters as defined in table 4.3, and were performed at 25°C in folded-capillary electrophoresis

cuvettes. Prior to each first measurement, a given sample was incubated for 180 seconds within the instrument for thermal equilibration. In between of the coupled size and Zeta potential determinations, as well as after each titration step, the measurement was prefaced by another 20 seconds of incubation.

Results of liposomal size determinations are given as the average vesicle diameter calculated as the arithmetic mean (z-average) with range from at least two independent preparations. Each single measurement enclosed a 12-fold size determination and was automatically assessed by the cumulant analysis tool provided by the manufacturer's software. Of note, as a quality marker, the polydispersity index (PDI) of each single measurement was monitored. In the context of Zetasizer-based experiments, the PDI is a dimensionless correlative measure of the distribution width for a recorded set of intensity signals, thus, particle sizes. By definition, the PDI can range from 0 (ideal monodisperse, or uniform) to 1 (broad distribution of data, without deducible correlation). Results associated with a PDI > 0.5 were excluded from further analysis.

The Zeta potential measurements of liposome preparations, performed immediately subsequent to each particle size determination, were done in analogy to the respective measurements on eukaryotic cells with identical input parameter settings (see section 4.2.5).

### **4.3.3 Probe Dilution Förster Resonance Energy Transfer Experiments**

A fluorescent probe dilution assay was performed in order to investigate peptide intercalation into phospholipid liposomes by so called Förster Resonance Energy Transfer (FRET) spectroscopy. Upon excitation of a fluorophore (donor) the process of resonance energy transfer to another molecule (acceptor) can occur if the emission spectrum of the former overlaps the absorption spectrum of the latter (Förster 1948). The transfer takes place without the appearance of an intermediate photon but by dipole-dipole interactions of the donor-acceptor pair (FRET pair). Besides the relative orientation of donor and acceptor transition dipoles, the efficiency of the transfer is dependent on the extent of the spectral overlap and, especially, on the distance between donor and acceptor molecules. Here, NBD- (donor dye) and Rhodamine-labeled (acceptor dye) labeled phosphatidylethanolamine (PE) served as a FRET pair.

Liposomes used were composed of either natural L- $\alpha$ -PC only, or a 90:10 mixture of L- $\alpha$ -PC and -PS, or L- $\alpha$ -PS only. During liposome preparation, lipid-conjugated FRET pair dyes were

introduced by the inclusion of 1 mol-% each of NBD-PE and Rh-PE. The total lipid concentration was 1 mM (see section 4.3.1). Preceding a measurement, liposome samples diluted 1:100 in buffer A (10  $\mu$ M) were equilibrated at 37°C in a thermostat (Haake F3; Thermo Fisher Scientific, Braunschweig, Germany) for several minutes.

All FRET experiments were conducted at 37°C on a SPEX-III Fluorolog spectrofluorometer with dual-channel detection (SPEX Industries, Edison, NJ, USA). Precision quartz cuvettes of type 109.000F-QS (Hellma Analytics, Müllheim, Germany) with a 10 mm light path were used for all FRET experiments. A miniature magnetic rod allowed continuous stirring of samples within the measurement chamber of the Fluorolog instrument, which is equipped with an appropriate rotating magnetic field. Donor-specific excitation was achieved at 470 nm with fixed slit width of 1 mm. Initially, apertures of emission paths I and II for donor and acceptor detection, respectively, were set manually to achieve ~200,000 counts per second. The fluorescence intensities of donor ( $I_D$ ) and acceptor ( $I_A$ ) were followed simultaneously over time at 531 nm and at 593 nm, respectively. After 50 seconds, a peptide sample was added from 100  $\mu$ M stocks (in 0.01 % TFA) to reach final concentrations of either 0.2, 0.4, or 0.8  $\mu$ M, and the signal was continuously recorded for another 250 seconds. Negative controls were measured after addition of 0.01 % TFA instead of peptide at a volume equivalent to a peptide molarity 0.8  $\mu$ M. All experiments were done at least in duplicates.

The equilibrium distribution of NBD- and Rh-coupled lipids throughout the liposomal membrane results in a steady state-like signal according to the average donor-acceptor distance. Upon addition and subsequent intercalation of peptide molecules, the mean distance between the two fluorophore species increases. The resulting decrease in the average spatial proximity of donor and acceptor dyes was followed as the ratio of their respective emission intensities ( $I_D/I_A$ ). This ratio is termed “FRET signal” in the following.

For quantitative evaluation, the arithmetic mean of the experimentally achieved level of FRET signal ( $F_{Exp}$ ) was calculated as percent increase ( $\%F$ ) compared to the mean FRET signal during the equilibration phase ( $F_0$ ) according to equation 6.5:

$$\%F = 100 \cdot \left( \frac{F_{Exp}}{F_0} \right) \quad (6.5)$$

Time frames of at least 30 seconds were included in the determination of the respective mean values.

#### 4.3.4 Measurement of Intrinsic Tryptophan Fluorescence

Tryptophan (Trp) fluorescence experiments were conducted in order to characterize peptide-membrane interactions in terms of peptide intercalation depth and, regarding NK-2, also molecular orientation.

The aromatic amino acid tryptophan is a fluorophore whose wavelength at maximum emission intensity is highly sensitive to changes in the polarity of its solvent surrounding. Hence, tryptophan fluorescence can be used as a highly sensitive intrinsic hydrophobicity probe. In case a distinct tryptophan-bearing part of a peptide is completely surrounded by an aqueous phase, its emission intensity maximum typically occurs at a specific wavelength around 350 nm. However, when the same tryptophan residue is located in a hydrophobic environment, for example upon integration into the core of a phospholipid membrane, the emission wavelength maximum of the fluorophore shifts to a lower value (see figure 4.2). Therefore, this phenomenon is called *blue shift* and is well-established as a measure for the degree of intercalation of tryptophan-bearing peptides into biomembranes (Lakowicz 2006, pp. 529-576).

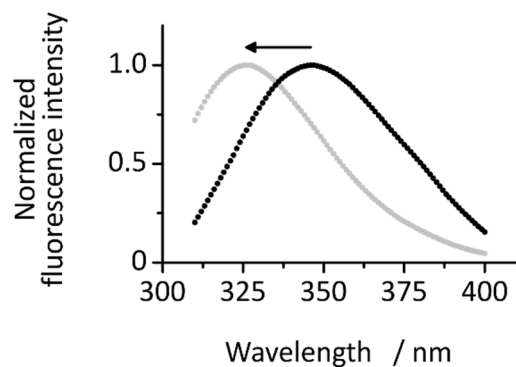


**Figure 4.2: Exemplary representation of a blue shift phenomenon.** Depicted are normalized fluorescence emission spectra of the single-Trp peptide F14W in buffer (black) and subsequent to incubation with liposomes made of natural phosphatidylserine (grey) recorded after excitation of the intrinsic tryptophan residue at 295 nm. Upon membrane intercalation of the respective residue, the wavelength at maximum emission intensity shifts to lower values (blue shift) as indicated by the arrow.

Three distinct single-Trp variants of NK-2 as well as the natural single-Trp peptide melittin served as test objects. The NK-2 derivatives are termed I2W, F14W, and G25W with amino acid residue substitutions to tryptophan in close-to-amino-terminal (Ile-2), mid-structure (Phe-14) and close-to-carboxy-terminal (Gly-25) positions, respectively (see figure 4.3). For each measurement, stocks of each peptide (1 mM in 0.01% TFA) were freshly diluted in buffer A to reach a final concentration of 250  $\mu$ M. Preparation of extruded unilamellar liposomes (1 mM) was performed according to the standard protocol (see section 4.3.1). Lipid compositions were chosen to roughly mimic membranes of pathologically modified (PC:PS = 80:20, 50:50, and PS only) and healthy eukaryotic cells (PC only).

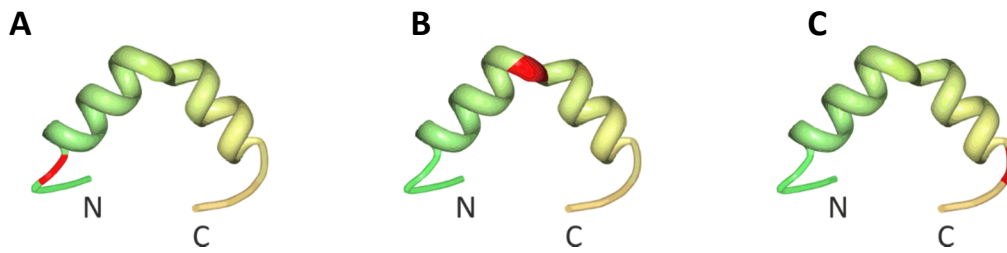


**Figure 4.3: Three distinct single-Trp variants of parent peptide NK-2.** The position of the introduced tryptophan residue was indicated in red color for peptides I2W (A), F14W (B), and G25W (C), respectively. The underlying ribbon model represents residues 39 to 65 of the originating NK-lysin structure referring to the Protein Database record 1NKL (Liepinsh et al. 1997), and was created and modified using Protein Workshop (Moreland et al. 2005).

Tryptophan fluorescence experiments were conducted in all-black, flat-bottomed 96-well microtiter plates (Nunclon; Greiner Bio-One, Frickenhausen, Germany). Measurements were performed at 37°C on a Tecan infinite M200pro fluorescence microtiter plate reader (Tecan, Crailsheim, Germany) controlled by the provided Magellan® software. The bandwidth of the excitation double monochromator was lower or equal to 5 nm, while the emission bandwidth was fixed to 20 nm. The latter required the minimum difference between excitation and emission wavelength to be  $\geq 25$  nm.

The total volume per well was set to 100  $\mu$ l comprising liposome pre-dilutions (87  $\mu$ l), peptide stock solutions (8  $\mu$ l), and demineralized water (5  $\mu$ l). Peptides were added from 250- $\mu$ M-stocks to liposomes pre-diluted in buffer A to yield final well concentrations of 20  $\mu$ M and 300  $\mu$ M, respectively, resulting in a peptide-to-lipid ratio of 1:15. After addition of all components, the microtiter plates were shaken for 10 seconds and subsequently incubated at 37°C within the plate reader for 5 minutes. This shaking and incubation step was repeated once. Measurements were carried out after another shaking step and further 5 minutes of incubating the plate.

Excitation was done at 280 nm and emission spectra were recorded from 310 to 400 nm at a step width of 1 nm, averaging ten reads per data point (called “no. of flashes”).

Resulting raw data were corrected for the contribution of light scattering in the presence of vesicles, i.e. blank reduction (spectra of liposomes in buffer served as blanks). Blank reduced raw data were then exported and post-processed well-wise by MATLAB software (version R2014a (8.3.0.532), MathWorks Inc., Natick, MA, USA) with a Savitzky-Golay smoothing algorithm using a 2<sup>nd</sup> order polynomial filter function and a filter window frame size of 21 nm (see appendix figure A.2). As a rule of thumb, for single-peak Gaussian-like spectrum

data, smoothing frame size should be less than peak width at half maximum (Savitzky and Golay 1964).

All experiments were done in duplicates and performed independently at least twice using individually prepared liposomes and peptide dilutions. Smoothed spectra of each run were used to extract the respective wavelengths at highest emission intensity. For the calculation of the blue shift ( $BS$ ), the mean value of all recorded wavelengths at maximum emission intensity of a given peptide incubated in the presence of defined liposomes ( $\lambda_{\max, \text{peptideX, liposomeY}}$ ) was subtracted from the mean maximum wavelength of the respective peptide in buffer alone ( $\lambda_{\max, \text{peptideX}}$ ):

$$BS_{\text{peptideX, liposomeY}} = \lambda_{\max, \text{peptideX}} - \lambda_{\max, \text{peptideX, liposomeY}} \quad (6.6)$$

The error of the blue shift ( $s_{BS_{\text{peptideX, liposomeY}}}$ ) was calculated according to equation 6.7:

$$s_{BS_{\text{peptideX, liposomeY}}} = \sqrt{\left(s_{\lambda_{\max, \text{peptideX}}}\right)^2 + \left(s_{\lambda_{\max, \text{peptideX, liposomeY}}}\right)^2} \quad (6.7)$$

### 4.3.5 Potassium Iodide Fluorescence Quenching

Quenching in terms of fluorescence spectrometry generally describes the diminishing of detectable fluorescence intensity due to various influences. When a fluorophore in the excited state is deactivated upon contact with another molecule in solution, the occurrence is referred to as collisional or dynamic quenching and the deactivating molecule is named a quencher. Halogens, such as iodide ( $I^-$ ), as well as heavy atoms, acrylamide or oxygen may all act as quenchers, yet the exact mechanism of interaction varies with the fluorophore-quencher pair. The decrease in fluorescence intensity can occur due to electron transfer, spin-orbit coupling or intersystem crossing to the triplet state between such pairs. This diffusion-dependent molecular collision phenomenon is the most common type of quenching effect. Apart from this, quenchers may form non-fluorescent complexes with fluorophores. This process is frequently termed static quenching as it can already occur in the energetic ground state. Both, dynamic as well as static quenching mechanisms require close spatial proximity between quencher and fluorophore. The internal conversion of light absorbed by a fluorophore into

vibrational and/or thermal energy can also decrease the intensity of emitted fluorescence. Finally, some non-molecular effects such as high optical densities or changes in the system temperature may cause signal quenching effects. (Lakowicz 2006, p. 11-18; Bu et al. 2004)

For the here-described assay, potassium iodide (KI) was deployed as a quencher well-soluble in aqueous surroundings. In general, KI-induced decreases in the fluorescence emission intensity are reversible via removal of the quencher molecules. To avoid the risk of I<sub>2</sub> formation, which could interact e.g. with nonpolar membrane regions, sodium thiosulfate (Na<sub>2</sub>S<sub>2</sub>O<sub>3</sub>) was added as a reducing agent to the quencher stock solution (7 M KI, 3.5 mM Na<sub>2</sub>S<sub>2</sub>O<sub>3</sub>, pH 8.55). Of note, buffer A contains 150 mM NaCl, which is necessary in order to maintain a constant ionic strength in the presence of I<sup>-</sup> (Lakowicz 2006, p. 290).

In principle, liposomes of PC and PS at equal shares were prepared according to the procedure given in section 4.3.1 with the following alterations: For the purpose of fluorescence labelling, the lipid mixtures enclosed 1 mol-% NBD-PE (Molecular Probes, Eugene, OR, USA), and the liposomes remained non-extruded subsequent to sonification and thermocycling. All measurements were carried out in 101-QS precision quartz cuvettes (Hellma Analytics, Müllheim, Germany) at 37°C on the SPEX-III Fluorolog spectrometer (SPEX industries, Edison, NJ, USA). Excitation was done at 470 nm with the excitation path aperture fixed at 3 mm, while the emission slit width was manually adjusted to set the starting intensity to approximately 200,000 counts per second. The samples were continuously stirred within the instrument as described before.

At first, each sample contained a 1:100 dilution (in buffer A) of the liposome stock solution, and its emission intensity was recorded for approximately 100 seconds until a stable signal was reached. In a second step, the quencher solution was injected to yield final concentrations of KI and Na<sub>2</sub>S<sub>2</sub>O<sub>3</sub> of 800 mM and 0.4 mM, respectively. A decrease in fluorescence intensity becomes detectable resulting from the iodide-induced quenching of fluorophore molecules in the outer leaflet of the liposomal membranes. For the following 400 seconds, the system was allowed to reach a steady state level ( $I_0$ ). The residual fluorescence emission is caused by NBD-groups in the liposomal inner membrane leaflet, where the fluorophores are inaccessible for the membrane-impermeant quencher molecules. Hereafter, peptides were added from stock solutions (1 mM in 0.01 % TFA) to yield a molar concentration of 3 μM (NK11) or 1 μM (all other peptides), and putative signal changes ( $I_{\text{peptide}}$ ) were recorded for about

100 seconds. In a last step, Triton X-100 was added to ensure complete membrane disintegration and to achieve the level of maximum fluorescence quenching ( $I_{100}$ ).

In order to assess any buffer-related influences, reference spectra were recorded for each experimental run after adding an equivalent amount of buffer A instead of quencher solution to the liposome sample ( $I_{\text{buffer}}$ ). In general, the arithmetic mean of steady-state fluorescence emission intensities were used for evaluation. Equation 6.8 was used to determine the percent quenching as the difference in the relative emission decreases induced by peptide addition or control treatment (buffer). Final results were calculated as the mean with standard deviation from three independent experiments conducted using a minimum of two individual liposomal preparations in total.

$$\begin{aligned} \% \text{ Quenching} &= \% \text{ KI-induced quenching} - \% \text{ Buffer-induced quenching} \\ \Rightarrow \% \text{ Quenching} &= \frac{(I_0 - I_{\text{peptide}})}{(I_0 - I_{100})} \cdot 100 \% - \frac{(I_0 - I_{\text{buffer}})}{(I_0 - I_{100})} \cdot 100 \% \end{aligned} \quad (6.8)$$

#### 4.3.6 Dye Release Test

Calcein is a membrane-impermeable fluorescent dye with well-defined excitation and emission wavelength maxima at around 495 nm and 515 nm, respectively. The exact characteristics of calcein fluorescence are dependent on various conditions, e.g. buffer composition, pH, and temperature. At high molar concentrations of  $\geq 20$  mM, the calcein fluorescence emission intensity decreases due to collisional quenching mechanisms, i.e. self-quenching (Horobin 2002, p. 249). The release of calcein from the internal volume of a liposome leads to the dilution of the dye in the surrounding buffer. The resulting dequenching of the fluorescence can be followed as the increase in the detected emission intensity.

In principle, liposomes made PC and PS at equal shares were prepared according to the general procedure given in section 4.3.1. Modifications to the standard protocol were as follows: Dried and desiccated lipid films were rehydrated in 288  $\mu\text{l}$  of buffer *IN* including 5 mg, i.e. 28 mM, of calcein (Sigma-Aldrich, Steinheim, Germany) and 20  $\mu\text{l}$  of 1 M NaOH, and dissolved by thorough vortexing. After ultra-sonification to clarity and thermocycling according to the standard protocol, another 262  $\mu\text{l}$  of buffer *IN* were added, followed by regular extrusion. For buffer exchange and separation of lipid vesicles from non-encapsulated

calcein, extruded samples were applied to a PD MidiTrap G25 column (GE Healthcare, Uppsala, Sweden) pre-equilibrated with buffer *OUT*. After sample application, elution was done by the stepwise addition of buffer *OUT* and equivolume fraction collection in Eppendorf cups. Fractions containing calcein-encapsulating liposomes in a close-to-calcein-free solvent surrounding were identified by fraction-wise analysis of average particle diameters and Zeta potentials as well as UV absorption measurements.

Calcein release tests were performed in half-micro UV cuvettes (VWR International, Hannover, Germany) on an RF-5301 PC spectrofluorometer (Shimadzu Deutschland, Duisburg, Germany) controlled by Panorama Fluorescence 2.1 software provided by the manufacturer. The instrument uses a xenon lamp of 150 W as light source and a photo-multiplier (R3788-02) for detecting fluorescence emission at right angle relative to the excitation beam. Excitation and emission detection were done at 495 and 513 nm, respectively, with bandwidths set to 3 nm.

Each sample enclosed liposomes diluted 1:200 in buffer *OUT* to a total volume of 1000  $\mu$ l. Signals were recorded at an interval of 1 measurement/second. At first, a baseline was recorded for diluted liposomes only. After not less than 90 seconds, peptide solution was added and distributed rapidly by repeated inversion of the parafilm-sealed cuvette. Peptides were added from stocks (1 mM in 0.01% TFA) to adjust the final peptide concentration to either 0.3  $\mu$ M or 3  $\mu$ M (NK11 only). Subsequent changes in the calcein fluorescence were recorded for up to 10 minutes before finally dissolving remaining lipid vesicles by the addition of 10  $\mu$ l of Triton X-100 from a buffer-diluted stock to set the detergent concentration to 0.2 %v/v.

Emission intensities recorded within 10 seconds after Triton addition were averaged and represented the level of 100 % dye release ( $R_{100}$ ), while the mean fluorescence emission within the last 20 seconds prior to peptide application were considered to reflect the 0 % level of calcein release ( $R_0$ ). The percentage of calcein release (% $R$ ) was calculated according to equation 6.9, as a quantitative measure for peptide-induced membrane permeabilization.

$$\%R = 100 \cdot \left( \frac{R_{\text{peptide}} - R_0}{R_{100} - R_0} \right) \quad (6.9)$$

Whereby  $R_{\text{peptide}}$  represents the mean fluorescence intensity over a period of at least 20 seconds after any peptide-induced signal change had reached a steady-state plateau.

## 5 RESULTS

### 5.1 Peptide Characterization

#### 5.1.1 Peptide Design

All NK-2-derived peptides used in the scope of this thesis have been designed based on rational considerations, as stated above. This ensemble of structural NK-2 variants comprised single- and multiple-residue substitution variants, as well as several shortened variants with C-terminal, N-terminal and intrasequential omissions of (consecutive) residues. Also combinations of substitutions and shortenings have been realized. In total, sequence lengths varied between 10 to 27 amino acid residues.

The helical wheel plots given in figure 5.1 schematically depict cross sections of the amino acid distribution within a presumed continuous  $\alpha$ -helical conformation of peptide NK-2. In addition, the specific sites and substituents of all single-residue modified variants as well as exemplary alterations in shortened NK-2 derivatives are indicated.

Obviously, most single-residue modifications were realized within the predominantly hydrophobic face of the helical cross section. Special emphasis laid on two distinct alterations regarding positions 7 and 21. On the one hand, the single free thiolate group of Cys-7 is anticipated to be prone to oxidation-related stability issues and putatively promotes peptide dimerization. The replacement of this non-functional cysteine by either alanine (e.g. C7A), leucine (C7L), or serine (e.g. C7S) could avoid such issues and concomitantly preserve the degree of polarity of the hydrophobic helix face. On the other hand, the negative charge of Asp-21 reduces the peptide's cationic net charge, while it additionally contradicts the overall amphipathic helix profile due to its anticipated localization within the hydrophobic cross-sectional moiety. An exchange of Asp-21 to lysine (D21K) enhanced the net positive charge by +2 to +12, while the alternative substitution to leucine (D21L) yielded a net charge of +11 and enlarged the size of the peptide's hydrophobic arc referring to the helical cross-section. Following a similar rationale, another single residue alteration comprised the replacement of the positive charge of either Arg-4 or Arg-17 by hydrophobic leucine (R4L, R17L). The introduction of a single tryptophan residue at three distinct intramolecular positions of NK-2 (I2W, F14W, and G25W) enabled fluorescence spectrometry-based investigations on peptide-membrane interactions. Moreover, changing the single methionine residue (Met-11) to leucine

could avoid potential detrimental consequences of oxidation to methionine sulfoxide, and concomitantly retains a similar hydrophobicity at this position. Variants like C7A-D21K and C7A-M11L-D21K combine also multiple substitutions in their sequence.

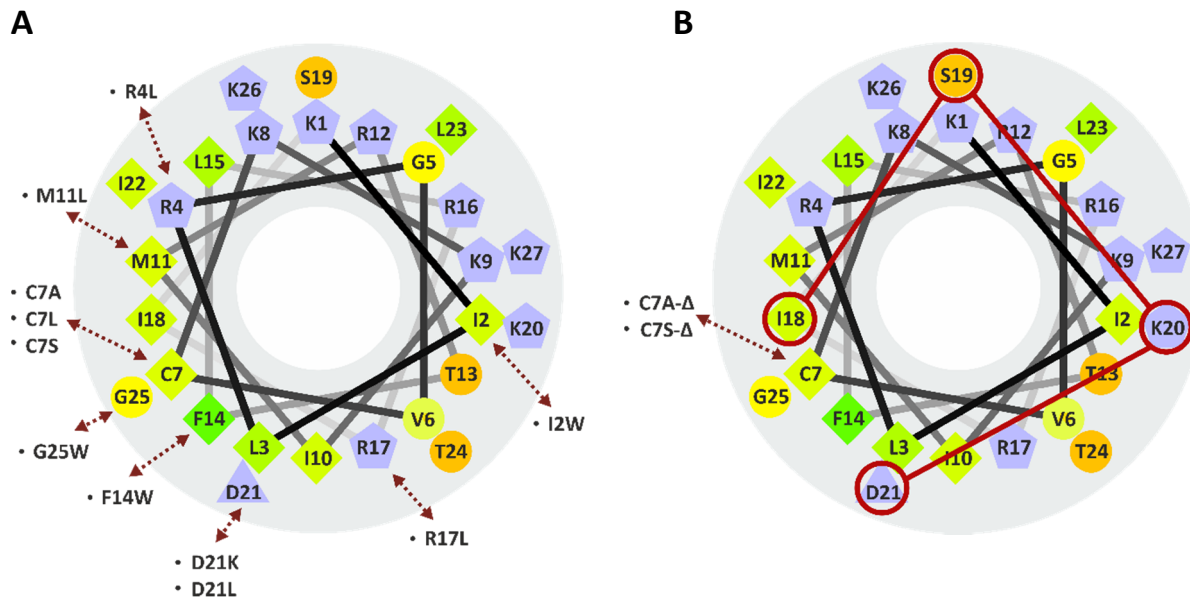


**Figure 5.1: Helical wheel plots of peptide NK-2 and exemplified structural modifications.** Symbol- and color-coding is compliant with figure 2.5. Hydrophobic residues (diamonds) were coded green, with pure green representing the most hydrophobic residue and the intensity of green decreasing proportionally to the hydrophobicity. Hydrophilic non-charged residues (circles) are coded orange. Glycine is coded in yellow reflecting the level of about zero hydrophobicity/hydrophilicity. Residues being charged under physiological conditions were colored in light purple, with triangles and pentagons reflecting acidic and basic residues, respectively. Moreover, in (A), the sites of amino acid residue exchanges were marked by red-dotted double arrows for several single-substitution variants of NK-2, each one named either according to the respective modification. Additionally, (B) representatively depicts the omission of four consecutive residues from positions 18 to 21 (red lines and circles). The underlying helical wheel plots were modified after creation with the web-based calculation tool introduced before (web source, Armstrong and Zidovetzki 2015).

As a second class of sequence modifications, also distinct peptide shortenings were realized by different means. In consideration of the parent structure of NK-2, such alterations basically followed the premise to exert limited and defined impacts on the charge and hydrophobicity patterns of the resulting sequence. A first approach was the deletion of four consecutive residues at distinct positions (e.g. C7A-Δ, NK23a, NK23b, and C7S-Δ). By this approach, a stretch of residues matching approximately the size of one helical turn (~3.6 residues) was omitted, thus, a minimal disturbance of the overall amphipathic helix profile was expected. Other shortened variants feature the deletion of one or more carboxy- and/or amino-terminal residues. This is exemplified by derivative I10 representing the overlapping ten amino acid

residues of variant C20, comprising the 20 C-terminal residues of NK-2, and N17, enclosing the N-terminal 17 residues of variant C7S. Finally, also extensive shortenings of the parent structure were realized by the omission of multiple helical turn segments. Peptide NK11, for instance, misses overall four of such 4-residue-stretches, resulting in an amino acid sequence of only eleven residues.

### 5.1.2 Sequence- and Structure-Inherent Peptide Properties

For all NK-2 variants a range of physicochemical properties was calculated by the aid of the Profilegraph software tool. Assuming a physiological pH value, determined parameters enclosed each peptide's molecular net charge ( $Q$ ), mean hydrophobicity ( $H$ ), as well as the average and local maximum hydrophobic moments ( $\mu H$ ). Moment calculations were initially done over a sliding window of 7 amino acid residues. All determined values are summarized in table 5.1 and displayed together with each peptide's amino acid sequence, the total residue count ( $n$ ), the mean charge per residue ( $Q/n$ ), as well as the ratio of hydrophobicity to net ( $H/Q$ ) and average residual charge ( $H/(Q/n)$ ). All properties were additionally calculated for each peptide's amino- and carboxy-terminal sequence moieties. Correspondingly determined values are tabulated in the supplemental to this thesis (appendix table A.2), while a visual overview on all calculated results is given in the box plot representations of figure 5.2. Out of this overall rather extensive information, without discussing each data set in detail, several findings of general relevance could be emphasized. Of note, statements made in the following primarily address NK-2 and its variants. Intentionally, the results for the non-NK-2-related reference peptide melittin will be put into context subsequently.

As a first striking feature, the net charges of all NK-2-derived peptides varied markedly from +6 to +12, well-reflecting both their generally polycationic, yet versatile charge-related nature. Moreover, an about equivalent contribution of the N- and C-terminal sequence parts to the overall peptide's net charge could be deduced. Furthermore, fluctuations of the net charge correlated roughly with the length of the amino acid sequence ( $n$ ), which could be demonstrated for the complete sequence itself as well as for the N- and C-terminal moieties. Consequently, the average portion of net charge per residue,  $Q/n$ , was found to span a quite consistent range of values in all sequence parts, and ranged between a minimum and maximum of +0.23 and +0.63, respectively.

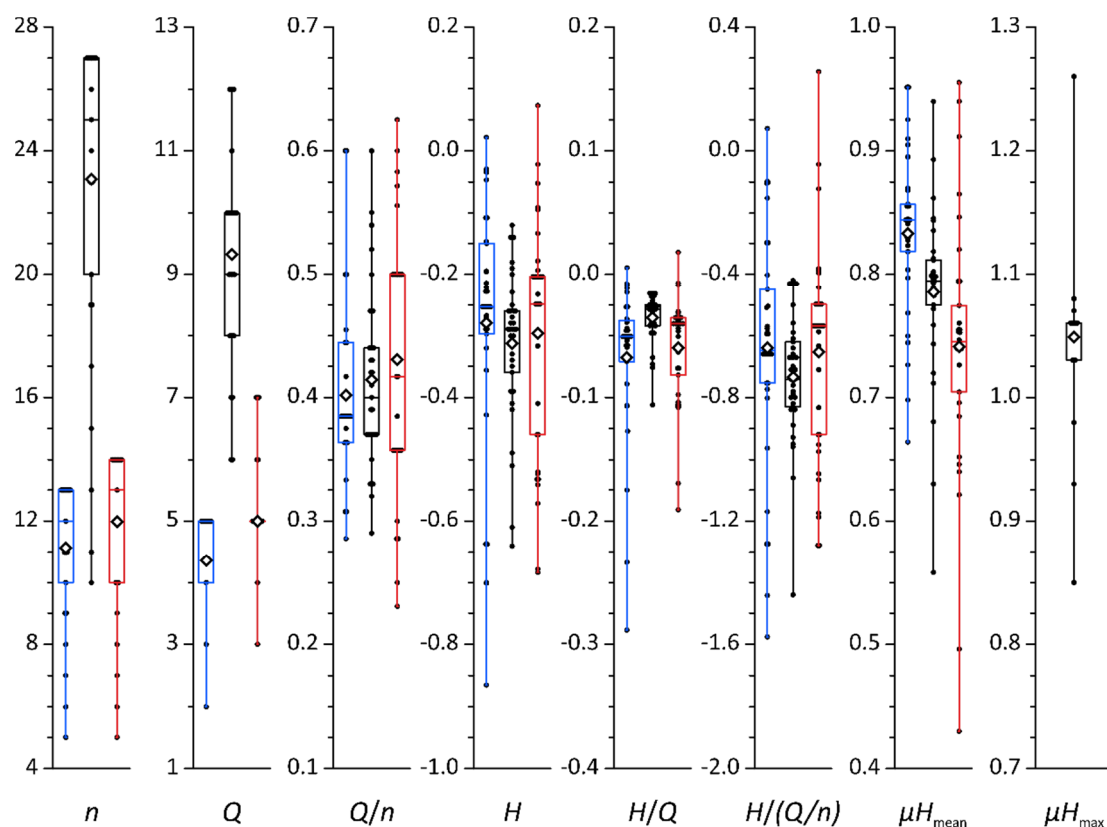


**Figure 5.2: Value distribution of calculated peptide properties.** All parameters were calculated assuming a physiological pH and under consideration of Eisenberg’s Normalized Consensus scale. The box plot representations display the distribution of each set of parameters determined over the full sequence length (black lines), as well as separately for amino-terminal (blue lines) and carboxy-terminal (red lines) segments. The top and bottom horizontal lines of each box frame reflect the upper and lower quartiles of the distributions, respectively. The median is delineated by an additional horizontal line and the arithmetic mean is represented by a black open diamond symbol. Bars span maximum and minimum values, respectively.

According to the underlying Normalized Consensus scale, the mean hydrophobicity ( $H$ ) of an arbitrary sequence of amino acid residues could theoretically adopt values from  $-2.53$  (arginine) to  $+1.38$  (isoleucine). For the investigated set of peptides,  $H$  values were found to vary between  $-0.64$  (I10) up to the highest full-sequence average of  $-0.12$  (NK-2-KKK), reflecting an overall rather intermediate to low mean hydrophobicity. In despite, individual contributions from terminal segments were more versatile, ranging from  $-0.87$  for the N-terminal part of peptide NK11 to  $+0.07$  for the C-terminal sequence of R17L. Regardless of this versatility, extrema in one moiety are in many cases apparently balanced out by the complementary segment leading to comparably narrow distributions of the overall  $H/Q$  and  $H/(Q/n)$  values. The strong linear interdependency of  $H$  and  $Q/n$ , substantiated by figure 5.3, is a consequence of the rationale-based design of the NK-2 derivatives in the course of which the proportion between charged and hydrophobic residues was intentionally kept in balance.

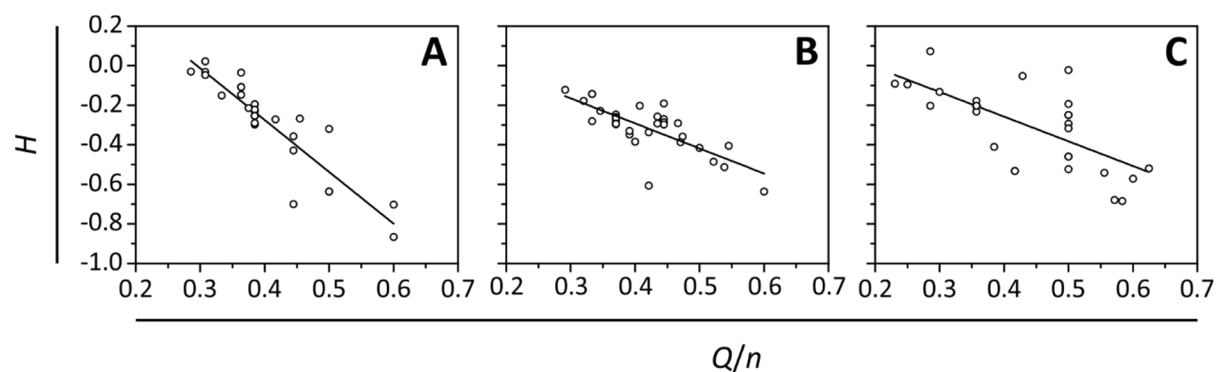


**Figure 5.3: Linear interdependency of the peptide hydrophobicity and the mean charge per residue .** The average hydrophobicity ( $H$ ) and the mean charge per amino acid residue ( $Q/n$ ) were calculated for each peptide's full length sequence (B) as well as individually for the N-terminal (A) and C-terminal (C) segments. The proportionality of both parameters is reflected by linear fittings.

As a measure of the amphipathicity in a presumed  $\alpha$ -helical peptide conformation, hydrophobic moments ( $\mu H$ ) were initially calculated considering complete peptide sequences only. This was done because the 7-residue sliding window underlying the respective calculations is not appropriately applicable if windows overlapping both terminal moieties would have been skipped in the first place. Nevertheless, hydrophobic moments were averaged ( $\mu H_{\text{mean}}$ ) also for notionally separated amino- and carboxy-terminal segments. A detailed overview on the calculated moments is given in table 5.2.

Overall, the full-sequence  $\mu H_{\text{mean}}$  values ranged from 0.56 to 0.94, which basically pointed at a pronounced amphiphilic character of the peptides in general. This tendency is underpinned by the observed local maximum hydrophobic moments ( $\mu H_{\text{max}}$ ), identifying the stretch of two consecutive helical turns of highest amphipathicity. Even variant NK11, the peptide of lowest average hydrophobic moment ( $\mu H_{\text{mean}}(\text{NK11}) = 0.56$ ), possesses a 7-residue window of marked amphipathicity with  $\mu H_{\text{max}}$  of 0.85. In total,  $\mu H_{\text{max}}$  adopted values between 0.85 (NK11) and 1.26 (NK19b-KR). However, 29 peptides featured a  $\mu H_{\text{max}}$  between 1.03 and 1.08, with a remarkable 22-fold occurrence of a maximum value of 1.06 in 20 different peptides. Of note, variants M11L and C7A-M11L-D21K were the only peptides with two windows of identical maximum amphipathicity, with a consistent localization at positions 13 and 17 (of 27). The abundance of this repeatedly found maximum hydrophobic moment value could be primarily assigned to the amino acid motif FLRRISK. This composition is a strongly amphipathic pairwise combination of hydrophobic (phenylalanine, leucine, isoleucine) and charged (arginine, lysine) residues, and obviously highly conserved within the set of NK-2 derivatives. With regard to the double-maximum derivatives mentioned above, the methionine-to-leucine ex-

change at position 11 apparently yielded another stretch of similar amphipathicity (ILRTFLR). Yet, apart from the overall high average amphipathicity, a remarkable gradual decline in the hydrophobic moment was observed between the mid-structural part and the C-terminus for most peptide variants. The minimum hydrophobic moments ( $\mu H_{\min}$ ) were frequently found to be as low as about 0.24, and were predominantly associated with the rightmost calculation windows. It could be inferred from the amino acid sequence of the corresponding windows that this minimum amphipathicity is mainly caused by the stretch of four adjacent non-charged residues ILTG spanning more than one helical turn (~3.6 residues). By contrast, the N-terminal peptide moieties basically feature a rather even distribution of high amphipathicity. An exception to this tendency is observed only with variants R4L and C7A-K8L-D21K, where the exchange of a basic residue (Arg-4 and Lys-8, respectively) to hydrophobic leucine again yielded non-charged 4-residue segments obviously perturbing the amphipathicity in the surrounding region.

Expectedly, the analysis of the non-NK-2-related reference peptide melittin led to an entirely divergent set of values. Exemplarily, in direct comparison to NK-2 (+0.37), melittin possesses a markedly reduced  $Q/n$  ratio of +0.23, as it is similarly large (26 versus 27 residues), but has a lower net charge of +6 instead of +10. Besides, four of melittin's five positively charged amino acid residues are clustered at positions 21 to 24, which is in close proximity to the additionally amidated C-terminus. Consequently, the amino-terminal peptide segment featured a strong mean hydrophobicity of +0.55 and a  $H/(Q/n)$  ratio of +7.18. Among all investigated peptides, melittin's amino acid sequence was the only one with a positive average hydrophobicity  $H$  of +0.10. Moreover, the determined mean and maximum hydrophobic moments of melittin were comparably low adopting values of 0.43 and 0.80, respectively.

Altogether, the conclusions drawn from the conducted software-assisted peptide property determinations underpin the apparent use of the applied set of NK-2 variants in order to study differential effects of distinct structural modifications. The substantially divergent features of melittin make this peptide a worthy reference to NK-2-derived sequences. Overall, the interpretation of these calculated, purely sequence- and structure-inherent properties is thought to be of special value when being brought into context with functional data from empirical biological and non-biological experiments. In the following chapters, the outcome of corresponding cell- and liposome-based investigations will be separately presented, before selected cross-correlations are discussed in a separate result chapter (see section 5.10).

## Results

**Table 5.1: Overview on peptide sequences and structure-related peptide properties.** Computer-assisted calculations were done with the Profilegraph software based on the Normalized Consensus hydrophobicity scale introduced by Eisenberg et al. (1984) for peptides NK-2 and 33 derivatives thereof, as well as the reference peptide melittin. Peptides are sorted in the order of decreasing sequence length ( $n$ ), and accordingly assigned a numerical identifier (ID). Referring to the sequence of NK-2, residue changes are indicated by bold type letters, while hyphens represent omissions. All peptides, except C7S-OH, were synthesized with amidated C-termini. Determined parameters enclosed each peptide's net charge ( $Q$ ) and average charge per residue ( $Q/n$ ) at physiological pH, the mean hydrophobicity ( $H$ ), as well as the average (index: mean) and local maximum (index: max) hydrophobic moments ( $\mu H$ ). The moments were initially calculated over a sliding window of 7 residues. Finally, the proportions of hydrophobicity to net ( $H/Q$ ) and average residual charge ( $H/(Q/n)$ ) were determined. Background grey-scale coding delineates single-substitution (IDs 2-13), multiple-substitution (IDs 14-16), and deletion (IDs 17-34) variants of parent peptide NK-2 (ID 1).

ID	Peptide	Amino acid sequence	$n$	$Q$	$Q/n$	$H$	$H/Q$	$H/(Q/n)$	$\mu H_{\text{mean}}$	$\mu H_{\text{max}}$	$\mu H_{\text{min}}$
1	NK-2	KILRGVCKKIMRTFLRRISKDILTGKK	27	+10	+0.37	-0.28	-0.028	-0.74	0.79	1.06	0.24
2	I2W	KWLRGVCKKIMRTFLRRISKDILTGKK	27	+10	+0.37	-0.30	-0.030	-0.80	0.78	1.06	0.24
3	R4L	KIL <b>L</b> GVCKKIMRTFLRRISKDILTGKK	27	+9	+0.33	-0.14	-0.016	-0.43	0.72	1.06	0.24
4	C7A	KILRGV <b>A</b> KKIMRTFLRRISKDILTGKK	27	+10	+0.37	-0.26	-0.026	-0.71	0.79	1.06	0.24
5	C7L	KILRGV <b>L</b> KKIMRTFLRRISKDILTGKK	27	+10	+0.37	-0.25	-0.025	-0.67	0.80	1.06	0.24
6	C7S	KILRGV <b>S</b> KKIMRTFLRRISKDILTGKK	27	+10	+0.37	-0.29	-0.029	-0.79	0.78	1.06	0.24
7	C7S-OH	KILRGV <b>S</b> KKIMRTFLRRISKDILTGKK-OH	27	+9	+0.33	-0.28	-0.031	-0.84	0.78	1.06	0.24
8	M11L	KILRGVCKK <b>I</b> LRTFLRRISKDILTGKK	27	+10	+0.37	-0.26	-0.026	-0.70	0.80	1.06	0.24
9	F14W	KILRGVCKKIMRT <b>W</b> LRRISKDILTGKK	27	+10	+0.37	-0.29	-0.029	-0.78	0.77	1.03	0.24
10	R17L	KILRGVCKKIMRTFL <b>R</b> LISKDILTGKK	27	+9	+0.33	-0.14	-0.016	-0.43	0.74	1.06	0.24
11	D21K	KILRGVCKKIMRTFLRRISK <b>K</b> ILTGKK	27	+12	+0.44	-0.30	-0.025	-0.67	0.80	1.06	0.25
12	D21L	KILRGVCKKIMRTFLRRISK <b>L</b> ILTGKK	27	+11	+0.41	-0.20	-0.018	-0.50	0.79	1.07	0.35
13	G25W	KILRGVCKKIMRTFLRRISKDIL <b>T</b> WKK	27	+10	+0.37	-0.26	-0.026	-0.71	0.80	1.06	0.28
14	C7A-D21K	KILRGV <b>A</b> KKIMRTFLRRISK <b>K</b> ILTGKK	27	+12	+0.44	-0.29	-0.024	-0.64	0.80	1.06	0.25
15	C7A-K8L-D21K	KILRGV <b>A</b> LKIMRTFLRRISK <b>K</b> ILTGKK	27	+12	+0.44	-0.19	-0.016	-0.43	0.71	1.06	0.25
16	C7A-M11L-D21K	KILRGV <b>A</b> KK <b>I</b> LRTFLRRISK <b>K</b> ILTGKK	27	+12	+0.44	-0.27	-0.023	-0.61	0.81	1.06	0.25
17	NK-2-K	-ILRGVCKKIMRTFLRRISKDILTGKK	26	+9	+0.35	-0.23	-0.025	-0.66	0.79	1.06	0.24
18	NK-2-KK	KILRGVCKKIMRTFLRRISKDIL <b>T</b> G--	25	+8	+0.32	-0.18	-0.022	-0.56	0.85	1.06	0.44
19	NK-2-KKK	-ILRGVCKKIMRTFLRRISKDIL <b>T</b> G--	24	+7	+0.29	-0.12	-0.018	-0.42	0.84	1.06	0.44
20	C7A-Δ	KILRGV <b>A</b> KKIMRTFLRR----ILTGKK	23	+10	+0.43	-0.26	-0.026	-0.59	0.81	1.03	0.32
21	L3K-C7A-F14K-Δ	K <b>I</b> KRGV <b>A</b> KKIMRT <b>K</b> LRR----ILTGKK	23	+12	+0.52	-0.49	-0.040	-0.93	0.68	0.98	0.32
22	NK23a	K <b>I</b> ---- <b>S</b> KKIMRTFLRRISKDILTGKK	23	+9	+0.39	-0.35	-0.039	-0.89	0.79	1.06	0.24
23	NK23b	KILRGV <b>S</b> KKIM----RRISKDILTGKK	23	+9	+0.39	-0.33	-0.037	-0.84	0.76	1.08	0.24
24	NK23c (C7S-Δ)	KILRGV <b>S</b> KKIMRTFLRR----ILTGKK	23	+10	+0.43	-0.29	-0.029	-0.67	0.80	1.03	0.32
25	C20	----- <b>K</b> KIMRTFLRRISKDILTGKK	20	+8	+0.40	-0.39	-0.048	-0.96	0.79	1.06	0.24
26	C20-DK	----- <b>K</b> KIMRTFLRRISK <b>K</b> ILTGKK	20	+10	+0.50	-0.42	-0.042	-0.83	0.80	1.06	0.25
27	NK19a	K <b>I</b> ---- <b>S</b> KKIMRTFLRR----ILTGKK	19	+9	+0.47	-0.36	-0.040	-0.76	0.82	1.03	0.32
28	NK19b	KILRGV <b>S</b> KKIM---- <b>R</b> R----ILTGKK	19	+8	+0.42	-0.34	-0.042	-0.80	0.77	1.08	0.32
29	NK19b-KR	<b>R</b> ILRGV <b>S</b> <b>R</b> RIM---- <b>R</b> R----IL <b>T</b> G <b>R</b> R	19	+8	+0.42	-0.61	-0.076	-1.44	0.86	1.26	0.28
30	N17	KILRGV <b>S</b> KKIMRTFLRR-----	17	+8	+0.47	-0.39	-0.048	-0.82	0.84	1.03	0.48
31	NK15	KILRGV <b>S</b> K----- <b>R</b> ----ILTGKK	15	+7	+0.47	-0.29	-0.042	-0.62	0.63	0.93	0.32
32	NK13	K <b>I</b> ---- <b>S</b> KKIMRTFLRR-----	13	+7	+0.54	-0.51	-0.073	-0.95	0.89	1.03	0.75
33	NK11	K <b>I</b> ---- <b>S</b> K----- <b>R</b> ----ILTGKK	11	+6	+0.55	-0.41	-0.068	-0.74	0.56	0.85	0.32
34	I10	----- <b>K</b> KIMRTFLRR-----	10	+6	+0.60	-0.64	-0.106	-1.06	0.94	1.03	0.85
35	Melittin*	GIGAVLKVLTGTPALISWIKRKRQQ	26	+6	+0.23	+0.10	+0.017	+0.44	0.43	0.80	0.25

\* reference peptide (not derived from NK-2)

## Results

**Table 5.2: Average hydrophobic moment ( $\mu H_{\text{mean}}$ ) per 7-residue calculation window.** Hydrophobic moments were determined for all peptides as the mean over each stretch of 7 consecutive amino acid residues based on the Normalized Consensus scale. The terminal three windows remained unconsidered (cut or greyed) due to the undefined pre- and post-terminal environment. A color gradient is applied to rate the relative magnitude of each segments moment with pure blue and pure red representing the level of lowest and highest  $\mu H$ , respectively. A thick vertical line virtually separates N- from C-terminal segments of each peptide, while both minimum and maximum values are highlighted in bold type.

ID	Peptide	$\mu H_{\text{mean}}$ per 7-residue window																				
1	NK-2	0.87	0.91	0.69	0.76	0.52	0.94	0.87	1.00	0.85	1.03	0.88	0.99	0.85	<b>1.06</b>	0.97	1.03	0.86	0.54	0.44	0.27	<b>0.24</b>
2	I2W	0.80	0.84	0.69	0.76	0.52	0.94	0.87	1.00	0.85	1.03	0.88	0.99	0.85	<b>1.06</b>	0.97	1.03	0.86	0.54	0.44	0.27	<b>0.24</b>
3	R4L	0.42	0.43	0.45	0.47	0.52	0.94	0.87	1.00	0.85	1.03	0.88	0.99	0.85	<b>1.06</b>	0.97	1.03	0.86	0.54	0.44	0.27	<b>0.24</b>
4	C7A	0.86	0.90	0.70	0.77	0.55	0.98	0.91	1.00	0.85	1.03	0.88	0.99	0.85	<b>1.06</b>	0.97	1.03	0.86	0.54	0.44	0.27	<b>0.24</b>
5	C7L	0.85	0.88	0.72	0.78	0.60	<b>1.03</b>	0.96	1.00	0.85	1.03	0.88	0.99	0.85	<b>1.06</b>	0.97	1.03	0.86	0.54	0.44	0.27	<b>0.24</b>
6	C7S	0.88	0.93	0.68	0.75	0.48	0.89	0.82	1.00	0.85	1.03	0.88	0.99	0.85	<b>1.06</b>	0.97	1.03	0.86	0.54	0.44	0.27	<b>0.24</b>
7	C7S-OH	0.88	0.93	0.68	0.75	0.48	0.89	0.82	1.00	0.85	1.03	0.88	0.99	0.85	<b>1.06</b>	0.97	1.03	0.86	0.54	0.44	0.27	<b>0.24</b>
8	M11L	0.87	0.91	0.69	0.76	0.53	0.95	0.89	1.02	0.89	<b>1.06</b>	0.94	0.99	0.85	<b>1.06</b>	0.97	1.03	0.86	0.54	0.44	0.27	<b>0.24</b>
9	F14W	0.87	0.91	0.69	0.76	0.52	0.94	0.87	0.95	0.80	0.97	0.84	0.95	0.82	<b>1.03</b>	0.97	1.03	0.86	0.54	0.44	0.27	<b>0.24</b>
10	R17L	0.87	0.91	0.69	0.76	0.52	0.94	0.87	1.00	0.85	1.03	0.95	<b>1.06</b>	0.78	0.94	0.73	0.80	0.42	0.54	0.44	0.27	<b>0.24</b>
11	D21K	0.87	0.91	0.69	0.76	0.52	0.94	0.87	1.00	0.85	1.03	0.88	0.99	0.85	<b>1.06</b>	0.98	1.04	0.90	0.57	0.48	0.30	<b>0.25</b>
12	D21L	0.87	0.91	0.69	0.76	0.52	0.94	0.87	1.00	0.85	1.03	0.88	0.99	0.85	<b>1.06</b>	1.00	<b>1.07</b>	0.76	0.54	0.40	<b>0.35</b>	0.38
13	G25W	0.87	0.91	0.69	0.76	0.52	0.94	0.87	1.00	0.85	1.03	0.88	0.99	0.85	<b>1.06</b>	0.97	1.03	0.86	0.54	0.45	0.30	<b>0.28</b>
14	C7A-D21K	0.86	0.90	0.70	0.77	0.55	0.98	0.91	1.00	0.85	1.03	0.88	0.99	0.85	<b>1.06</b>	0.98	1.04	0.90	0.57	0.48	0.30	<b>0.25</b>
15	C7A-K8L-D21K	0.86	0.57	<b>0.33</b>	0.40	<b>0.34</b>	0.74	0.72	0.80	0.85	1.03	0.88	0.99	0.85	<b>1.06</b>	0.98	1.04	0.90	0.57	0.48	0.30	<b>0.25</b>
16	C7A-M11L-D21K	0.86	0.90	0.70	0.77	0.56	0.99	0.93	1.02	0.89	<b>1.06</b>	0.94	0.99	0.85	<b>1.06</b>	0.98	1.04	0.90	0.57	0.48	0.30	<b>0.25</b>
17	NK-2-K	0.91	0.69	0.76	0.52	0.94	0.87	1.00	0.85	1.03	0.88	0.99	0.85	<b>1.06</b>	0.97	1.03	0.86	0.54	0.44	0.27	<b>0.24</b>	
18	NK-2-KK	0.87	0.91	0.69	0.76	0.52	0.94	0.87	1.00	0.85		1.03	0.88	0.99	0.85	<b>1.06</b>	0.97	1.03	0.86	0.54	<b>0.44</b>	
19	NK-2-KKK	0.91	0.69	0.76	0.52	0.94	0.87	1.00	0.85	1.03		0.88	0.99	0.85	<b>1.06</b>	0.97	1.03	0.86	0.54	<b>0.44</b>		
20	C7A-Δ		0.86	0.90	0.70	0.77	0.55	0.98	0.91	1.00		0.85	<b>1.03</b>	0.88	0.99	0.88	0.88	0.83	0.49	<b>0.32</b>		
21	L3K-C7A-F14K-Δ			0.73	0.79	0.45	0.77	0.55	<b>0.98</b>	0.91	0.63	0.48	0.65	0.63	0.72	0.82	0.82	0.83	0.49	<b>0.32</b>		
22	NK23a			0.75	0.92	0.82	1.00	0.85	1.03	0.88	0.99	0.85	<b>1.06</b>	0.97	1.03	0.86	0.54	0.44	0.27	<b>0.24</b>		
23	NK23b			0.88	0.93	0.68	0.75	0.48	0.89	0.86	<b>1.08</b>	1.01	1.03	0.92	1.03	0.86	0.54	0.44	0.27	<b>0.24</b>		
24	NK23c (C7S-Δ)			0.88	0.93	0.68	0.75	0.48	0.89	0.82	1.00	0.85	<b>1.03</b>	0.88	0.99	0.88	0.88	0.83	0.49	<b>0.32</b>		
25	C20				1.00	0.85	1.03	0.88	0.99	0.85	<b>1.06</b>	0.97	1.03	0.86	0.54	0.44	0.27	<b>0.24</b>				
26	C20-DK				1.00	0.85	1.03	0.88	0.99	0.85	<b>1.06</b>	0.98	1.04	0.90	0.57	0.48	0.30	<b>0.25</b>				
27	NK19a					0.75	0.92	0.82	1.00	0.85	<b>1.03</b>	0.88	0.99	0.88	0.88	0.83	0.49	<b>0.32</b>				
28	NK19b					0.88	0.93	0.68	0.75	0.48	0.89	0.86	<b>1.08</b>	1.05	0.85	0.77	0.49	<b>0.32</b>				
29	NK19b-KR					0.99	1.06	0.80	0.87	0.66	1.08	1.04	<b>1.26</b>	1.19	0.85	0.77	0.35	<b>0.28</b>				
30	N17						0.88	0.93	0.68	0.75	<b>0.48</b>	0.89	0.82	1.00	0.85	<b>1.03</b>	0.88					
31	NK15							0.88	<b>0.93</b>	0.66	0.72	0.56	0.63	0.58	0.39	<b>0.32</b>						
32	NK13								<b>0.75</b>	0.92	0.82	1.00	0.85	<b>1.03</b>	0.88							
33	NK11									<b>0.85</b>	0.65	0.58	0.39	<b>0.32</b>								
34	I10									1.00	<b>0.85</b>	<b>1.03</b>	0.88									
35	Melittin	0.49	0.47	0.46	0.52	0.56	0.47	0.52	0.29	<b>0.25</b>	0.26	0.30	0.32	0.29	0.35	0.50	<b>0.80</b>	0.59	0.32	0.42	0.36	

## 5.2 Cell Type-Specific Membrane Surface Characteristics

Prior to investigations on cellular interactions with peptides, crucial surface properties of each cell type were characterized by different approaches. Flow cytometry analysis was applied to identify potential specificities in the cell-specific surface PS exposure. In addition, the average Zeta potential of each cell type was determined as a comparative measure of the overall accessible surface charge.

The level of cell surface-exposed PS was determined for five cell lines including two directly patient-derived CRC cells. Annexin V binds to PS with high affinity and selectivity, and FITC-labeling of annexin V enabled quantitative flow cytometric analysis. Dead cell exclusion was accomplished by propidium iodide (PI) staining.

Figure 5.4 representatively depicts the outcome of a flow cytometric investigation of unstained (non-filled histograms) and FITC-annexin V-stained (grey-filled histograms) CRC cells. In principle, the geometric mean fluorescence intensities (MFI) of both groups were used to calculate a respective quotient for each cell type. This signal ratio of stained versus unstained cells served as a measure to compare the relative levels of surface-exposed PS. Detailed results for all cell types are given in figure 5.5.

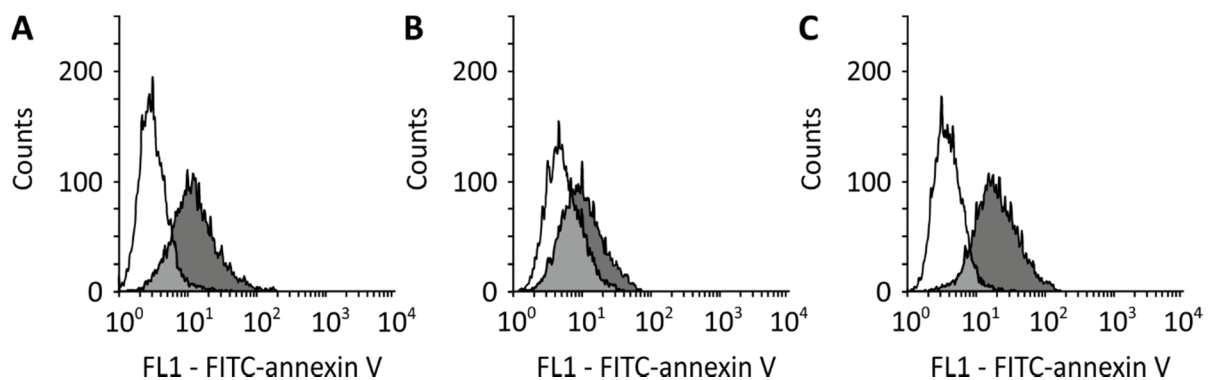


**Figure 5.4: Representative results of the flow cytometric assessment of the surface PS levels on CRC cells.** Depicted are exemplary overlay histograms of the FL1 (FITC-annexin V) fluorescence signals of annexin V-stained (grey) and unstained control (white) cells of type HROC24 (A), HROC107 (B), and HCT116 (C). The respective quotient of geometric mean fluorescence intensity (MFI) was calculated for all cell lines tested and served as a marker for the corresponding level of surface-exposed PS. Pre-gating of the PI-negative population enabled the exclusion of signals from dead cells *a priori*. Gates were set manually and kept constant for all experiments and reproductions analyzing a given cell type. Software-based evaluation was done using Flowing Software 2.5.1 (Turku University, Finland).

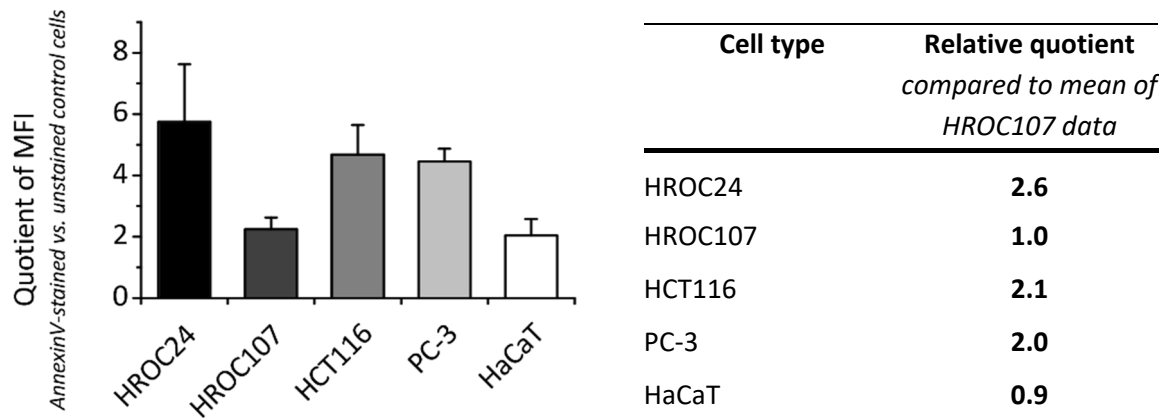


**Figure 5.5: Surface exposure of PS on various cell lines as assessed by flow cytometry analysis after FITC-annexin V-staining.** The surface levels of PS were determined as the quotient of the geometric mean fluorescence intensity (MFI) of FITC-annexin V-stained versus unstained control cells for each cell line. The column plot in (A) depicts the absolute quotient, while quantities in (B) are expressed in relation to HROC107 cells, which showed the lowest exposure levels of PS among the involved cancer cells (B). Results are given as arithmetic means with standard deviations from at least three independently conducted experiments.

Generally speaking, the levels of cell surface-exposed PS were found to vary remarkably among the investigated set of cells, and the cell types were accordingly classified. HROC107 cells exposed PS on their surface at a level as low as that of non-cancerous HaCaT cells. Both cell types will be addressed as poorly PS-exposing, or '*low-PS*', cells in the following. In sharp contrast to this, HROC24, HCT116 as well as PC-3 cells reproducibly demonstrated to possess 2.0- to 2.6-fold higher MFI quotients, thus surface PS levels. Hence, the latter three human cancer cell types could be attributed to be highly PS-exposing, or '*high-PS*' cells.

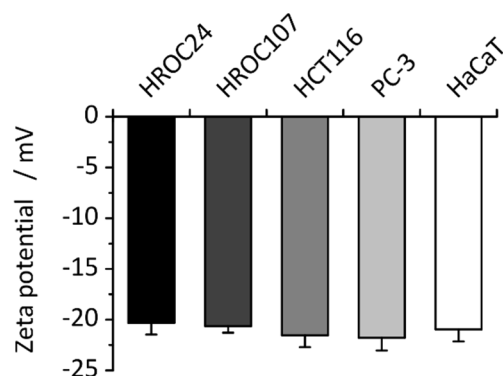


**Figure 5.6: Cell surface Zeta potentials of all cell lines under investigation.** The Zeta potentials were determined at 25°C for samples of 200,000 cells/mL in 40 mM HEPES buffer (pH 7.4). All measurements were carried out on a Zetasizer Nano ZS with input parameters as defined in table 4.3. Data represent mean values with standard deviations of at least three independent cell preparations.

Intriguingly, as can be deduced from figure 5.6, the average Zeta potentials of the investigated cell types did not show significant differences ranging from about -20.3 mV (HROC107) to -21.4 mV (PC-3). This observation stood in striking contrast to the marked differences in the PS exposure. Apparently, the abundance of the anionic phospholipid did not govern the overall level of surface charge of a given cell type. Apart from this, the uniformity in the cellular Zeta potential happened to be favorable in terms of directly comparing the effects upon titration with peptides.

### 5.3 Peptide Cytotoxicity

Two distinct cellular test systems were deployed to scrutinize peptide-induced effects on cultivated human cells by MTT-based metabolic activity tests.

Firstly, the same set of 35 peptides, for which the software-assisted property characterization was performed (see section 5.1), was assessed in terms of peptide-specific activities against two model cell lines, including the PC-3 prostate cancer cell line as well as attributably healthy HaCaT human keratinocytes. Here, the main focus was put on gathering comprehensive quantitative cytotoxicity data in order to subsequently enable a detailed view on structure-activity relationships.

Secondly, the cytotoxic potentials of six selected peptides, including NK-2, four derivatives thereof, and melittin, were tested against three distinct CRC cell lines, enclosing patient-derived HROC24 and HROC107 cells, as well as the commercially available colon cancer model cell line HCT116. Inferring from the above-described cell type-specific characteristics, this model system appeared to have good prospect in providing further details on the hypothesized PS-related peptide activity.

Of note, for both approaches, the corresponding cytotoxicity assays were conducted using two distinct buffer conditions, i.e. (i) PBS/medium as well as (ii) complete medium. (see also section 2.1.2.4). Adding to this, particular variations of both buffer systems were additionally tested for their basic influence on the cytotoxic potential of certain peptides.

### 5.3.1 Comprehensive Investigations on the Cytotoxicity of NK-2-Derived Peptides against PC-3 and HaCaT Cells

Figure 5.7 exemplarily depicts representative results from MTT assays performed under PBS/medium and complete medium conditions after treating human prostate cancer (PC-3) cells with various concentrations of peptide NK-2 and selected derivatives thereof. In general, the individual peptide effects, indirectly measured as the residual metabolic activity of vital cells, were found to be strongly dependent on the respective peptide molarity. For instance, under PBS assay conditions (figure 5.7A), the parent peptide NK-2 did not markedly reduce the PC-3 metabolic activity at concentrations lower or equal to 0.3  $\mu\text{M}$ . With increasing peptide molarity a gradual decrease of the residual cell viability was observed, finally dropping to 0 % survival at molarities  $\geq 30 \mu\text{M}$ . In comparison, derivatives C7A-D21K and C7S- $\Delta$  showed a very similar order of effectiveness, yet having a slightly steeper or flatter slope, respectively.

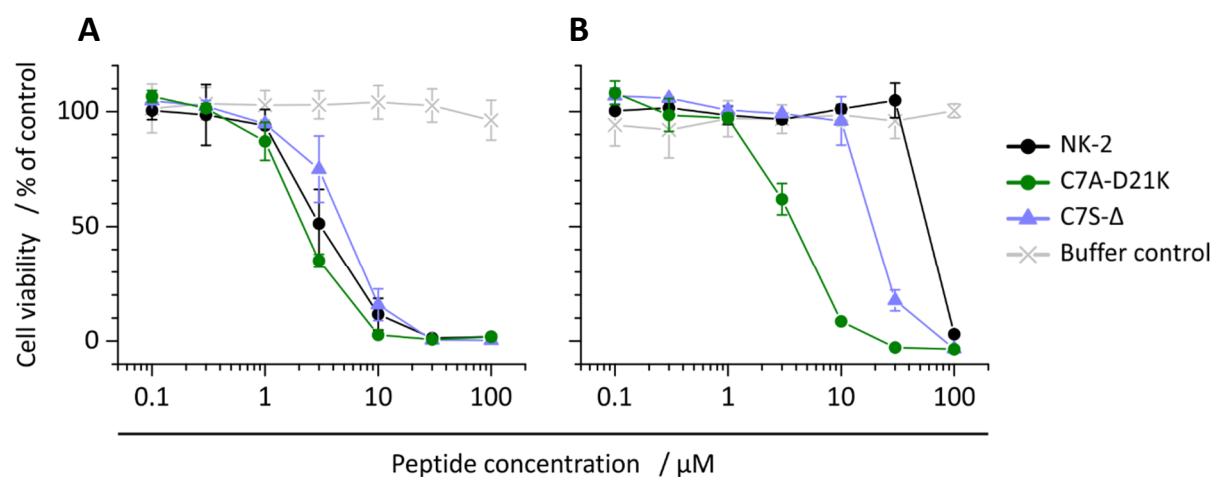


**Figure 5.7: Exemplary MTT results illustrating the concentration- and buffer-dependent *in vitro* cytotoxicity of selected NK-2 variants against PC-3 prostate cancer cells.** Cytotoxicity assays based on the conversion of yellowish MTT into purple formazan by viable cells were conducted at 37°C under PBS/medium conditions (A) as well as in complete medium (B). Representatively chosen data depict the outcome after a 4 h treatment of equal counts of PC-3 cells with indicated concentrations of peptides NK-2 (black circles), C7A-D21K (green circles), and C7S- $\Delta$  (violet triangles). Peptides were administered from stocks, and buffer toxicity was ruled out through incubation with equivalent volumes of the dissolvent, i.e. 0.01 % TFA (light grey crosses). Positive and negative control experiments were included in each run by incubating cells in buffer/medium alone (100 %) or under addition of 5 % Triton X-100 (0 %), respectively. Each data point was calculated as the mean residual cell viability (%) with standard deviation (error bars).

As opposed to this similarity, strongly differential activities were observed for the very same peptides when the assay was conducted in complete cell culture medium while keeping all

other conditions constant (figure 5.7B). Here, peptides NK-2 and C7S- $\Delta$  remained void of detectable activity up to concentrations of 30 and 10  $\mu\text{M}$ , respectively, whereas C7A-D21K almost completely maintained its effectiveness.

Apparently, the investigated peptide molarity range was appropriate to cover a broad spectrum of activity, hence, to differentially assess the degree of cytotoxicity exhibited by distinct peptide concentrations. In general, the molar peptide concentration at which the metabolic activity of peptide-treated cells becomes diminished by 50 % is defined as the  $\text{IC}_{50}$  value. For the already introduced pool of 35 peptides, corresponding values were determined from sigmoidal fittings of experimental titration curves as given in table 5.3.

A color-code was applied in order to visually categorize the extensive  $\text{IC}_{50}$  data, and to facilitate the comparative interpretation.  $\text{IC}_{50}$  values of  $\leq 2.5 \mu\text{M}$  were classified as most cytotoxic and coded in pure green. In despite, values of  $\geq 100 \mu\text{M}$  were highlighted in red, and considered to represent peptide ineffectiveness. Gradual differences in between of these two extremes were illustrated by attributing specific color nuances to distinct peptide activity levels, which is defined in details in the color key accompanying the result table. From the given overview of cytotoxicity data, several general tendencies emerged and should be emphasized in the following.

First of all, it could be stated that PBS conditions allowed many peptides to exert potent cytotoxicity in general. Among all 35 employed peptides, 19 NK-2-related peptides as well as melittin were found to kill PC-3 prostate cancer cells with  $\text{IC}_{50}$  values below 5  $\mu\text{M}$ . In this scope, peptides C7A-D21K and C7A-M11L-D21K demonstrated to be the most potent NK-2 variants against cancer cells with mean  $\text{IC}_{50}$  values of 2.1 and 1.7  $\mu\text{M}$ , respectively.

As another striking aspect, a marked decrease in the cytotoxic activity was observed for the majority of NK-2-derived peptides when conducting the MTT test in complete medium instead of PBS/medium conditions. Especially the parent peptide NK-2, as is also deducible from the above-given exemplary data, underwent an outright inactivation in full medium by factors of around 10- and 20-fold against HaCaT and PC-3 cells, respectively. Likewise, and regardless of the cell line treated, most NK-2 derivatives were inactivated in medium, too. In terms of the intended potential future application of NK-2 in cancer therapy, at a first glance, this observation basically impeded and questioned its therapeutic perspectives.

**Table 5.3: Cytotoxicity of NK-2-derived peptides and melittin against PC-3 and HaCaT cells.** Metabolic activity tests based on the conversion of MTT by viable cells were conducted in both PBS/medium and in complete medium conditions. Given data represent mean IC<sub>50</sub> values (μM) with standard deviations. IC<sub>50</sub> values were derived from sigmoidal fitting curves after incubation of cells (4 h) with distinct peptides at molarities from 0.1 to 100 μM. In case fitting was unsuccessful, values were estimated (≈), or classified as being considerably larger than 100 μM (>> 100). Cells incubated in PBS/medium or complete medium served as positive controls, whereas negative control was accounted for by treating cells with 5 % Triton X-100 dissolved in the respective buffer. A color-coding was applied to categorize the obtained IC<sub>50</sub> values from highly cytotoxic (green) to ineffective (red) (see color key, in μM). Of note, peptides inactive in favorable PBS/medium conditions were excluded from MTT experiments in complete medium (i.e. *not done*).

ID	Peptide	n	PC-3		HaCaT		
			PBS/medium	Medium	PBS/medium	Medium	
1	NK-2	27	3.4 ± 0.2	≈ 80	8.7 ± 0.8	≈ 100	
2	I2W	27	2.9 ± 0.1	≈ 30	6.6 ± 1.5	≈ 35	
3	R4L	27	2.6 ± 0.1	≈ 80	7.0 ± 0.7	≈ 80	
4	C7A	27	3.3 ± 0.5	8.8 ± 0.4	7.2 ± 1.2	17.7 ± 1.6	
5	C7L	27	3.2 ± 0.4	3.6 ± 0.2	2.5 ± 0.1	10.4 ± 0.4	
6	C7S	27	8.3 ± 0.7	≈ 30	11.4 ± 1.3	≈ 90	
7	C7S-OH	27	9.1 ± 0.8	≈ 40	11.5 ± 1.4	37 ± 6	
8	M11L	27	3.8 ± 0.4	≈ 50	7.6 ± 1.0	>> 100	
9	F14W	27	3.7 ± 0.1	≈ 100	10.6 ± 1.3	≈ 100	
10	R17L	27	3.1 ± 0.2	≈ 30	6.7 ± 1.5	≈ 70	
11	D21K	27	3.4 ± 0.5	23.7 ± 1.6	3.6 ± 0.2	≈ 50	
12	D21L	27	3.0 ± 0.2	14.9 ± 0.6	4.7 ± 1.7	≈ 30	
13	G25W	27	4.1 ± 0.3	≈ 30	6.1 ± 0.6	≈ 35	
14	C7A-D21K	27	2.1 ± 0.1	3.7 ± 0.3	3.1 ± 0.3	12.9 ± 1.6	≤ 2.5
15	C7A-K8L-D21K	27	2.5 ± 0.1	3.2 ± 0.2	2.0 ± 0.0	10.4 ± 0.4	≤ 5.0
16	C7A-M11L-D21K	27	1.7 ± 0.1	3.2 ± 0.3	4.3 ± 0.3	16.4 ± 0.6	≤ 10.0
17	NK-2-K	26	2.8 ± 0.2	>> 100	6.0 ± 0.7	≈ 100	≤ 30.0
18	NK-2-KK	25	3.6 ± 0.2	≈ 100	7.7 ± 0.6	>> 100	≤ 60
19	NK-2-KKK	24	3.2 ± 0.2	≈ 100	7.4 ± 1.3	≈ 100	≤ 99
20	C7A-Δ	23	4.3 ± 0.3	5.9 ± 0.6	3.6 ± 0.7	12.8 ± 0.6	≥ 100
21	L3K-C7A-F14K-Δ	23	≈ 100	not done	≈ 100	not done	
22	NK23a	23	13.9 ± 3.3	>> 100	19.4 ± 2.9	>> 100	
23	NK23b	23	≈ 100	>> 100	≈ 60	>> 100	
24	NK23c	23	3.8 ± 0.2	20.5 ± 1.7	10.0 ± 2.3	≈ 30	
25	C20	20	≈ 80	>> 100	≈ 150	>> 100	
26	C20-DK	20	21.6 ± 1.3	>> 100	≈ 30	>> 100	
27	NK19a	19	11.2 ± 1.7	≈ 80	12.7 ± 0.5	>> 100	
28	NK19b	19	≈ 100	not done	≈ 50	not done	
29	NK19b-KR	19	≈ 80	not done	≈ 30	not done	
30	N17	17	>> 100	not done	≈ 100	not done	
31	NK15	15	>> 100	not done	>> 100	not done	
32	NK13	13	>> 100	not done	>> 100	not done	
33	NK11	11	>> 100	>> 100	>> 100	>> 100	
34	I10	10	>> 100	not done	>> 100	not done	
35	Melittin	26	0.9 ± 0.0	1.1 ± 0.0	1.1 ± 0.0	3.1 ± 0.1	

However, an apparent activity re-establishment under complete medium conditions was achieved with several distinct NK-2 variants. Namely, such medium-active variants featuring  $IC_{50}$  values of below 10  $\mu$ M comprised two single-substitution derivatives (C7A, C7L), one double-substitution variant (C7A-D21K), as well as two triple-substitution variants (C7A-K8L-D21K, C7A-M11L-D21K). It is suggestive that the exchange of the single cysteine residue at position 7 is related to this phenomenon.

Noticeably, changing the Cysteine at position 7 to rather polar serine (e.g. in variants C7S and C7S- $\Delta$ ) did not yield derivatives with satisfactory effectiveness in medium. In despite, even a truncated derivative of C7A, with a deletion of four consecutive residues from position 18 to 21 (C7A- $\Delta$ ), effectively inhibited the cellular metabolic activity in medium. In fact, C7A- $\Delta$  turned out to be the only peptide among any shortened variants of NK-2 being also sufficiently active in complete medium – while peptides NK23a, C7S- $\Delta$ , and NK19a (all comprising a C7S substitution) exhibited a substantial level of effectiveness only in case PBS/medium conditions were applied, but lost their activity in medium. Any other shortenings led to peptides void of demonstrable effectiveness already under PBS conditions.

Melittin was found to effectively impair the cellular metabolic activity, regardless of the medium conditions and, especially, the targeted cell type. This underlines the potent but vastly unselective melittin activity, and apparently points at a particularly different mode of action as compared to NK-2 and derivatives thereof.

Finally, it should be pointed out that non-cancerous HaCaT cells turned out to be basically susceptible to anti-cancer cell active peptides, as well, albeit in many cases to a lesser extent. In fact, under complete medium conditions, the highest degree of selectivity for cancer cells was again demonstrated for the overall most potent NK-2 variants C7A-D21K and C7A-M11L-D21K. For these derivatives, preferential killing of prostate cancer over normal cells by factors of about 3.5 and 5.1 could be determined, respectively.

### 5.3.2 Cytotoxicity of Selected Peptides against Colorectal Cancer Cells

The triplet of colorectal carcinoma (CRC) cells was assessed in MTT tests regarding their susceptibility to selected peptides. Chosen peptides comprised the parent peptide NK-2 as the lead structure as well as three promising derivatives thereof, namely C7A, C7A-D21K, and C7A- $\Delta$ . In addition, the extensively shortened NK-2 variant NK11 was included as a putative

## Results

negative control while melittin served as a knowingly potent but non-selective reference. Results obtained from cytotoxicity tests in the two distinct buffer conditions are summarized in table 5.4.

Here again, the parent peptide NK-2 was found to be well-effective against all CRC cell lines for as long as the MTT test was performed in PBS/medium. In line with this, all basically active peptides consistently inhibited HROC107 cells with poorer efficiency in comparison to HCT116 and especially HROC24 colon cancer cells, regardless of the buffer condition. However, switching the solvent surrounding to complete cell culture medium instead, led to an extensive inhibition of NK-2's cytotoxic efficacy. Meanwhile, the three C7A-substitution variants exhibited differential degrees of activity improvement compared to the parent peptide.

**Table 5.4: Cytotoxicity of selected NK-2-derived peptides against human colorectal cancer cells.** MTT assays were conducted under PBS/medium conditions (A) as well as in complete medium (B). Given data represent mean  $IC_{50}$  values ( $\mu M$ ) with standard deviations. Peptides were added to confluent cell-covered cavities of a 96-well plate.  $IC_{50}$  values were derived from sigmoidal fitting curves after incubation of cells for 4 h with distinct peptides at molarities between 0.1 and 100  $\mu M$ . In case fitting was unsuccessful, values were estimated ( $\approx$ ), or classified as being considerably larger than 100  $\mu M$  ( $\gg 100$ ). Cells incubated in PBS/medium or complete medium served as positive controls, whereas negative control was accounted for by treating cells with 5 % Triton X-100 in the respective buffer condition.

**A**  $IC_{50}$  ( $\mu M$ ) in PBS + 10 % complete medium

Cell line	NK-2	C7A	C7A- $\Delta$	C7A-D21K	NK11	Melittin
HROC24	7.5 $\pm$ 0.7	2.3 $\pm$ 1.6	3.3 $\pm$ 0.5	1.7 $\pm$ 0.6	$\gg 100$	1.0 $\pm$ 0.0
HROC107	8.5 $\pm$ 0.9	7.2 $\pm$ 0.6	7.1 $\pm$ 0.8	5.7 $\pm$ 0.4	$\gg 100$	1.6 $\pm$ 0.1
HCT116	9.1 $\pm$ 0.5	6.3 $\pm$ 0.6	6.8 $\pm$ 0.7	4.7 $\pm$ 0.7	$\gg 100$	1.1 $\pm$ 0.0

**B**  $IC_{50}$  ( $\mu M$ ) in complete medium

Cell line	NK-2	C7A	C7A- $\Delta$	C7A-D21K	NK11	Melittin
HROC24	$\approx 100$	25.7 $\pm$ 2.3	17.0 $\pm$ 0.6	12.2 $\pm$ 0.9	$\gg 100$	2.3 $\pm$ 0.1
HROC107	$\approx 110$	$\approx 48$	$\approx 55$	35.7 $\pm$ 3.5	$\gg 100$	2.3 $\pm$ 0.1
HCT116	$\approx 100$	30.1 $\pm$ 1.1	20.8 $\pm$ 1.0	19.0 $\pm$ 1.6	$\gg 100$	3.0 $\pm$ 0.0

With a closer look on the two patient-derived CRC cells, HROC24 and HROC107, the highest selectivities of toxicity were found for peptide C7A- $\Delta$  and C7A-D21K with 3.2-fold and 2.9-fold higher  $IC_{50}$  values, respectively, towards HROC24 cells under full medium conditions.

## Results

Representatively, the concentration-dependent peptide activity under complete medium conditions against the two patient-derived HROC cell types is illustrated in figure 5.8.

Once more, derivative C7A-D21K turned out to be the overall most effective peptide in complete medium with the lowest  $IC_{50}$  values among all tested NK-2-related peptides. With mean  $IC_{50}$  values of 12.2  $\mu$ M, 19.0  $\mu$ M, and 35.7  $\mu$ M against HROC24, HCT116, and HROC107 cells, respectively, even the most improved variant C7A-D21K was not as effective as observed with the PC-3 human prostate cancer model.

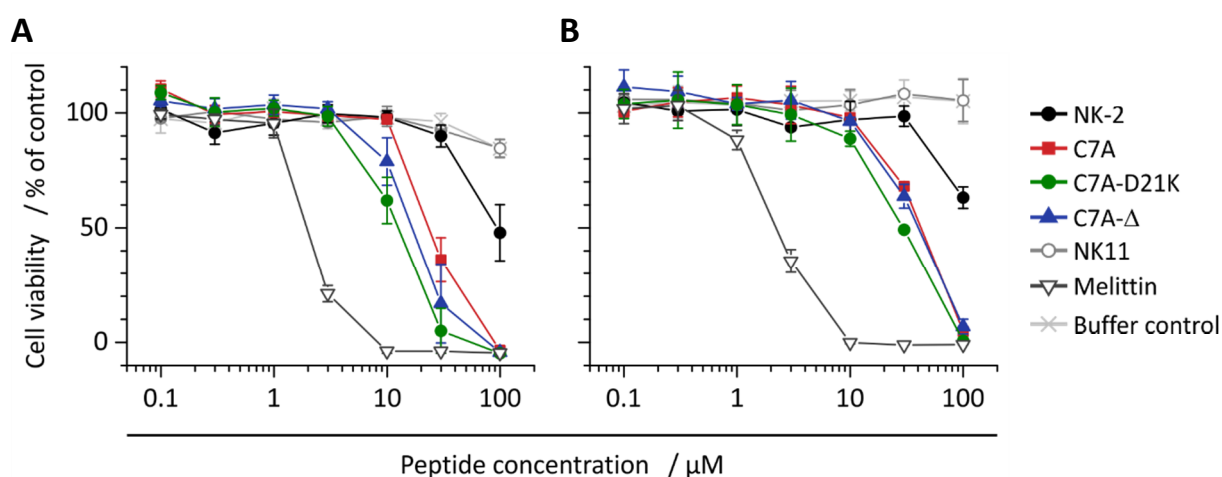


**Figure 5.8: Representative results of cytotoxicity tests in complete medium with patient-derived CRC cells.** MTT assays were performed in complete medium to test the effectiveness of selected peptides (as indicated) against HROC24 (A) and HROC107 (B) cells. The experimental setup was identical with conditions described for figure 5.7. Each data point represents the mean residual cell viability (%) with standard deviation at the indicated peptide concentration.

The anticipated inactivity of NK11 was strikingly underlined by  $IC_{50}$  values exceeding a peptide concentration of 100  $\mu$ M by far, irrespective of the buffer condition or the cell type treated. In contrast to this, melittin proved to be highly active against all cell lines with only minor declines in the corresponding  $IC_{50}$  values under full medium conditions.

### 5.3.3 Influences of Buffer Components on the Potency of Selected Peptides

Having found the afore-described marked divergences in the cytotoxic potential of numerous peptides depending on whether PBS/medium or complete medium was used for toxicity testing, the potential impacts of major buffer components were elucidated in separate experiments. MTT tests under variation of the solvent condition were performed with HaCaT normal keratinocytes treated with peptides NK-2, as the lead structure proven to forfeit

activity in complete medium, C7A-D21K, as a derivative of the parent peptide with comparably well-sustained medium activity, and the non-NK-2-related reference peptide melittin, demonstrating potent activity under both assay conditions tested so far. The outcome is illustrated by figure 5.9.

Unequivocally, the highest overall peptide activities (i.e. lowest  $IC_{50}$  values) were obtained from experiments performed in PBS/medium. Augmenting this condition with a DMEM-equivalent concentration (4.5 g/l) of glucose (figure 5.9, variant I) exerted only minor, if any, inhibitory effects on the peptide activity. In despite, divalent metal cations present at their respective DMEM levels (200 mg/l each) provoked considerable decreases in the cytotoxic potentials of all three examined peptides. In this regard, the activity of NK-2 was apparently more sensitive to  $Ca^{2+}$  (II) than to  $Mg^{2+}$  (III), whereas the type of metal ion did not seem to make a difference for the response of C7A-D21K or melittin.

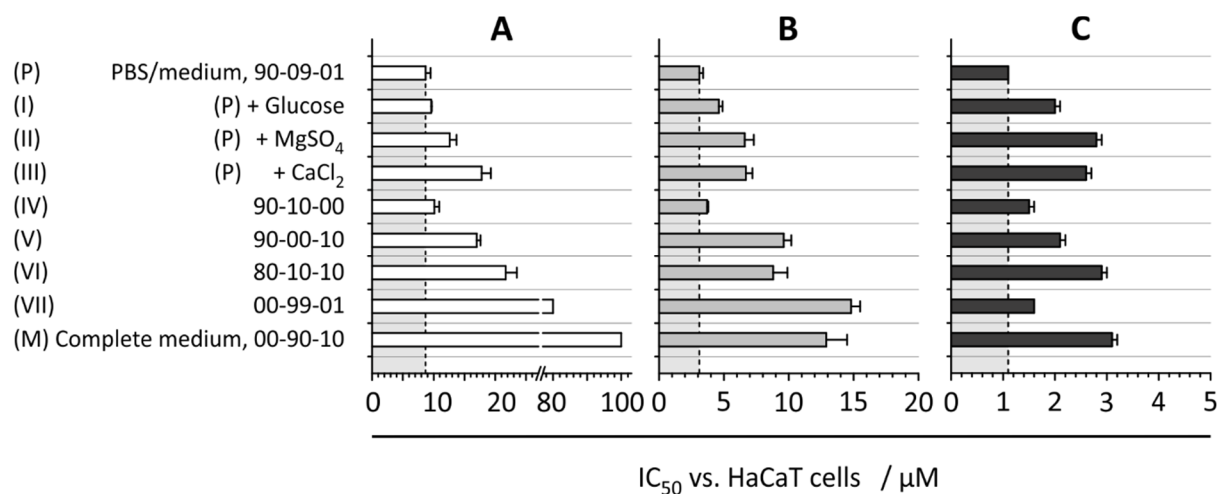


**Figure 5.9: Impact of buffer components on the cytotoxicity of selected peptides against HaCaT cells.**  $IC_{50}$  values against HaCaT normal keratinocytes were assessed for peptides NK-2 (A), C7A-D21K (B), and melittin (C) in MTT tests performed under variation of the buffer conditions. Cells were grown in complete medium to confluence in the wells of a 96-well tissue culture plate. Washing and incubation with peptides for 4 h was done with the indicated buffer (refer to tables 3.8 and 3.9 for details). Shortcuts given in the form XX-YY-ZZ represent the volumetric percentages of the three main buffer components PBS (XX), DMEM (YY) and FBS (ZZ), respectively. Further additives are accordingly delineated. The shaded area in each plot facilitates visual comparison to PBS/medium conditions. The x-axis in (A) was subjected to a scale break for enhanced resolution.

The alteration of the mixing proportions of PBS, DMEM, and FBS revealed, on the one hand, that the complete withdrawal of FBS (IV) yielded  $IC_{50}$  values almost fully equivalent to the most favorable PBS/medium conditions. On the other hand, increasing the FBS portion to 10 % (V, VI, and complete medium) was accompanied by a marked drop in peptide activities, with

the strongest (negative) effect on the potency of NK-2 and a considerably lower but similar (relative) impact on the activities of C7A-D21K and melittin. Nonetheless, most critical declines in peptide activity (down to virtual inactivity) were observed for the parent peptide NK-2 when buffer conditions were used featuring high DMEM contents concomitantly supplemented with FBS only at low (1 % in VII) or raised (10 % in complete medium) proportions. Although the potency of peptide C7A-D21K was affected too under such conditions, the corresponding drop in effectiveness was considerably less pronounced.

### 5.4 Visualization of Peptide-Induced Effects on Colorectal Cancer Cells

Concentration- and time-dependent effects of selected Rhodamine-labeled NK-2-derived peptides were studied by fluorescence microscopy analysis for the treatment of patient-derived CRC cell lines HROC24 (high-PS) and HROC107 (low-PS). Combined phase contrast and fluorescence microscopy was applied to visualize peptide-cell interactions. Labeling with red fluorescent Rhodamine (Rh) enabled tracing of the peptide localization. Selected Rh-labeled peptides included in these experiments encompassed the lead structure NK-2 as well as its most effective derivative C7A-D21K, and the inactive control variant NK11. Cell permeabilization events were monitored by concomitant incubation with the membrane-impermeant nucleic acid stain Sytox green.

Figure 5.10 illustrates the time course of representative experimental series involving HROC24 (A-L) and HROC107 (M-X) cells upon incubation with peptides Rh-NK-2 (A-F, M-R) and Rh-C7A-D21K (G-L, S-X) at a molar concentration of 10  $\mu$ M. Initial binding of Rh-labeled peptides to the cell surface was observed as a red peripheral seam. The permeabilization of affected cells was visualized by a bright Sytox-induced green fluorescence emission of the respective cell nuclei. At extended incubation periods, the coincident massive cellular intake of labeled peptides frequently led to a bright yellow overlay fluorescence found in an increasing number of cells over time. Of note, even long-term incubation with peptides at highest molarities did not lead to disruptive membrane lysis with either of the cells. This could be substantiated by the fact that no cellular debris or aggregates thereof were observable.

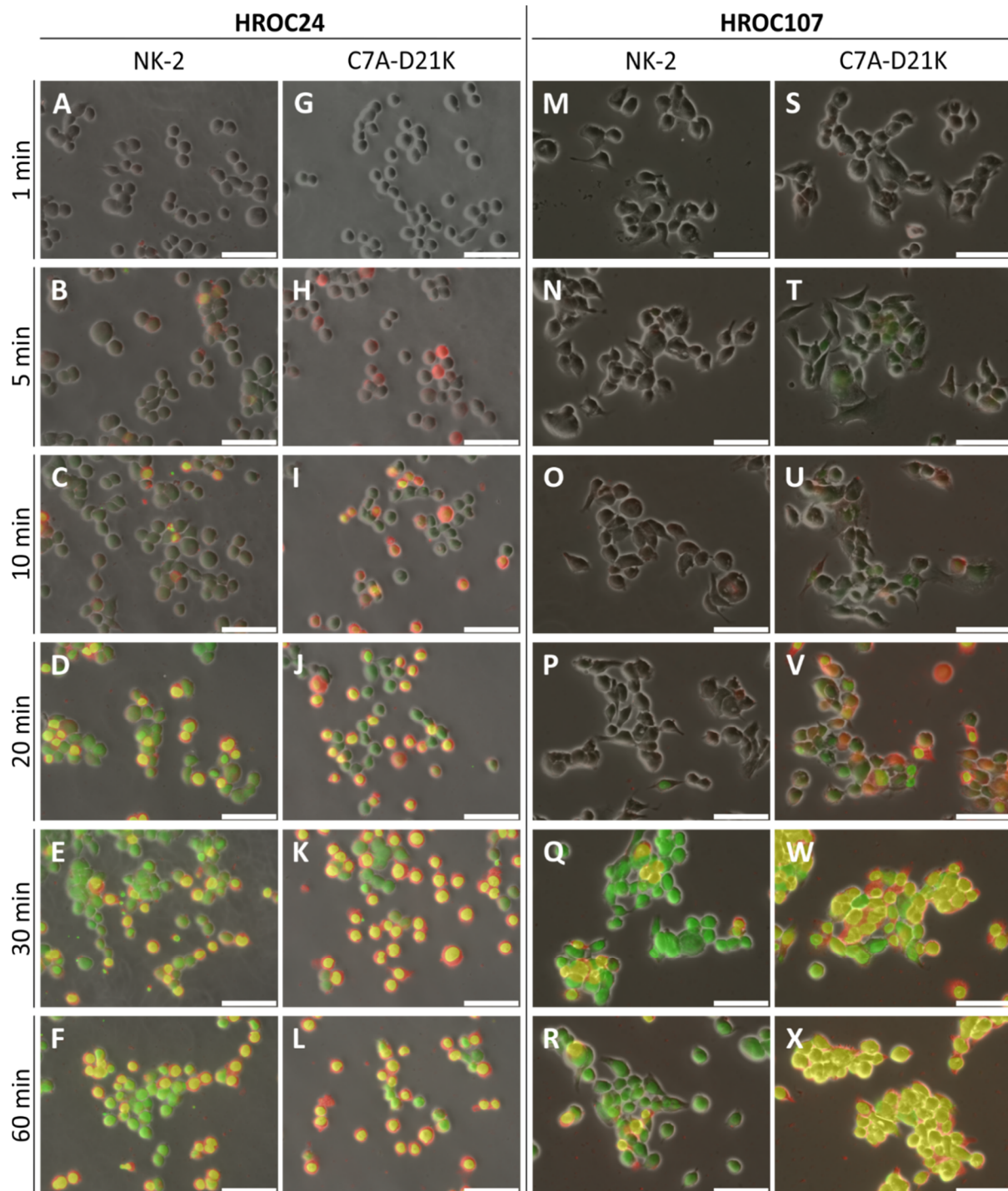


**Figure 5.10: Fluorescence microscopy analysis of high- and low-PS CRC cell types.** Equal counts of HROC24 (A-L) and HROC107 (M-X) cells seeded on glass cover slips were treated with 10  $\mu$ M of fluorescently labeled peptides Rh-NK-2 (A-F, M-R) or Rh-C7A-D21K (G-L, S-X) in PBS over indicated periods of time. For dead cell indication, all preparations were additionally incubated in the presence of 3  $\mu$ M of the membrane-impermeant nucleic acid stain Sytox green, which shows a bright green fluorescence upon DNA intercalation. Bright yellow fluorescence reflects overlay signals from internalized Rh-peptides and Sytox green. Selected images display the outcome of representative experiments for each time point. Scale bars: 50  $\mu$ m.

## Results

For high-PS HROC24 cells, incidences of peptide accumulation at the cell surface were typically registered within 5 minutes from peptide addition, and first cells showing yellow overlay fluorescence were observed after 5-10 minutes. Obviously, similar kinetics applied for both peptides with regard to the initial step of cell surface binding (occurrence of red seams), and finally, complete mortality was reached for both peptides after about 20 minutes. However, overall, the number of readily permeabilized cells grew faster for Rh-C7A-D21K, and almost all HROC24 cells finally displayed bright yellow overlay fluorescence.

In comparison, a shift in the interaction kinetics was evident for the peptide treatment of low-PS HROC107 cells. For Rh-C7A-D21K, first binding events were recorded after 5-10 minutes, while the occurrence of Rh-NK-2-binding to HROC107 cells was not registered earlier than 10 minutes from peptide addition. Both peptides were capable of achieving a level of complete cell killing within the monitored 60-minutes timeframe, however, considerably faster kinetics were observed for the administration of peptide Rh-C7A-D21K. Moreover, subsequent to cell membrane permeabilization, peptide internalization was less pronounced with NK-2, while intracellular C7A-D21K appearance was finally visible in virtually every cell. This could reflect a somewhat altered mechanism of action of Rh-C7A-D21K as compared to the parent peptide NK-2.

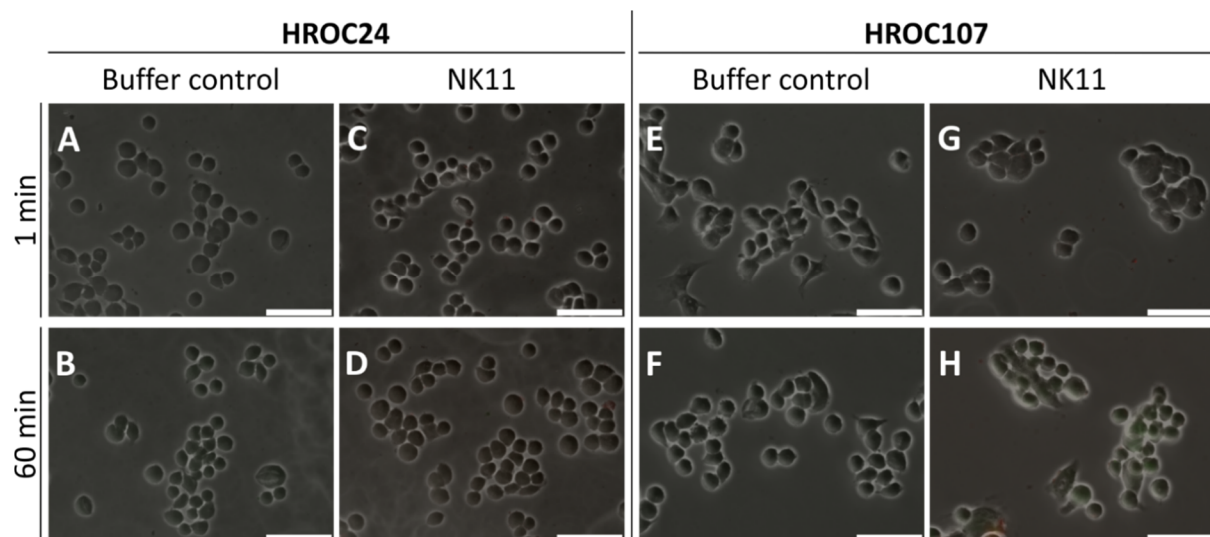


**Figure 5.11: Control treatment of high- and low-PS CRC cells.** Equal counts of HROC24 (A-D) and HROC107 (E-H) cells seeded on glass cover slips were incubated either in PBS only for buffer control (A-B, E-F) or were treated with 10  $\mu$ M of the knowingly inactive NK-2 variant Rh-NK11 (C-D, G-H) for indicated periods of time. Dead cell indication was accomplished by the concomitant incubation of all cell samples in the presence of 3  $\mu$ M Sytox green. Selected images display the outcome of representative experiments for each time point. Scale bars: 50  $\mu$ m.

In control experiments, equivalently prepared cell samples were incubated either with PBS only or with the Rh-conjugated inactive NK-2 derivative Rh-NK11 for identical periods of time. As anticipated, peptide NK11 remained strictly void of activity and accordingly treated cells closely resembled the also non-affected PBS buffer controls. A diffuse red background shimmer was visible in NK11-treated cell samples over the entire imaging period, apparently caused by non-accumulated but freely dissolved Rh-labeled peptide (see figure 5.11).

Finally, in special consideration of the phase contrast images, general morphological differences were observed between both cell types tested. While populations of HROC24 cells appeared to be very homogeneous in terms of a spherical shape and rather narrow size distribution, the dimensions and shapes found with HROC107 cells appeared to be comparably versatile. Here, larger and predominantly rounded morphologies were prevalent, yet, also considerable occurrences of stretched cell shapes were registered. Both CRC cell types grew consistently in monolayers, with HROC107 cells tending to build slightly denser clusters of cells. Overall, such distinctions in cellular appearance and growth behavior were not highly incisive, but still thought to impact on the cumulative surface area accessible for any peptides to interact with. Yet, the major differential responses of HROC24 and HROC107 cells could only be owed to a limited degree to these morphological influences.

### **5.5 Changes in the Surface Zeta Potential of CRC Cells upon Peptide Interaction**

The compensation of the negative cellular Zeta potential was used as a marker to assess binding of selected cationic amphipathic peptides to three distinct CRC cell lines (figure 5.12). For this purpose, samples of these cells were titrated with increasing concentrations of NK-2-derived peptides, melittin or equivalent volumes of the peptide solvent, 0.01% TFA, as buffer control. Cell surface Zeta potentials were determined subsequent to each compound addition step.

Titration of peptides to the CRC cells in all cases led to a dose-dependent decrease of the (absolute) cellular Zeta potential, strongly suggesting peptide binding or at least firm association to the cell membrane. For the interaction of peptides with HROC107 cells, the compensation of the cell surface Zeta potential was consistently reached at comparably higher

peptide concentrations than for the treatment of other cells. This pointed at an obviously weaker peptide interaction with the cell surface of HROC107 cells. Overall, the course of the peptide-induced change in the surface Zeta potential of the commercial reference CRC cell line, namely HCT116, closely resembled the results obtained for HROC24 cells.

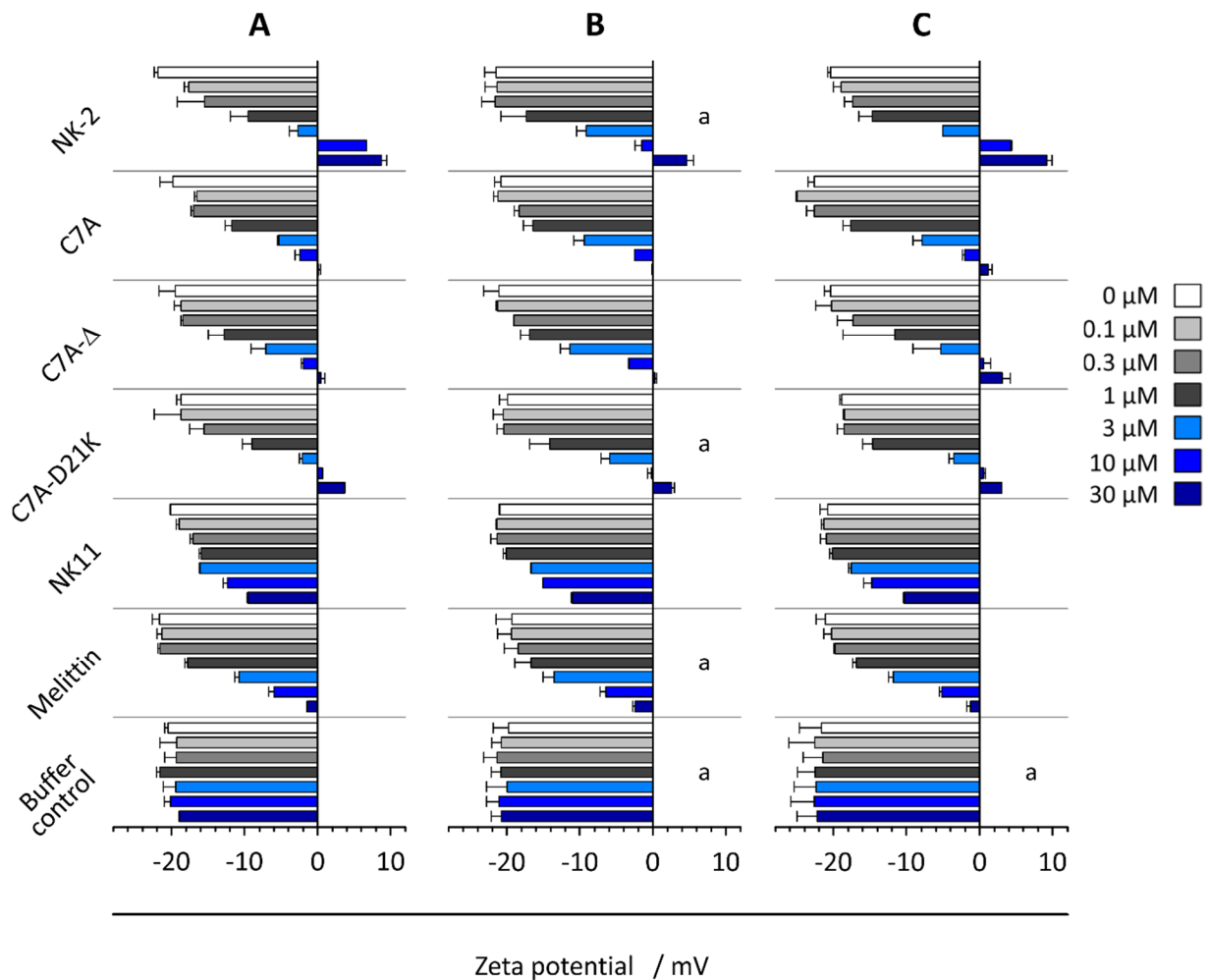


**Figure 5.12: Changes in the surface Zeta potential of distinct CRC cell types upon treatment with selected peptides.** Samples of  $2 \times 10^5$  cells suspended in HEPES buffer (40 mM, pH 7.4) were sequentially titrated with peptides at indicated concentrations (see color key). Results shown comprise cell lines HROC24 (A), HROC107 (B), and HCT116 (C). After each peptide addition step, the cell surface Zeta potential was determined at 25°C in a six-fold repeated measurement cycle (of 20 runs/cycle) with a Zetasizer Nano ZS. In case three or more independent experiments were performed, data represent mean values with standard deviation (a). All other results are given as mean with range.

Recalling parts of the previous findings of this work, it should be emphasized that almost indistinguishable Zeta potentials had been found in the initial untreated state of each cell line. Thus, differential responses to the incubation with NK-2 peptides are supposed to be related to other distinctions in the respective cellular surface constitution. With HROC24 and HCT116 cells being attributably high-PS cell types as opposed to the low-PS HROC107 cell line, Zeta

potential studies strongly supported the cellular surface PS exposure to play a pivotal role. Notably, for the reference peptide melittin only negligible differences in the binding behavior towards distinct cell types were determined, indicating a basically divergent interaction mechanism.

In the investigated peptide concentration range, the phenomenon of overcompensation of the Zeta potential was observed for peptide NK-2 and the three C7A-substitution variants. Ideally, the addition of increasing peptide concentrations to initially negatively charged particles (cells) leads, at some point, to an equilibrium state, where the surface Zeta potential becomes fully depleted ( $\pm 0$  mV). Beyond that point, overcompensation can only be realized when furtherly added peptides bind to or at least firmly associate with the cellular surface void of a considerable Zeta potential. Lacking an electrostatic driving force, such an effect would most probably be established due to hydrophobic interactions. The degree of overcompensation was found to be more pronounced for the treatment of CRC cells with peptide NK-2 than with any other peptide assessed. In fact NK-2 was the only peptide to unequivocally overcompensate the Zeta potential of high-PS HROC24 and HCT116 cells already at 10  $\mu$ M. This is especially of note as the net charge of variant C7A-D21K (+12) is even higher than that of NK-2, C7A and C7A- $\Delta$  (all +10). Adding to this, the change in the cellular Zeta potential after incubation with melittin was stronger than after treatment with NK11, although both peptides possess an identical net charge (+6). These observations underline that the phenomenon of Zeta potential compensation is not simply driven by stoichiometric summation of charges. Instead, peptide-specific interactions with particular cellular surface structures are apparently important.

Of note, with none of the investigated cell types the addition of TFA (buffer control) led to any changes in the surface Zeta potentials, thus observed effects were considered explicitly peptide-induced.

## 5.6 Changes in Liposomal Size and Zeta Potential upon Peptide Interaction

Complementary to the cell-based experimental series described above, also the binding behavior of selected peptides to liposomal membranes was studied. As opposed to the highly polydisperse cellular samples, here, quite homogeneous particle size distributions were achieved. The well-established preparation of defined unilamellar lipid vesicles enabled a reliable determination of mean particle diameters in addition to the respective surface Zeta potentials.

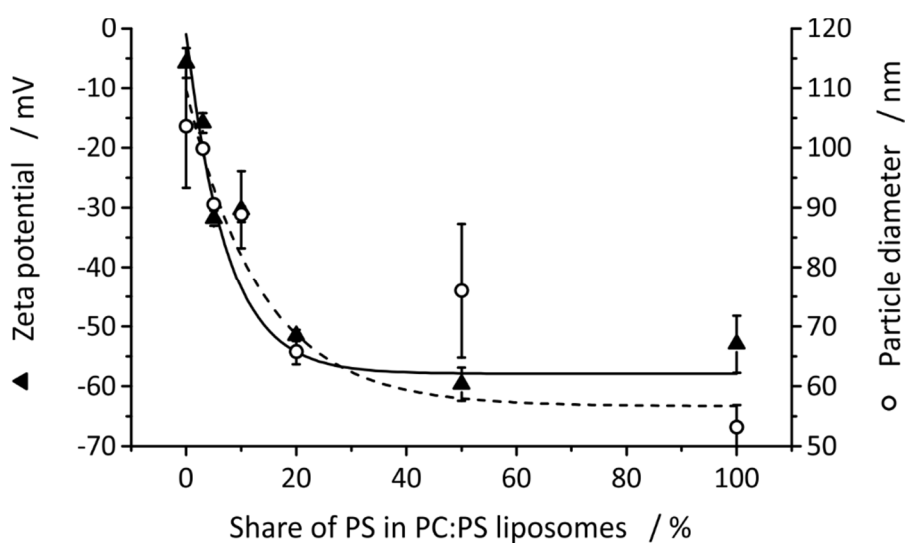


**Figure 5.13: Average size and Zeta potential of liposomes composed of PC and PS in various proportions.** Particle diameters (open circles) and Zeta potentials (filled triangles) were assessed by DLS measurements on a Zetasizer Nano ZS. Given are mean values with range. For perceptibility, fittings were done according to an exponential decay function as indicated by dashed and solid lines for size and Zeta potential determinations, respectively.

Results given in figure 5.13 depict obtained average dimensions and surface Zeta potentials of PC:PS liposomes of distinct phospholipid ratios before adding any peptides. Basically, both parameters were found to decrease with increasing shares of PS in the overall lipid composition. Determined values ranged from pure L- $\alpha$ -PC vesicles with a mean diameter of about 103 nm and an only slightly negative potential of  $-5$  mV, to purely L- $\alpha$ -PS-constituted liposomes of about half the size (ca. 53 nm) and a pronounced negative Zeta potential (ca.  $-53$  mV). Of note, considering the standard deviations of the measurements, the average size and Zeta potentials of liposomes containing 20, 50, or 100 % PS were found to possess similar characteristics, which is reflected by the plateau state reached in the exponential decay fitting.

The reduction of the liposomal Zeta potential was comprehensibly explainable, as a higher portion of anionic charge was introduced upon elevation of the PS content. However, the concomitant decline in the average particle diameter was less obvious. It might be suggested that raising the PS portion in the overall membrane lipid composition could have led to enhanced repulsive forces between the lipid head groups inducing intensified curvature strain, thus, yielding smaller average particle diameters.

Putative alterations in both investigated parameters were studied by DLS-based Zetasizer measurements for the sequential titration of vesicles of distinct lipid compositions with NK-2-derived peptides (and controls). Roughly, apart from NK11, all NK-2 variants were basically found to be capable of provoking an overcompensation of the liposomal surface Zeta potential, regardless of the actual membrane composition (see figure 5.14). Here again, just like with cells, NK-2 showed the strongest overcompensation behavior, while no Zeta potentials  $\geq 0$  mV were obtained for NK11.

In the applied concentration range, NK11 was the only peptide apparently not interacting with liposomes exclusively made of PC (figure 5.14, column A), as considerable changes were neither observed in the average particle dimensions nor in the Zeta potentials. All other peptides were found to increase the Zeta potential of PC liposomes about proportional to the amount of peptides added. This was reflected by a consistent (log) linear change in the corresponding potential, suggesting at least a partial association of peptide molecules to the liposomal surface. Yet, no alterations of the average diameter of PC liposomes were found with any of the peptides.

Instead, regarding liposomes being partially or completely made of PS (columns B-D), an irregular pattern was observable: In reaction to the first peptide titration steps (up to  $0.3 \mu\text{M}$ ), only minor increases in the Zeta potential values were achieved, regardless of the particular peptide added. However, at a certain molarity range, peptide addition typically led to an abrupt, disproportionate rise in the Zeta potential. This pointed at some kind of transition in the peptide-membrane interaction behavior and was generally found at peptide molarities  $\geq 1 \mu\text{M}$ .

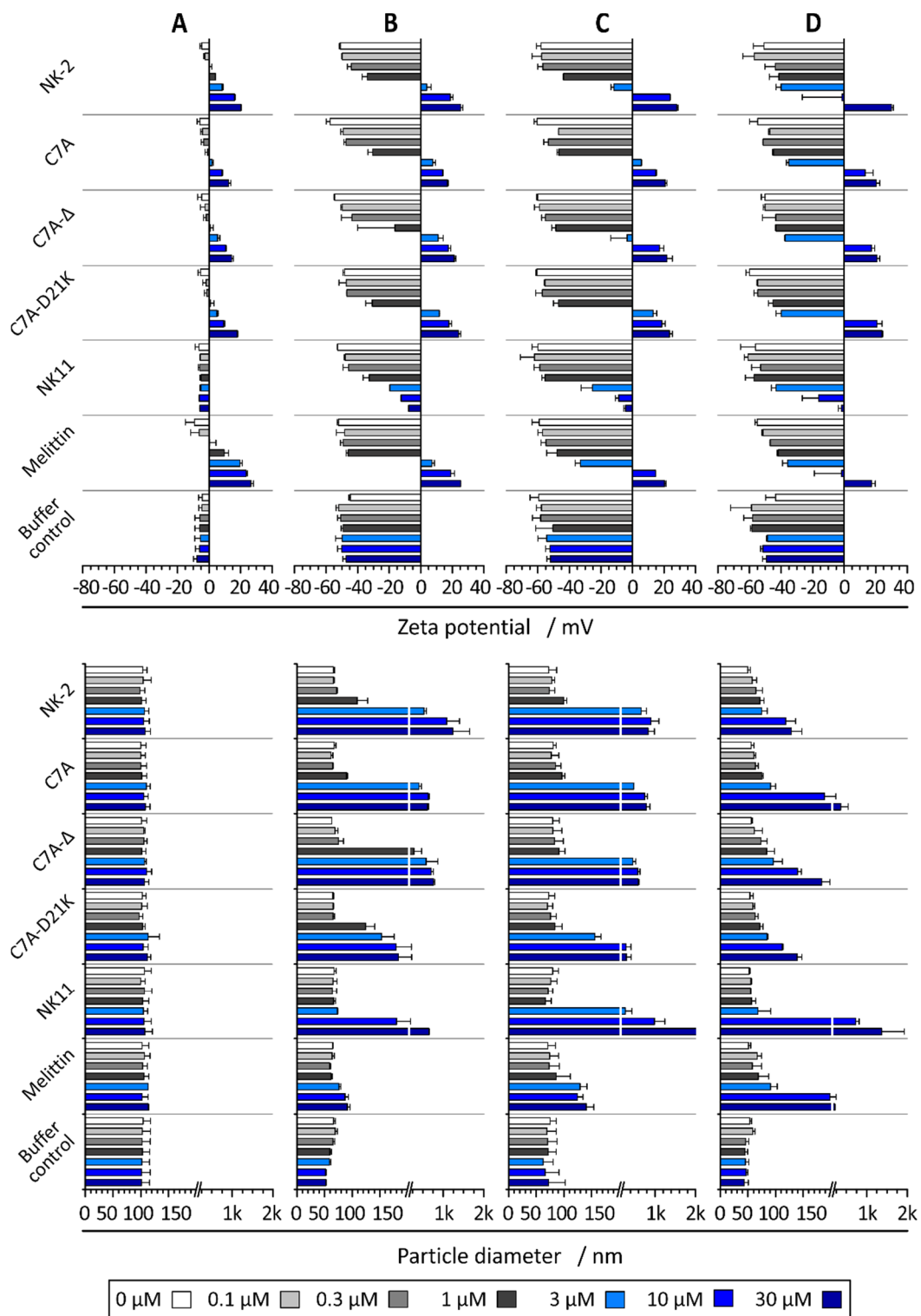


**Figure 5.14: Changes in Zeta potential and size of liposomes upon treatment with selected peptides.** Liposomes (50  $\mu$ M) made of PC only (A), PC:PS-mixtures at ratios of 80:20 (B) or 50:50 (C), or PS only (D) were titrated with progressive concentrations (see color key) of indicated peptides as well as equivalent volumes of 0.01 % TFA (buffer control). Prior to the first as well as after each peptide addition step, the Zeta potential (upper panel) as well as the liposomal size (bottom panel) were determined on a Zetasizer Nano ZS in six- and three-fold repeated measurement cycles, respectively. Data represent mean values with range from a minimum of two independent experimental series. For the depiction of size determination results, a break was introduced to the x-axis at a value of 200 nm, with labeling increments of 10 and 200 nm (minor ticks) before and after the break point, respectively.

Apparently, such a sharp change in the surface Zeta potential (by typically  $\geq +30$  mV to values mostly  $\geq -10$  mV) coincided with an increase of the mean lipid vesicle particle size. This marked enlargement was differentially pronounced, but loosely related to the portion of PS in the membrane lipid composition. The higher the share of PS, the more peptide was needed to induce such an extensive and abrupt change in the Zeta potential and particle diameter.

It is suggestive that in case the liposomal Zeta potential was reduced to a certain level, repellent forces between the poorly net-charged particles became too small to sustain a stable suspension. Consequently, the probability of aggregation events would have increased, and potentially formed aggregates could have provided platforms also for interactions with hydrophobic regions of amphipathic peptides. In resemblance to the observations made with CRC cells, this, in turn, could promote the phenomenon of overcompensation. Finally, huge particles have been constituted with considerable positive Zeta potentials. As both Zeta potential and size determinations are based on DLS measurements, such tremendously enlarged particles contributed disproportionately strong to the calculated cumulative results (scattered light is proportional to the 6<sup>th</sup> power of the particle radius).

Interestingly, also titration with peptide NK11 led to the formation of enlarged particles, though no marked drop in the Zeta potential was observed with this NK-2 variant. Probably, the association of peptide NK11 to the particle surface was considerably less firm than with other peptides. Hence, upon application of an electrical field, comparably fewer molecules could have endured the arising shear forces to reside within the slipping plane around the moving particle. Nonetheless, as no forces were applied during size determinations, even the less tightly associated NK11 molecules could have promoted particle aggregation processes at least at higher peptide molarities.

Of note, liposomes made of zwitterionic PC only did not show any aggregation effects – neither at their low initial Zeta potentials of around  $-5$  mV in the untreated state, nor during any state of peptide-induced (over)compensation of the surface potential. This implicates that the level of surface charge was not the (sole) determinant parameter leading to liposome aggregation. Instead, the preceding binding of amphipathic peptides seems to be mandatory to mediate or at least initiate the particle growth. And this required association of peptides was obviously dependent on the presence of a certain share of anionic PS on the liposomal surface.

It should be pointed out that such tremendous increases in size had not been observed for the titration of peptides to cells. Although the pronounced polydispersity of such biological samples prevented the determination of a size distribution based on DLS measurements, cell samples were occasionally checked by visual means under a phase contrast lab microscope. In this regard, neither cellular debris nor aggregates were observable (not shown).

## 5.7 Membrane Intercalation of NK-2 Peptides

Peptide integration into phospholipid membranes composed of natural PC, PS and a 90:10 mixture thereof was assessed by a FRET pair probe dilution assay. Membrane intercalation of peptides was monitored by fluorescence spectroscopy as the increase of the ratio of donor to acceptor emission intensity (FRET signal) in dependence on time.

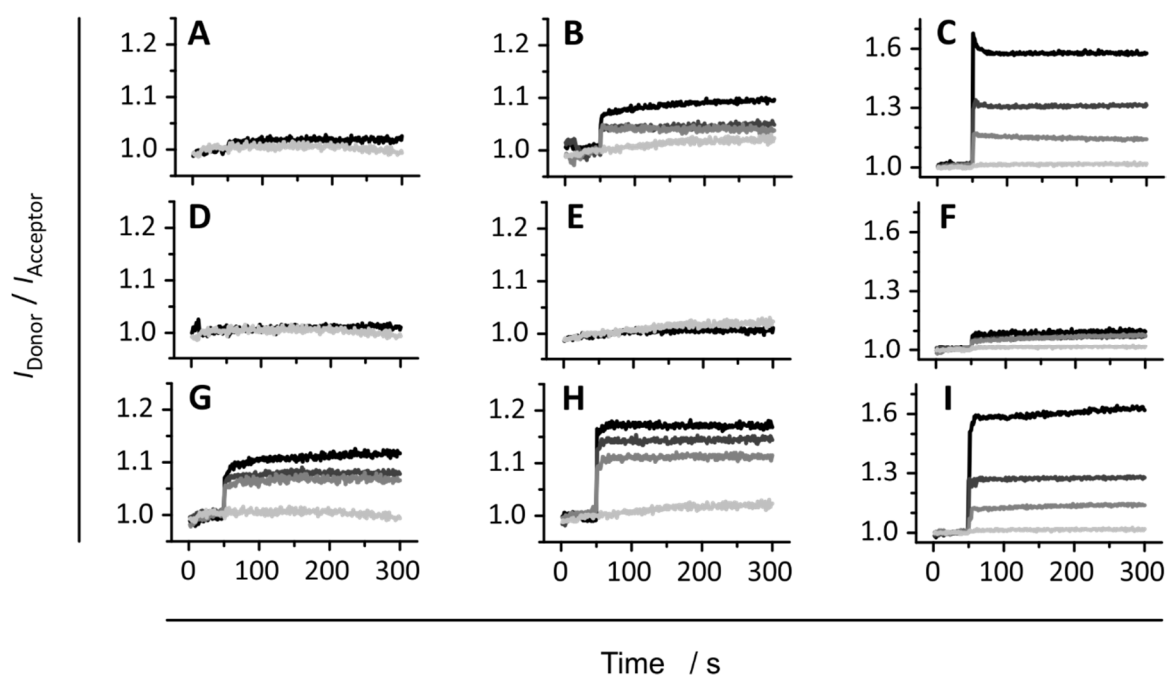


**Figure 5.15: Membrane intercalation of selected peptides as probed by FRET spectroscopy.** Representative data sets depicting the FRET signals upon peptide addition to liposomes (10  $\mu$ M total lipid concentration) made of PC only (left column), a mixture of PC and PS at a ratio of 90:10 (center column), and PS only (right column). The liposomes were double-doped during preparation with 1 % each of Rh- and NBD-coupled phosphatidylethanolamine. Treatment comprised the addition of peptides NK-2 (A, B, C), NK11 (D, E, F), and melittin (G, H, I) at different concentrations: 0.2  $\mu$ M (grey), 0.4  $\mu$ M (dark grey), and 0.8  $\mu$ M (black). Peptides were added from 100- $\mu$ M-stocks in 0.01 % TFA at time point 50 seconds. Accordingly, each preparation was controlled for solvent effects using a volume of 0.01 % TFA equivalent to 0.8  $\mu$ M (light grey). All measurements were carried out at 37°C with excitation at 470 nm and simultaneous detection of donor and acceptor emissions at 531 and 593 nm, respectively.

Figure 5.15 exemplarily displays the typical outcome of selected FRET experiments. In principle, the degree of membrane intercalation was dependent on the peptide concentration, as well as on the presence and amount of PS found in the liposomal membrane composition.

The representative data sets depict typically observed peptide-specific differences:

For parent peptide NK-2 no considerable FRET signal changes were obtained after addition to zwitterionic PC liposomes (A), reflecting a lack of membrane insertion. By contrast, the abundance of PS in the membrane lipid composition promoted NK-2 intercalation, as moderate to extensive FRET signal enhancements of up to ~10 and ~60 % were observed upon peptide addition to liposomes made of PC:PS = 90:10 (B) or 100 % PS (C), respectively. In comparison, peptide NK-2's shortened derivative NK11 (C-E) did not lead to substantial changes in the FRET signal. A maximum response of around 10 % FRET increase was obtained for the highest peptide molarity with pure PS liposomes. Thus, NK11 was considered to feature basically poor membrane insertion abilities. Instead, melittin already showed substantial concentration dependent insertion into PC membranes (G) with up to ~12 % increased FRET signals upon peptide addition. Slightly enhanced melittin-induced FRET signal changes with a maximum of about 18 % were observed for PC:PS (90:10) liposomes (H). This rather poor difference pointed at a minor influence of PS on the membrane intercalation behavior of peptide melittin. Overall, liposomes purely made of anionic PS obviously allowed for the largest extents of peptide intercalation. With a FRET signal enhancement of up to ~60 %, melittin (I) was found to insert into PS membranes as effective as NK-2 (C).

In a simplified scheme, the membrane insertion behaviors of peptides NK-2 (A-C), NK11 (D-F), and melittin (G-I) could be characterized as clearly PS-correlated, poorly selective and weak, as well as hardly selective but strong, respectively.

In principle, the findings described above for the exemplary data sets could be transferred to the more comprehensive investigations which enclosed 30 peptides in total. Corresponding results were summarized in figure 5.16. For the sake of comparability, the mean percent increase in FRET signal was calculated in relation to a peptide molarity of 0.8  $\mu\text{M}$ .

Overall, NK-2-derived peptide variants inserted very poorly into zwitterionic PC liposomes. At the highest peptide molarities the median FRET increase was as low as 2.5 %, with a minimum and maximum percent signal change of 0.5 and 10.3 %, respectively.

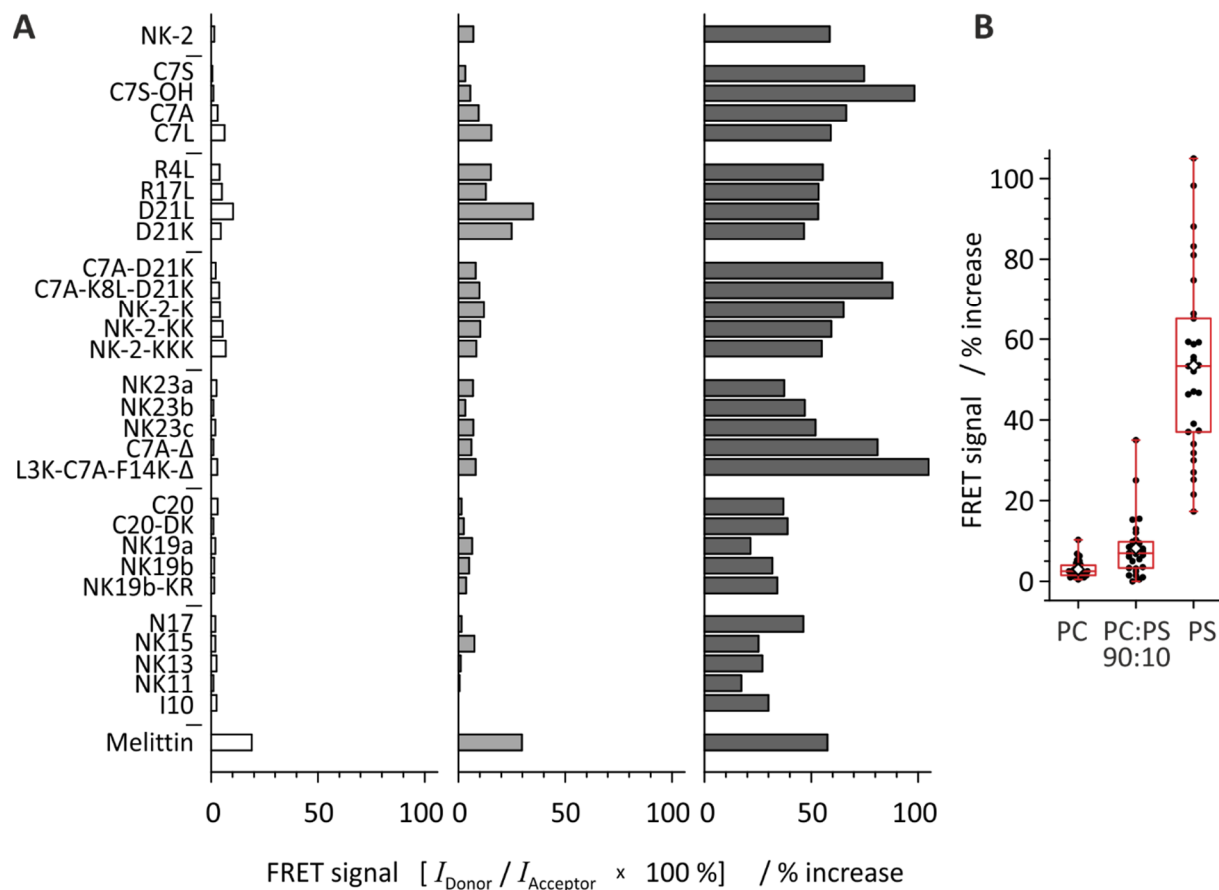


**Figure 5.16: Peptide intercalation into liposomal phospholipid membranes determined by probe dilution FRET experiments.** (A) Liposomes (10  $\mu$ M total lipid) were made of either PC (white), PS (dark grey), or a mixture of PC and PS at a molar ratio of 90:10 (grey). For FRET pair labeling, liposomes were prepared together with phosphatidylethanolamine conjugated with either NBD or Lissamine-Rhodamine (1 mol-% each) as donor and acceptor dyes, respectively. Double-doped liposomes were independently treated with 0.2, 0.4 and 0.8  $\mu$ M of the indicated peptides at 37°C. Given values represent percent changes in the FRET signal, i.e. the emission intensity ratio of donor ( $I_{\text{Donor}}$ ) to acceptor ( $I_{\text{Acceptor}}$ ), after excitation at 470 nm and simultaneous detection at 531 nm and 593 nm. Any results shown were calculated in relation to a peptide concentration of 0.8  $\mu$ M. Box plots in (B) summarize the distribution of these numeric results. From top to bottom, horizontal lines represent upper quartile, median, and lower quartile, respectively. Bars indicate maximum and minimum values. The arithmetic mean over the distributions is reflected by a black open diamond symbol. Of note, results for peptides C7A, C7A- $\Delta$ , C7A-D21K, and NK11 have been partially used in the publication of Maletzki and co-workers (2014), while melittin results were calculated in consideration of data already published by Hanulova et al. (2009).

Apparently, liposomal membranes became more susceptible to peptide integration when containing a share of 10 % PS. Yet, peptide-specific differential responses were observed with this membrane composition. On the one hand, the majority of NK-2 variants induced roughly three- to five-fold increased FRET signals as compared to the responses upon their addition to PC liposomes. As an interesting fact, the membrane insertion improvement of the Cys-7

substitution variants correlated nicely with the hydrophobicity of their respective substituent residue, i.e. C7L > C7A > NK-2 > C7S. Altering NK-2's sole negatively charged aspartic acid in variants D21L and D21K yielded derivatives of decisively enhanced intercalation ability. On the other hand, several derivatives did not exhibit considerably improved membrane insertion. Especially, most of the extensively shortened variants of the parent peptide NK-2 (e.g. I10, NK11, NK13, NK15, C20, C20-DK) apparently lacked the ability to induce a noteworthy FRET signal enhancement.

For the interactions of peptides with liposomes purely made of natural PS, these tendencies were basically confirmed. Yet, a marked increase of the FRET signal was consistently observed. With this membrane constitution, even variants I10 or NK11 induced substantial FRET signal changes. Putatively, the high density of negative charges on the liposomal membrane surface solely constituted by PS exerted strong electrostatic attraction forces on the cationic peptides. Consequently promoted firm peptide association could potentially lead to a similar shift in the FRET signal without necessarily being owed to a peptide insertion into the lipid bilayer.

In conclusion, it could be stated that the presence and abundance of the anionic membrane lipid constituent PS had a strongly positive influence on the membrane insertion ability of all peptides. Explicitly, most NK-2-derived peptide variants demonstrated a selective membrane intercalation into PS-comprising membranes. This tendency is underpinned especially in comparison to the reference peptide melittin, which exhibited only minor selectiveness towards the membrane composition.

### 5.8 Peptide Orientation upon Membrane Intercalation

Tryptophan fluorescence experiments were carried out in the absence and presence of liposomes constituted of different shares of PC and PS. Three distinct single-Trp variants of NK-2, termed I2W, F14W, and G25W with amino acid residue substitutions to tryptophan in close-to-amino-terminal, mid-structure, and close-to-carboxy-terminal positions, respectively, were used as test probes. In addition, the natural single-Trp (Trp-19) peptide melittin served as a reference. The so called blue shift represents a measure for the hydrophobicity of the solvent environment in close proximity to the tryptophan side chain. The larger the blue shift, the better a given tryptophan residue is shielded from the surrounding aqueous phase.

Consequently, for the applied experimental setup, a large blue shift indicated a more pronounced integration of the respective part of the molecule into the hydrophobic core of the lipid bilayer and *vice versa*.

In general, the results given in figure 5.17 revealed two clear tendencies. First of all, the degree of intercalation of any tested peptide appeared to be strongly correlated to the share of PS found on a given membrane. However, secondly, obvious differences were observable in comparison of the intercalation characteristics of each single-Trp peptide.

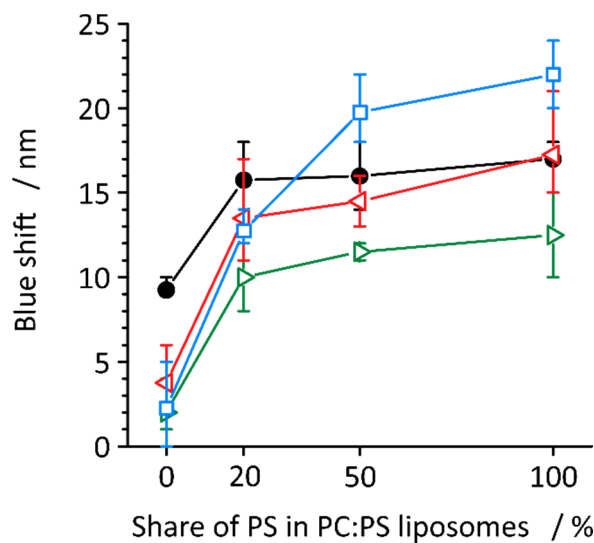


**Figure 5.17: Blue shift of the wavelength at maximum tryptophan fluorescence intensity after incubation of PC:PS liposomes with peptides.** Single-Trp residues from NK-2-derived peptides I2W (red), F14W (blue), and G25W (green), as well as melittin (black) served as intrinsic hydrophobicity sensors. The molar peptide-lipid ratio was set to 1:15 in buffer A. All measurements were carried out at 37°C. Resulting raw data were corrected for the contribution of light scattering in the presence of vesicles (spectra of liposomes in buffer served as reference). Post-experimental spectra processing enabled the reproducible determination of signal peaks of maximum emission intensity. Depicted are mean blue shifts from experiments done in duplicates and performed independently at least twice. Bottom and top error bars represent minimum and maximum blue shifts, respectively.

Melittin was found to be the only tested peptide clearly integrating into zwitterionic liposomal membranes solely made of PC (blue shift ~10 nm). This stressed, once again, the effective but vastly unselective membrane interaction of the reference peptide. For negatively charged membranes, the intercalation depth of melittin apparently increased substantially leading to an about 1.5-fold higher blue shift. However, the degree of membrane interaction remains almost invariant, irrespective of the amount of PS present in a membrane, clearly reflected by the blue shift stagnating at a steady level of around 16 nm.

In contrast to this, none of the three single-Trp variants of NK-2 was found to integrate considerably into purely zwitterionic PC membranes. Upon increasing the share of PS in the membrane total lipid composition, the derivatives demonstrated differential membrane intercalation characteristics. Generally speaking, all NK-2 variants experienced substantial increases of their respective intercalation depths in relation to the membrane PS content. Yet, both the amino-terminal peptide moiety (I2W) and, especially, the mid-part (F14W) were found to integrate to a considerably higher extent than the close-to-carboxy-terminal part of NK-2 (G25W). Finally, upon interaction with liposomal membranes made of PS only, the mid-structure tryptophan present in F14W induced the highest blue shift (~22 nm), followed by the close-to-amino-terminal Trp-exchange variant I2W (~17 nm) and G25W (~12.5 nm). Nevertheless, at a lower PS content of 20 % of the total membrane lipid, the mid-structure and amino-terminal segments of NK-2 integrated to very similar extents.

### 5.9 Peptide-Induced Permeabilization of PS-Comprising Membranes

The capability of selected peptides to permeabilize PS-containing lipid vesicle membranes was exemplified in two distinct proof-of-principle experimental approaches: (i) The peptide-induced release of the membrane-impermeant dye calcein encapsulated in such vesicles at self-quenching molarities, as well as (ii) the fluorescence quenching of NBD-labels on the inner liposomal surface upon peptide-induced internalization of potassium iodide. Figure 5.18 representatively illustrates the differential effects exerted by peptides NK-2, C7A-D21K, NK11, and melittin using liposomes consisting of PC and PS at equal shares.

Most prominently, in both setups C7A-D21K provoked a more than two-fold higher response than the parent peptide NK-2 itself, which underpinned the superior activity of the double-substitution derivative. The non-NK-2-related reference melittin was apparently the most effectively permeabilizing peptide, inducing a calcein release rate and percent NBD-quenching of approximately 80 % and 65 %, respectively, which is about twice and thrice as much as obtained with C7A-D21K. In despite, peptide NK11 remained void of considerable permeabilization activity even at a three- to ten-fold higher peptide molarity than applied for all other peptides. Furthermore, both experimental approaches enclosed buffer control

measurements (0.01 % TFA), with none of which considerable membrane permeabilization effects became evident (not shown).

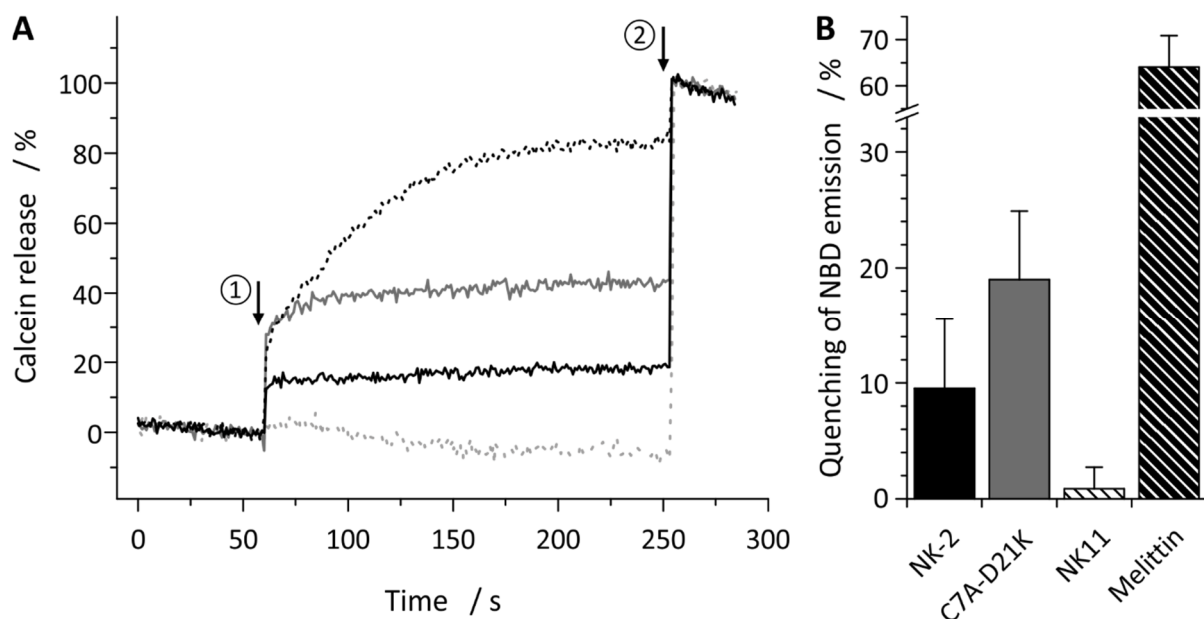


**Figure 5.18: Peptide-induced permeabilization of phospholipid liposomes.** Given data represent exemplary results from two distinct experimental approaches to assess the membrane permeabilization by peptides NK-2 (black), C7A-D21K (grey), NK11 (dashed grey line / black-hatched white column), and melittin (dashed black line / white-hatched black column). In both cases, liposomes composed of PC and PS at equal shares were used. (A) Leakage of liposome-encapsulated calcein was induced by the addition of peptides after about 60 seconds (①) at concentrations of 0.3  $\mu$ M (all but NK11) or 3  $\mu$ M (NK11), respectively. Full leakage was accomplished by adding 0.2 % Triton X-100 (②). The release rate at room temperature was followed over time after excitation at 495 nm and fluorescence emission detection at 513 nm. (B) Fluorophore emission intensity was quenched by potassium iodide before and after incubation of NBD-labeled liposomes with peptides at concentrations of 1  $\mu$ M (all but NK11) or 3  $\mu$ M (NK11), respectively. Here again, complete permeabilization was achieved by the addition of Triton X-100. Measurements were carried out at 37°C and emission signals were detected at 531 nm after excitation at 470 nm. Error bars represent standard deviations from three independent experiments.

Of note, in dye release experiments, a sharp signal increase was observed immediately after the addition of peptides NK-2 and C7A-D21K to calcein-encapsulating vesicles (see panel A). Here, the steady state level of the peptide-specific maximum dye release was typically reached in less than 30 seconds reflecting very rapid interaction kinetics. With peptide melittin instead, completion of the calcein leakage process was achieved much slower ( $\geq 150$  seconds after peptide addition), which clearly pointed at a divergent underlying mechanism of action.

## 5.10 Structure-Function Analyses

The previously determined sequence- (net charge  $Q$ , mean hydrophobicity  $H$ ) and structure-inherent (hydrophobic moment  $\mu H$ ) physicochemical properties of peptide NK-2 and its variants were brought into context with functional data from biological and liposome-based experiments.

The peptide concentration needed to diminish the metabolic activity of PC-3 human prostate cancer cells to 50 % ( $IC_{50}$ ) was comprehensively investigated for all 34 NK-2-related peptides by an MTT assay under PBS buffer conditions. Accordingly identified values served as a quantitative marker for peptide-specific anti-cancer cell activities. The  $IC_{50}$  values of peptides void of detectable activity in the scrutinized molarity range were arbitrarily set to 500  $\mu M$  (i.e.  $\gg 100 \mu M$  as in table 5.3). Of note, preference was given to MTT results achieved under PBS conditions as the limited number of peptides active in complete medium would have been too restrictive in the context of structure-function analyses. Complementary, the intercalation abilities of 29 of these peptide variants were assessed by a FRET probe dilution approach considering three distinct membrane compositions. The mean signal increase (percent FRET increase) calculated in relation to a peptide molarity of 0.8  $\mu M$  was likewise used for correlations with calculated parameters.

Overall, this enabled the investigation of potential interrelationships of more than 100 distinct combinations of functional and sequence-related data sets. Here, selected interdependencies and general tendencies are to be presented, representatively contrasted by clearly non-correlated factors.

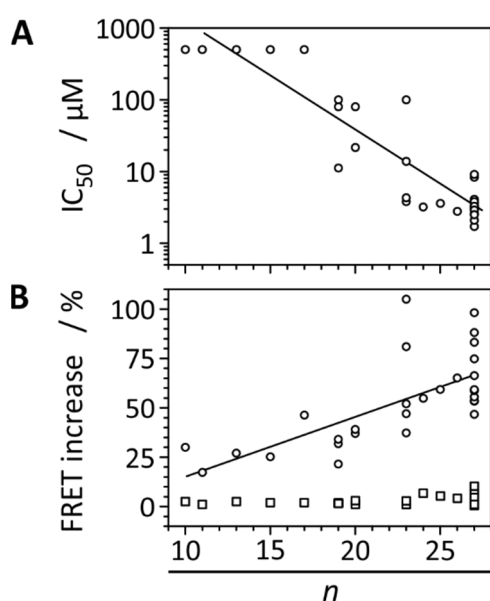


**Figure 5.19: Correlation of the anti-cancer cell activity and membrane intercalation properties of NK-2 derivatives with the peptide sequence length.** The total residue count ( $n$ ) was compared to (A) the log of peptide-specific mean  $IC_{50}$  values against PC-3 human prostate cancer cells deduced from MTT tests under PBS/medium conditions, as well as to (B) the peptide-induced FRET signal change obtained from probe dilution assays upon incubation of peptides with lipid vesicles made of either PS (open circles) or PC (open squares). Each symbol represents a single peptide.

First of all, as is perceptible from figure 5.19, NK-2 variants featuring less than 19 amino acid residues did generally not exert activity against PC-3 prostate cancer cells. Moreover, the efficiency of peptide intercalation into PS membranes, as determined by FRET probe dilution assays, tended to be facilitated with larger peptides, though the relation was less clear. Generally speaking, the applied semi-log linear fit is to be considered rather ambiguous due to the overall wide distribution of ordinate values, and the disproportionately high frequency of 27-residue peptides. As the extent of interaction of peptides with zwitterionic PC membranes was very low in general, no correlation could be deduced in this regard.

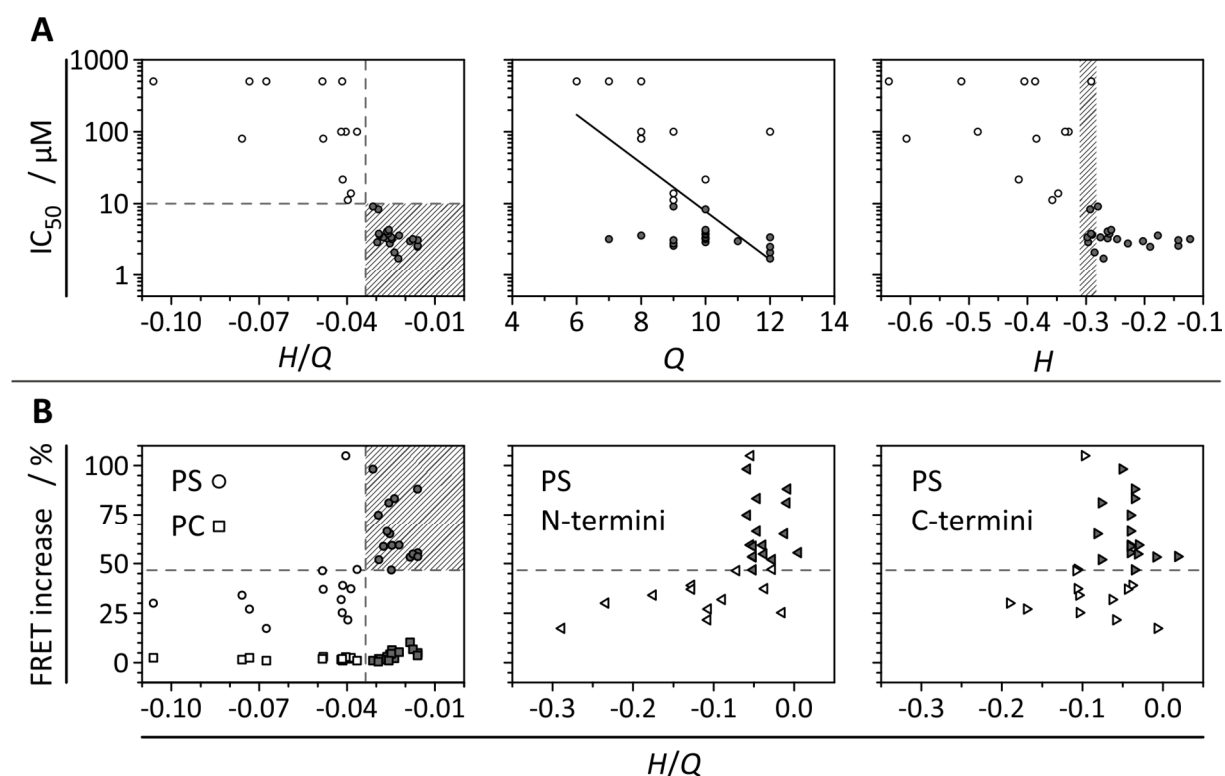


**Figure 5.20: Correlation of peptide-specific functional data with the net charge and the mean hydrophobicity.** Each symbol represents a single peptide with grey filled symbols indicating peptides with pronounced anti-cancer cell activity (i.e.  $IC_{50} \leq 10 \mu M$ ). Panel A illustrates interdependencies of the log of the peptide-specific mean  $IC_{50}$  values against PC-3 human prostate cancer cells deduced from MTT tests under PBS conditions with the calculated average peptide hydrophobicity ( $H$ ), its net charge ( $Q$ ), as well as the ratio of both parameters ( $H/Q$ ). Panel B depicts the relation of the very same physicochemical peptide properties with the corresponding percent signal increase derived from FRET-based probe dilution experiments done in the presence of liposomes made of either PS (open circles) or PC (open squares). For the former, additionally, the distribution of  $H/Q$  ratios is given calculated separately for the amino- (left-pointing open triangles) and carboxy-terminal (right-pointing open triangles) peptide sequence moieties.

Apart from this, most strikingly, a critical value of around  $-0.03$  in the ratio of each peptide's mean hydrophobicity to net charge ( $H/Q$ ) could be identified providing a quite sharply

defined threshold below which peptides did not exert potent anti-cancer cell activity. The separate influences of both contributing parameters were differential: While no clear dependency was perceptible for the peptide's net charge alone, a disadvantageous impact of extremely low overall hydrophobicity ( $\leq -0.3$ ) became evident (see figure 5.20, panel A).

Although less dominantly, the  $H/Q$ -related threshold also seemed to play a crucial role for the ability of the peptides to intercalate into liposomal membranes (figure 5.20, panel B). For the ensemble of highly insertive peptides, a substantially narrower distribution of the  $H/Q$  parameter was observed in the amino- than in the carboxy-terminal sequence moieties. Yet, this relation was clearly unidirectional, as, in reverse, also comparably poorly intercalating peptides were found in the respective segment-specific  $H/Q$  ranges. Moreover, for particular peptide variants the hydrophobicity-to-net-charge ratio critically influenced the PS-selectivity of their insertion into lipid bilayers as they hardly change the FRET signal with PC liposomes but belong to the peptides which induced highest signal increases with PS lipid vesicles.

Both PC-3-related  $IC_{50}$  values and FRET signal increases were observed to be grossly independent from the peptide amphipathicity. This was exemplified in figure 5.21 for average ( $\mu H_{\text{mean}}$ ) as well as local peak ( $\mu H_{\text{max}}$ ) hydrophobic moments (i.e. the vector sum of hydrophobicity assuming a continuous  $\alpha$ -helical secondary structure) determined for complete peptide sequences, but held true likewise when N- and C-terminal moieties were considered separately (not shown). Nevertheless, peptides for which effective anti-cancer cell activity was observed possessed consistently high mean hydrophobic moments in a range of 0.7 to 0.85, combined with a narrowly defined 7-residue maximum moment of around 1.03 to 1.08. However, a reverse connection of amphipathicity to the log of  $IC_{50}$  and, especially, to the FRET signal could not be inferred, thus, no clear correlation was deducible between peptide-specific hydrophobic moments and either anticancer activity or intercalation behavior.

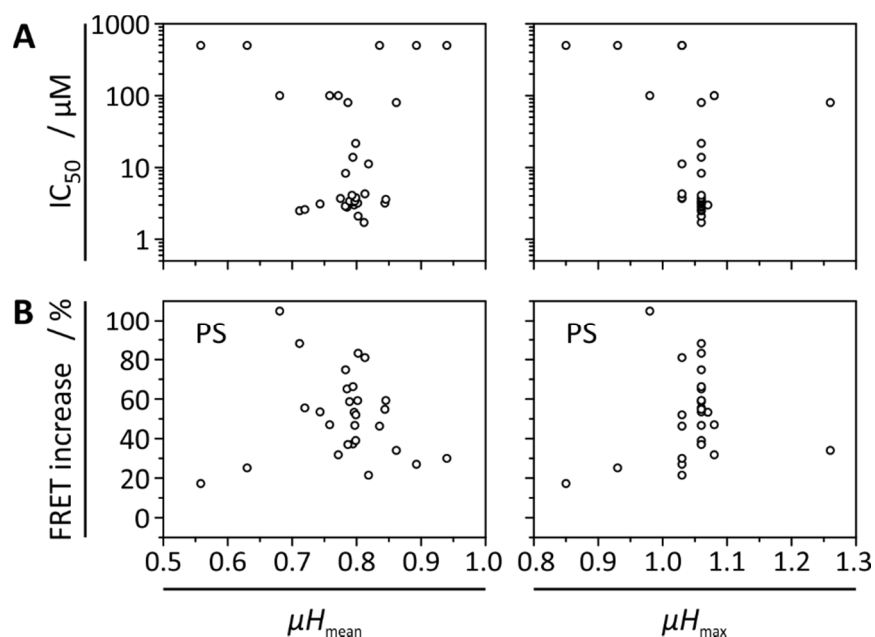


**Figure 5.21: Interdependencies between functional data and the peptide amphipathicity.** As a measure of amphipathicity, hydrophobic moments were calculated over a sliding window of 7 amino acid residues for all peptides presuming the adoption of a continuous  $\alpha$ -helical secondary structure based on the Normalized Consensus hydrophobicity scale. The moment value of the segment of highest hydrophobic moment ( $\mu H_{max}$ ) and the moment average over all 7-residue segments ( $\mu H_{mean}$ ) were compared with (A) the log of the peptide-specific mean  $IC_{50}$  values against PC-3 cancer cells deduced from MTT cytotoxicity tests under PBS/medium conditions and (B) the peptide-induced percent signal increase in FRET probe dilution assays using fluorescently double-doped liposomes made of PS. Each symbol (open circle) represents a single peptide.

In summary, apart from a roughly proportional relation with the peptide sequence length, overall no clearly linearly interdependent combinations of functional data and calculated structural peptide parameters were found – neither for complete sequences nor the separate scrutiny of amino- and carboxy-terminal peptide moieties. Instead, defined threshold areas or value ranges of particular physicochemical peptide properties could be identified as being vital for PS-selective membrane intercalation and, especially, anti-cancer cell activity. The overall sequence hydrophobicity ( $H$ ) was of basic importance, yet, the determining influence on the peptide functionality became strikingly pronounced when the corresponding net charge was taken into account additionally ( $H/Q$ ).

### 5.11 Cumulated Selectivities as a Measure of a Peptide's Anticancer Potency

Inferring from the various function-related data experimentally determined for the ensemble of distinct peptides, figure 5.22 summarizes crucial findings regarding the peptide-specific selectivity for cancerous cells as well as for the membrane abundance of PS. This approach was followed in order to narrow down the group of NK-2-derived peptides by identifying the most promising candidates.

In a first step, a so called cumulated selectivity value (CSV) was determined for each peptide. The CSV additively concatenates the selectivity factors deduced from (i) the ratio of peptide-specific  $IC_{50}$  values against HaCaT (low-PS human normal keratinocytes) over PC-3 (high-PS human prostate carcinoma) cells under complete medium conditions (grey columns), as well as from (ii) the FRET signal increase induced upon peptide incubation with liposomes made of a 90:10 mixture of PC and PS over the signal change with purely PC-constituted liposomes (red columns).

Accordingly sorted, this plot ranks the set of peptides in the order of decreasing cumulated selectivity. However, in this type of representation only the relative performance of the peptides is reflected. Hence, focusing on the aims of this thesis, the CSV of each peptide was additionally weighted by the corresponding level of anti-cancer cell activity under complete medium conditions. This was accomplished by dividing the CSV by the peptide-specific mean  $IC_{50}$  against PC-3 cells in medium to yield an activity-weighted cumulated selectivity value, termed A-CSV. The use of this weighted measure of each peptide's anti-cancer cell performance is well-exemplified by the lead structure peptide NK-2. It exhibited good selectivity for PS-comprising membranes as well as for cancerous over normal human cells. However, NK-2's poor activity in complete medium (with a mean  $IC_{50}$  against PC-3  $\approx 80 \mu\text{M}$ ) is adequately reflected by a very low A-CSV, which was normalized to equal 1.0 in order to easily express higher and lower values as multiples and fractions of it, respectively.

The essence of this evaluation approach is to identify the most promising peptide candidates for potential therapeutic use or further development. In fact, the number of such candidates concomitantly exerting potent anti-cancer cell activity in medium combined with high selectivity for PS-bearing membranes as well as for cancerous over normal human cells was successfully limited to a small group of NK-2-derived peptides. Namely, these variants

## Results

enclosed peptides C7A (A-CSV = 8.0), C7A- $\Delta$  (17.7), C7L (20.1), C7A-M11L-D21K (21.7), C7A-K8L-D21K (24.9), as well as C7A-D21K (26.2).

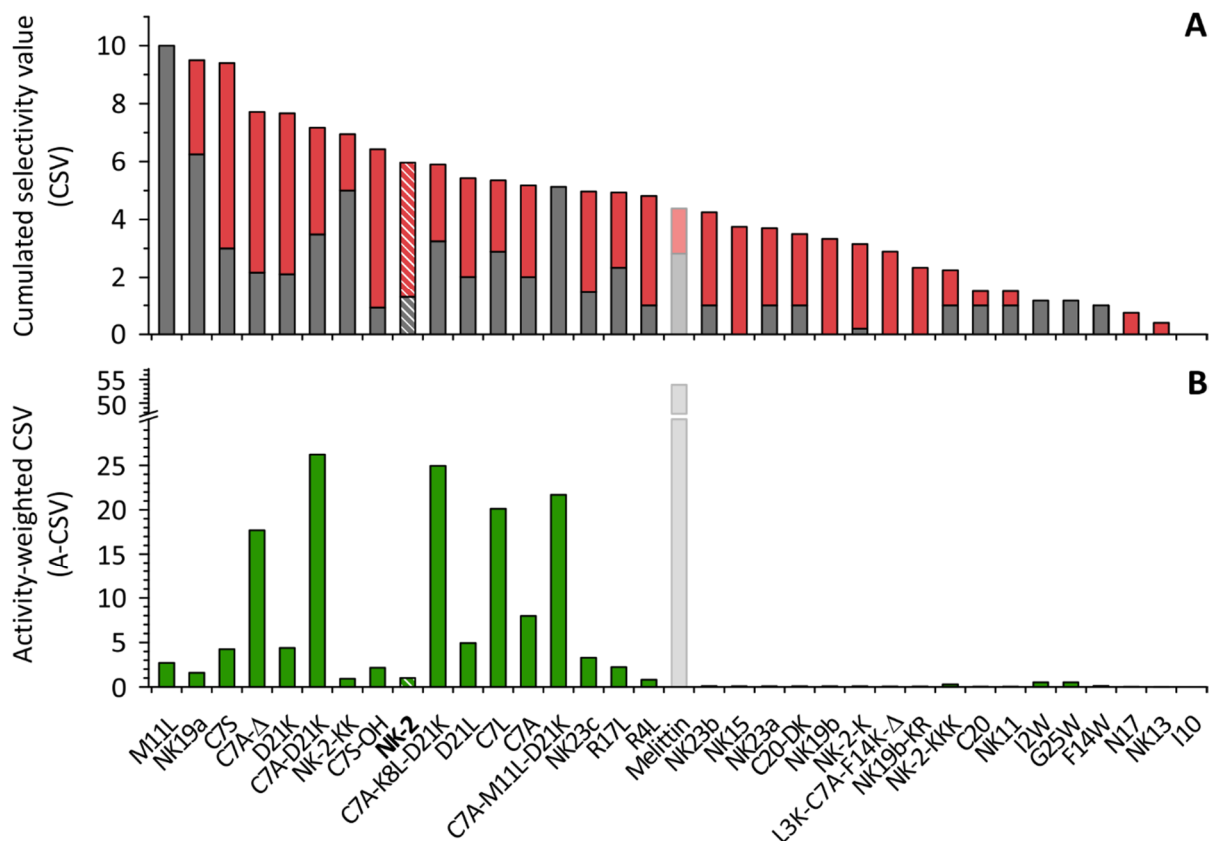


**Figure 5.22: Peptide-specific anti-cancer cell potency and selectivity.** The stacked column plot in (A) additively depicts the selectivity factors of peptides derived as the quotients of (i) their mean  $IC_{50}$  values towards human PC-3 prostate cancer cells over HaCaT normal keratinocytes in complete medium (grey columns) as well as of (ii) their membrane intercalation (% FRET signal increase) into liposomes made of PC:PS (90:10) over insertion into pure PC vesicles (red columns). In (B) the cumulated selectivities of each peptide given in (A) were additionally weighted through division by the corresponding  $IC_{50}$  against PC-3 cancer cells under complete medium conditions (activity gold standard). Notably, the data set in (B) was normalized so that NK-2 has an A-CSV of 1.0, and a break was introduced to the y-axis scale for enhanced resolution. Parent peptide NK-2 is highlighted by hatched columns, while faded columns represent the non-NK-related peptide melittin.

Particular concern must be given to peptide melittin as this non-NK-2-related reference peptide (faded-color columns) possessed the highest A-CSV. Nevertheless, as discussed before, melittin is not a suitable candidate for drug development due to its severe hemolytic potential as well as its marked toxicity also against non-cancerous HaCaT keratinocytes (mean  $IC_{50} = 3.1 \mu\text{M}$ ).

## 6 DISCUSSION

Peptide NK-2 and certain structural derivatives of this HDP originally described as the cationic core region of porcine NK-lysin have already been reported to exhibit anticancer activity against a representative range of human (Maletzki et al. 2014; Bankovic et al. 2013; Gross and Andrä 2012; Drechsler and Andrä 2011; Schröder-Borm et al. 2005) and even equine cancer cell lines (Gross et al. 2013).

In general, the nature of peptide-cell interactions is believed to be governed by the specific interplay between cell membrane-related parameters such as its composition and organization, on the one hand, and peptide-related influences such as its sequence and conformation, on the other hand (Gaspar et al. 2013; Harris et al. 2011; Hoskin and Ramamoorthy 2008).

Key aspects of these contributory factors have been under investigation in the course of this work. Both cell- as well as liposome-based experimental approaches enabled studies on mechanistic aspects underlying the anti-cancer cell activities of peptide NK-2 and improved variants. Structure-function relationships of more than 30 structural derivatives of the lead peptide NK-2 were examined in order to *identify highly promising anticancer variants and crucial sequence modifications* underlying their superior activity. Moreover, discussing the achieved results could contribute to understanding the characteristics of the anti-cancer cell effectiveness and selectivity, as well as of the peptides' *mode of action* and the involved "building blocks" comprising membrane binding, insertion and permeabilization, along with orientational information and interaction kinetics. Overall, general focus was put on the hypothesized *target specificity* of NK-2-related peptides *for membrane surface anionic phospholipid PS*.

### 6.1 Anticancer Activities of Peptide NK-2 and Structural Derivatives

The well-established PC-3 human prostate cancer cell line was used in conjunction with HaCaT normal human keratinocytes as a non-tumorigenic reference model to comprehensively assess the peptide-specific effectiveness against and selectivity towards cancerous over attributable healthy cells. The basic susceptibility of PC-3 cells to the parent peptide NK-2 has been documented previously (Gross and Andrä 2012). As a pertinent extension to the current knowledge, here, the use of overall more than 30 structural derivatives of the lead

structure NK-2 gave detailed insights into sequence-related features influencing the anti-cancer cell potency and selectiveness.

Most remarkably, also rarely considered patient-derived colorectal carcinoma (CRC) cells, namely HROC24 and HROC107 cells, were successfully targeted by selected NK-2-related peptides. To a limited degree, this has been reported before by Maletzki et al. (2014), and, for selected peptide derivatives, CRC cell type-specific toxicity could be strikingly underpinned in this thesis. As an appropriate reference, the cell cultures deployed here also entailed a commercially available CRC model cell line (HCT116).

As a first approach, the activity of each peptide variant was assessed against PC-3 as well as HaCaT cells by the common and widely used MTT test applying PBS/medium conditions, i.e. PBS buffer void of calcium and magnesium supplemented with 10 % DMEM cell culture medium again including 10 % heat-inactivated bovine serum. In addition, selected peptides were evaluated against all three distinct CRC cell types under equivalent assay conditions.

In this particular solvent environment, NK-2 and even a considerable number of its structural derivatives proved to be extraordinarily active against all cell types tested with  $IC_{50}$  values in a low micromolar range. Notably, also non-cancerous HaCaT cells were not spared from peptide toxicity. Although corresponding  $IC_{50}$  values were in most cases slightly increased, HaCaT keratinocytes were still substantially affected by peptide molarities assigned to be effective against cancerous cells, reflecting an intermediate degree of cancer cell selectivity under PBS/medium conditions.

In sharp contrast to the overall high potency of many peptides in PBS/medium conditions, a substantial inactivation was observed for peptide NK-2 and the majority of its variants when their cytotoxicity was alternatively assessed in complete medium, i.e. DMEM cell culture medium supplemented with 10 % FBS. To this end and in general regard of cytotoxicity-related findings of this thesis, it should be stated that the peptide anti-cancer cell performance in complete medium is to be considered as the *in vitro* activity gold standard, because this environment mimics physiological conditions much more closely than highly PBS-diluted assay conditions. Medium-related activity losses have been reported before for NK-2 (Gross et al. 2013; Drechsler and Andrä 2011; Schröder-Borm et al. 2005) as well as for other HDPs (Hancock and Sahl 2006; Mader and Hoskin 2006; Papo and Shai 2005; Papo et al. 2003), and

can provide a critical obstacle for the clinical development of peptide-based therapies in general (Yeung et al. 2011).

As has been outlined in details before (see section 2.1.2.4), putatively, several of the coarse cell culture medium ingredients could be causative for the peptide activity inhibition and low bioavailability frequently observed also in blood serum. Besides proteolysis, binding to serum components or electrostatic interference from elevated concentrations of salts and metal ions basically bear the potential to decrease peptide effectiveness. In fact, control experiments confirmed considerably detrimental but not eliminating impacts of  $\text{Ca}^{2+}$  and  $\text{Mg}^{2+}$  on the activities of peptides NK-2, C7A-D21K as well as melittin. Instead, a high proportion of either DMEM cell culture medium, or bovine serum, or, especially a combination of both components strongly impaired to fully depleted the activity of peptide NK-2.

One could assume that cells cultivated in complete medium might also be more sufficiently provided with conditions promoting cellular repair mechanisms, which probably prolongs their endurance to peptide attacks. However, a peptide incubation period of four hours was applied here and an accordingly upheld constitution of the membrane's barrier function is rather incompliant with the fast interaction kinetics of active peptide derivatives obtained here, e.g. in fluorescence microscopic analyses. Moreover, such a survival mechanism would have similarly impeded the effectiveness of any peptide tested, which, in fact, was not observed. Instead, a narrowly defined group of selected NK-2 variants proved to sustain their activity in complete medium and crucial underlying structural modifications of such derivatives could be identified.

NK-2 derivatives with preserved medium activity were strikingly limited to peptides comprising particular amino acid modifications. Explicitly, substituting the parent peptide's sole cysteine residue at position 7 was consistently proven to be key to this critical improvement. The free thiol group of a single cysteine side chain is commonly considered disadvantageous, e.g. in terms of being prone to unspecific oxidation and disulfide bridging (Cleland et al. 1993), accompanied by peptide stability and functionality issues (Haag et al. 2012; Li et al. 1995). Notably, Cys-7 in peptide NK-2 is equivalent to Cys-45 in the originating NK-lysin protein, where the thiol is involved in intramolecular disulfide bonding to Cys-35, which circumvents oxidation-related issues in the natural source (Liepinsh et al. 1997).

Here, in case of medium-active peptide variants, NK-2's Cys-7 was replaced by either alanine or leucine, both being attributably hydrophobic amino acid residues. The corresponding straight-forward single-residue substitution derivatives, C7A and C7L, featured only negligible, if any, changes concerning the set of calculated physicochemical peptide parameters. Moreover, in close resemblance to the conformational features of the parent peptide itself, it was proven for variant C7A to likewise adopt a predominantly  $\alpha$ -helical secondary structure in hydrophobic environments as well as in aqueous solutions in the presence of PS lipid vesicles (Gross et al. 2013). Hence, it is suggestive that these substitutions provided an improvement to the parent structure of NK-2 primarily through enhanced peptide stability rather than through direct alteration of its inherent biophysical parameters. In compliance with this finding, any other derivative featuring an accordingly exchanged Cys-7 residue exerted potent activity in medium. Namely, such peptides included the multiple-substitution variants C7A-D21K, C7A-K8L-D21K, and C7A-M11L-D21K, as well as the truncated derivative C7A- $\Delta$ . Apparently, these variants entailed an additional exchange or even deletion of the aspartate (D) residue at position 21. As this acidic residue impedes the overall polycationic peptide character, its exchange to a non-charged (L) or even basic amino acid residue (K) was expected to facilitate NK-2's interaction with putatively anionic target cell membranes by elevating the peptide net charge by +1 or even +2, respectively. Interestingly, derivatives D21L and D21K proved to be highly effective in PBS/medium, but provided only moderate activity enhancements in complete medium. This, in turn, implicated that Asp-21 is not the key position to be modified in order to improve medium activity, and concomitantly underpins the outstanding role of Cys-7. Further emphasizing this, the shortening of C7A to variant C7A- $\Delta$  by the omission of amino acid residues 18-21 (comprising Asp-21) was apparently possible without undergoing a critical activity inhibition under full medium conditions. As generally growing importance is assigned to the cost of goods and production during drug development processes (Agyei and Danquah 2011; Bray 2003), the reduction in size but not performance realized with this derivative provided a further substantial enhancement to the lead structure of NK-2.

Intriguingly, the probably most conservative exchange of Cys-7 to serine did not yield derivatives of satisfactory effectiveness against cancerous cells in medium. At a first glance, this was frankly unexpected, as variants C7S and C7S- $\Delta$  previously demonstrated enhanced effectiveness against various Gram-positive as well as Gram-negative bacterial strains even in

quite crude culture broth conditions (Gofman et al. 2010; Andrä et al. 2007). Nonetheless, the here-described low anti-cancer cell potential of C7S is in good agreement with findings from other groups. For example, the C7S-induced killing of LNCaP (lymph-node carcinoma of the prostate) cells was achieved at a comparably high (i.e. unfavorable)  $IC_{50}$  in medium of  $> 30 \mu M$  (Manavbasi 2012, peptide NKCS). Altogether, this should be taken as an indicator that different precepts might apply for the antibacterial and the anti-cancer cell activities of NK-2-derived peptides.

To this end, also some exemplary sequence modifications of ambivalent or even disadvantageous effects should be considered as valuable sources of information on the structural basis of the peptide functionality. In resemblance to the stability-enhancing substitution of Cys-7, the methionine residue at position 11 was exchanged to leucine in variant M11L. In general, sulfur-comprising methionine residues can be readily oxidized to methionine sulfoxide (Liang et al. 2012) which may cause structural alterations, aggregation and functional impairment of peptides (Stadtman et al. 2005). Nevertheless, variant M11L itself was virtually void of medium activity implying a profoundly less decisive role of the methionine residue for stability in medium as compared to Cys-7. Yet, the triple-substitution derivative C7A-M11L-D21K, combining the modifications of successful single-exchange variants, featured the lowest (i.e. best)  $IC_{50}$  in medium against PC-3 cells with concomitant highest selectivity for cancerous PC-3 over attributably healthy HaCaT cells.

The detrimental effect of perturbed amphipathicity on the medium-related peptide activity could be exemplarily underpinned by variant L3K-C7A-F14K- $\Delta$ , which is an alteration of the active peptide C7A- $\Delta$  enclosing two additional residue substitutions to lysine in close-to-N-terminal (L3K) and mid-structure (F14K) position. Strikingly, though L3K-C7A-F14K- $\Delta$  has a substantially increased overall net charge, it was found to be entirely void of activity already in PBS/medium conditions. This implicates that not charge itself but its defined positioning and counterbalancing, e.g. by rather non-polar segments, is determinant for the peptide functionality. This observation is basically in good agreement with findings from Harris and co-workers (2011) who concluded from analyses of a range of diverse anticancer HDPs that a functional impact of a peptide's net charge usually involves additional contributing factors. Heading in the same direction, here, comprehensive correlations of functional data with distinct physicochemical peptide properties revealed that the mean hydrophobicity ( $H$ ) and, more precisely, a well-defined balance between  $H$  and the net charge  $Q$  of a given peptide

(*H/Q* ratio) were most decisive for the respective variant's anticancer potential against PC-3 human prostate cancer cells, as well as – even though less unequivocally – for the ability to intercalate into PS-comprising membranes.

Apart from this, pronounced amphipathicity is a highly conserved characteristic of HDPs in general (Ebenhan et al. 2014; Jenssen et al. 2006). Here, peptide-specific hydrophobic moments were not found to correlate with functional features of the investigated NK-2 derivatives. This is believed to be owed to the generally high average amphipathicity which the majority of variants have in common, and which only slightly diverged from the moment values featured by the lead structure of NK-2. By all likelihood, this lack of interdependency is a consequence of the rationale-based design of the peptides in the course of which the sustained distribution pattern and balance of hydrophobic and charged residues, i.e. amphipathicity, had been major premises (Gross et al. 2013; Andrä et al. 2007).

Finally, it should be stated that NK-2 derivatives shorter than 20 amino acid residues consistently featured outright inactivity in terms of anti-cancer cell potency. In this regard it appears worth-mentioning that an ideal  $\alpha$ -helix of 20 residues is typically required to completely traverse the distance of 30 Å, which is the approximate thickness of the hydrocarbon core of phospholipid bilayer membranes (White and Wimley 1999; Hol 1985). Besides, also the inability to adopt a regular  $\alpha$ -helical conformation in membrane-mimetic environments, as it was shown e.g. for peptide NK11 (Andrä et al. 2007), impedes the exertion of effective membrane interactions, thus, cytotoxic activities.

Interestingly, Andrä et al. (2007) identified a minimum net charge of +8 along with the abundance of a highly amphipathic 7-residue segment to be determinant for the broad spectrum antibacterial activity of peptide NK-2 and a set of 18 (mostly shortened) derivatives thereof. Instead, they observed no correlation with the mean hydrophobicity. As these findings diverge considerably from the above-defined criteria for the anti-cancer cell activity, this can be taken as another supportive finding to propose that somewhat different principles appear to govern the interactions of peptide NK-2 with particular bacterial as opposed to human cancerous cells. This can be exemplarily substantiated by peptide N17, which demonstrated an outright inactivity against any mammalian cell line tested here, but exhibited a considerable degree of activity against several Gram-negative bacterial strains (Andrä et al. 2007).

## 6.2 Peptide Mode of Action and Impacts of Membrane Phosphatidylserine

As reviewed in the introduction to this thesis, an increased abundance of the anionic phospholipid PS, accounting for up to 10 % of the total lipid content (Riedl et al. 2011b; Schutters and Reutelingsperger 2010; Kirszberg et al. 2009), was observed on the surface of various human cancer cell types, including but not limited to neuroblastoma (Schröder-Born et al. 2005), multi-drug resistant lung carcinoma (Bankovic et al. 2013), hard-to-treat glioblastoma, or metastasis-derived melanoma (Riedl et al. 2011b) cells. Opposing this, due to an actively upheld asymmetric distribution of membrane constituents, PS is known to be virtually absent from the outer membrane leaflet of healthy mammalian cells (Beveris et al. 1996).

Consequently, PS has become more and more recognized as a putative anticancer target, with cationic membrane-active HDPs providing a major opportunity to selectively attack this cancer cell-specific marker (Huang et al. 2015; Liu et al. 2015; Gaspar et al. 2013). In this regard, it is the consensus view that the initial step of binding or association is predominantly driven by electrostatic interactions between the polycationic peptide and negatively charged factors on the target membrane surface. With respect to the specificities of cancerous cells, besides PS, mainly sulfated glycans as well as sialic acids are frequently regarded as anionic target structures potentially contributing to the charge-driven attraction of peptides to the cancer cell surface (Gross and Andrä 2012). However, as it has been reviewed in detail before, both must be considered non-ideal target candidates, e.g. due to their ubiquitous presence also on healthy human cells, and/or their ambivalent effects on peptide activities (see section 2.1.2).

Hence, in the scope of this thesis, special emphasis was put on the anionic phospholipid PS as a membrane-related factor of putatively crucial impact on the anticancer mode of action of peptide NK-2 and structurally improved derivatives thereof.

By introducing and assigning each peptide an A-CSV, i.e. an activity-weighted cumulated selectivity value, a quantitative marker was established in order to evaluate the ensemble of NK-2-related peptides in terms of their individual prospects as anticancer agents. This multi-parametric value classified each peptide according to its overall performance, taking into account the peptide-specific differences regarding (i) the cytotoxicity in complete medium against cancerous PC-3 as compared to normal HaCaT cells, as well as (ii) the FRET-deduced selectivities for PC:PS (90:10) over pure PC lipid membranes.

Following this approach, the group of overall 34 NK-2-related peptides was successfully narrowed down to six derivatives of highly promising anticancer performance. From these, in turn, three particular peptides were selected for subsequent in-depth investigations on the hypothesized PS-related interactions of NK-2-based peptides with both advanced cellular models of patient-derived CRC cells as well as with artificial membrane systems:

The double-substitution variant C7A-D21K (1) was chosen as the overall best-performing derivative, while peptide C7A- $\Delta$  (2) was selected as it provided outstanding improvement compared to NK-2, too, and entailed the additional productional benefit of being truncated by four residues. Moreover, though not being as high-rated as the former derivatives, also C7A (3) was included as it featured a still considerably better A-CSV as the parent peptide and, of special note, represents the most decisive single-residue substitution (Cys-7 to Ala) both greatly enhanced variants (1 and 2) have in common.

Complementary to these three improved variants, the selection peptides for follow-up studies obligatorily enclosed also NK-2 (4) as the parent structure originating any derivative thereof. Finally, the extensively shortened variant NK11 (5) was included as an evidentially inactive control peptide, while melittin (6) served as a non-NK-2 related reference known to be highly potent but likewise excessively hemolytic (see table 6.1, p. 104, as well as section 2.2.2).

It should be noted that the basically well-performing peptides C7L, C7A-K8L-D21K, and C7A-M11L-D21K were not considered in the follow-up investigations. On the one hand, their generally supreme A-CSVs were still inferior to that of C7A-D21K, and, on the other hand, their applicability was impaired by increased hemolytic activities (personal communication; see also table 6.1).

### 6.2.1 Cellular Selectivity

Generally speaking, the primarily investigated cellular model of cancerous PC-3 cells with the HaCaT cell line as a non-cancerous reference proved to be a valuable test system to basically elucidate the peptides' anti-cancer cell activities and specificities. In this regard, considerable degrees of selectivity for the tumorigenic over the normal human cell type became evident in the course of this work. Reduced activity of the lead peptide NK-2 against the HaCaT human normal keratinocyte cell line has been observed before, together with an overall minor hemolytic potential (Drechsler and Andrä 2011; Schröder-Borm et al. 2003; Andrä and Leippe

1999). Adding to this, NK-2 was also shown to be about non-toxic towards normal human lymphocytes (Schröder-Borm et al. 2005). In line with these findings, with the exception of peptide C7A, any of the here-identified NK-2 variants of enhanced anticancer performance has been proven to be of comparable or even lower toxicity towards human erythrocytes than the parent peptide. Table 6.1 outlines corresponding findings deduced from data published in Gross et al. (2013), which additionally underpins the destructive hemolytic potential of the reference peptide melittin.

Peptide	Hemolysis / % at 10 $\mu$ M
NK-2	19.4
C7A	32.8
C7A-D21K	22.3
C7A- $\Delta$	13.5
NK11	0.4
Melittin	92.4

**Table 6.1: Hemolytic activities of selected NK-2-related peptides and melittin.** Photometrically determined percent hemolysis of human erythrocytes freshly harvested from healthy donors by measuring the release of hemoglobin after incubation with indicated peptides at a concentration of 10  $\mu$ M. Values were deduced from data originally published in Gross et al. (2013). Background grey scaling denotes the type of sequence modification compared to NK-2 as introduced in table 5.1.

Importantly, flow cytometric analyses classified cancerous PC-3 cells as high-PS and attributably healthy HaCaT cells as low-PS, which provided general support for the hypothesized relevance of PS for the effectiveness and selectiveness of peptide NK-2. Both PC-3 (Watson et al. 2014; Boo et al. 2013; He et al. 2012) as well as HaCaT (Seo et al. 2012; Shim et al. 2008; Deyrieux and Wilson 2007) cells are well-reputed as cellular *in vitro* models and their common and widespread uses range from assay-based compound screening to studies on signaling pathways or cell differentiation, to name a few. However, in direct relation to each other, these cell lines feature a range of profound distinctions referring to their highly divergent cell type and origin. Comparisons are made between epithelial carcinoma cells from a bone metastasis of a malignancy of the prostate gland, on the one hand, and a spontaneously *in vitro* immortalized cell line of keratinocytes derived from histologically healthy skin tissue, on the other hand. The overall rather high degree of divergence between both cell types basically hampers the definition of individual influence factors putatively relevant for cellular interactions with the investigated peptides.

Thus, in order to further elucidate the significance of PS for the activities of NK-2-related peptides against cancer cells, in a second step, the previously identified ensemble of improved derivatives was further assessed using an advanced cellular test system of patient-derived

colon cancer cells. Both HROC24 and HROC107 cell lines were originally established from the colon ascendens of individual patients, demonstrating highly similar characteristics even down to the underlying genetic aberration (Maletzki et al. 2014; Maletzki et al. 2012; Linnebacher et al. 2010). Moreover, identical cultivation conditions were successfully applicable, which further stressed the similar demands of both CRC cell types. In line with these fundamental resemblances, here, experimental data additionally revealed a marked uniformity of both HROC cells with respect to their accessible surface charge as reflected by almost indifferent Zeta potentials.

Yet, in contrast to this high degree of congruence, pronounced differential responses were observed in the cell type-specific susceptibility towards selected NK-2 peptides. On the one hand, HROC107 cells demonstrated to be substantially less prone to the cytolytic effects exerted by active peptide variants than HROC24 cells. On the other hand, this cellular selectivity was emphasized by the preferential compensation of the surface Zeta potential of HROC24 cells upon incubation with any knowingly membranolytic NK-2 derivative.

In consistency with this, peptides NK-2 and C7A-D21K demonstrated superior effectiveness in terms of peptide binding to and permeabilization of HROC24 as compared to HROC107 cells, which was successfully monitored in a PBS solvent environment by fluorescence microscopic analyses. Confirmative results were also achieved with the commercially available colon cancer model cell line HCT116, which was found to be almost as well susceptible to the selected active NK-2 variants as HROC24 cells.

Against this background, it is of utmost importance that HROC24 and HCT116 cells were both found to possess comparably high levels of surface-bound PS (high-PS) as determined by flow cytometric analysis, while the surface PS levels of HROC107 cells were demonstrably lower (low-PS). These observations were in very good accordance with findings from Maletzki et al. (2014), the laboratory of whom originated the set of patient-derived HROC cell lines. Even though using a different fluorescent annexin V label (allophycocyanin), a roughly 3.5-fold higher surface PS level for HROC24 over HROC107 could be deduced from their previous study. This value correlates well with the ratio of 2.6 determined in the here-performed FITC-annexin V-based flow cytometry experiments. Adding to this, for the parent peptide NK-2, these findings correlate nicely to results of Schröder-Borm et al. (2005) who observed facilitated killing of leukemia cell lines featuring up to ten-fold higher surface PS contents as compared to normal lymphocytes.

Of special note, the observed almost indistinguishable levels of the cell surface net charge held true for all five cell lines under investigation. Obviously, the markedly differential interactions with NK-2-derived peptides cannot be owed to any profound deviations in the amount of accessible charge on the respective cellular surface. Instead, distinctions in the cell type-specific peptide susceptibility are strongly suggested to be attributable to a considerable extent to cell type-specific differences in the level of surface-exposed PS.

Under complete medium conditions, all three CRC cell lines tended to be less prone to the treatment with active variants of peptide NK-2 as compared to both non-CRC cell types, although the surface PS levels of high-PS (HROC24, HCT116, PC-3) and low-PS (HROC107, HaCaT) cell types were comparable within each group. This basically indicates that the cell surface PS exposure is not the sole influencing factor in this regard, and contributions from further (cancer) cell line-specific distinctions such as the membrane rigidity, the accessible surface area or the abundance and types of anionic carbohydrates have been addressed at the outset to this thesis (see section 2.1.2). However, it should be pointed out explicitly that a direct comparison and interpretation of  $IC_{50}$  values obtained for CRC and non-CRC cell types must be regarded rather inapplicable with respect to the above-discussed pronounced divergences between both classes of cell lines. Despite of this partial limitation, when considering the activities of individual peptides, a striking conformity existed in their selectivity for (i) PC-3 over HaCaT on the one hand, and (ii) HROC24 over HROC107 cells on the other. While the lead peptide NK-2 and its derivative NK11 generally lacked activity (thus, also selectivity) in complete medium, the enhanced variants C7A (2.0- and 2.1-fold selectivity for (i) and (ii), respectively), C7A- $\Delta$  (2.2- and 3.2-fold), and C7A-D21K (3.0- and 3.5-fold) exerted well-correlated selectivities for the respective high-PS types of both cellular test systems.

From a more general point of view, the here-observed variable degrees of PS surface exposure are most probably found likewise in comparison of other cancerous cells. Exemplarily, this assumption can be duly substantiated by Dobrzynska and co-workers (2005) showing that the membrane composition with respect to phospholipid contents and organization fluctuated tremendously among 18 tumors from individual patients all diagnosed with colorectal cancer of similar TNM stage. Consequently, it appears reasonable to assume that marked differences are to be expected regarding each individual malignancy's susceptibility even to the best-performing anticancer peptides.

## 6.2.2 Membrane Interaction Mechanisms

The spatial approximation of peptide molecules to the target cell membrane is a profound prerequisite for any effective interaction in the first place. As was deducible from light scattering measurements, apart from NK11, all of the selected peptides were apparently able to associate – to a very limited degree – with liposomal membranes reflecting the outward-facing leaflet of healthy human cells, here being simplistically constituted solely of zwitterionic natural PC. However, no interactions of higher grade, i.e. extensive particle aggregation coinciding with a disproportionate jump in the Zeta potential, were detectable in this regard. This indicates that in the presence of PC vesicles the peptide-membrane association might be too weak to enable a transition from an electrostatics- to a hydrophobicity-driven interaction. In line with this, probe dilution FRET as well as intrinsic tryptophan fluorescence spectrometry strongly supported this finding as poor to virtually no insertion into PC membranes was observable neither for NK-2 or its structurally enhanced derivatives, nor for any of its three single-Trp substitution variants. This is fully compliant with the outcome of numerous former investigations where only minor to completely absent interactions of peptide NK-2 with normal human membrane mimetics have been repeatedly proven (Ciobanasu et al. 2015; Gelhaus et al. 2008; Andrä et al. 2007; Schröder-Borm et al. 2005; Willumeit et al. 2005; Schröder-Borm et al. 2003).

Contrasting the peptides' poor interactions with PC membranes, both the degree of membrane binding of NK-2 as well as its intercalation ability increased substantially in case the target membrane was designed to mimic cancerous cellular surface conditions, i.e. liposomes made of mixtures of PC and anionic PS. To this end, it is proposed that – for peptide NK-2 and its active variants – the successful establishment of considerable hydrophobic interactions between bound peptide molecules and the lipid bilayer provides an important precondition for the subsequent process of intercalation. Notably, already quite low amounts of PS (10 % of the total lipid content) seemed to be sufficient to enable effective peptide-membrane interactions. For peptide NK-2, this is in very good agreement with findings from Schröder-Borm et al. (2005) demonstrating facilitated intercalation into PS-comprising (as compared to pure PC) lipid vesicle membranes. Adding to this, here, also the three structurally enhanced C7A-substitution variants proved to likewise preferentially bind to and insert into liposomal membranes in correlation to the membrane PS content.

Notably, peptides NK-2 as well as melittin both induced very similar changes in liposomal surface Zeta potentials. This was especially surprising as both peptides exert membrane-activity in considerably different manners with regard to selectivity, effectiveness, and mode of action (see also section 2.2). Moreover, the net charge of NK-2 is substantially higher ( $Q = +10$ ) than melittin's ( $Q = +6$ ). This suggests that the membrane association of melittin is more readily driven by hydrophobic effects than observed with NK-2, which strongly substantiates melittin's mostly unselective interaction with phospholipid bilayers, regardless of whether the membrane surface composition features e.g. anionic PS. In consistency with this, NK-2 as well as its enhanced derivatives preferentially compensated the cellular surface Zeta potentials of high-PS CRC cell lines, while for melittin no prioritization of any type of cell was noticed. With regard to membrane interaction mechanisms it is further to be recognized that on both, cells and PS-containing liposomes, the parent peptide NK-2 induced more extensive overcompensation effects than its derivatives of enhanced anticancer activity. Obviously, such C7A-substitution variants require minor extents of hydrophobic interactions with a target membrane to fully unfold their potential.

Another interesting mechanistic observation was made in probe dilution experiments when shortly after the addition of 0.8  $\mu\text{M}$  NK-2 to liposomes purely consisting of PS, the initially sharply raised FRET signal decreased by around 10 % within the range of about 50 seconds until reaching a steady state (see figure 5.15C). It is suggested that this phenomenon of an inverse kinetic might result from peptide-induced lipid demixing effects. If ordered lipid domains were initiated, donor and acceptor dyes could have come into closer proximity again leading to a certain decline of the detectable donor-to-acceptor emission ratio, i.e. FRET signal. Lohner and Blondelle (2005), for instance, described such a membrane disturbance mechanism for antimicrobial peptides via the formation of reordered lipid domains.

Furthermore, NK-2 as well as its most improved derivative C7A-D21K were representatively verified to be able to perturb the integrity of PC/PS lipid vesicle membranes, thus, to provoke bilayer permeabilization. For NK-2, preferential permeabilization of PS-comprising over solely PC-constituted lipid vesicles has been demonstrated before (Gelhaus et al. 2008), and here, C7A-D21K was even considerably more efficient than its parent peptide. However, with both peptides membrane impairment was generally sufficient to enable either efflux of calcein from the inner liposomal volume or the internalization of KI molecules. Of note, the complementary setups of both experimental approaches allow drawing the conclusion that the peptide-

induced membrane permeability was proven to be bidirectional and readily transmembrane. Adding to this, by the use of Rh-conjugates of the very same peptides, also cellular permeabilization accompanied by concomitant intracellular access of peptides and the membrane-impermeant nucleic acid stain Sytox green was comprehensibly visualized in fluorescence microscopic investigations with high-PS HROC24 and low-PS HROC107 cells. Mechanistically, these findings furthermore suggest that both NK-2 and C7A-D21K impede the membrane's barrier function via the formation of transient transmembrane pores. In line with this, such transient pores have been observed for NK-2 in planar lipid bilayer measurements at different types of bacterial membrane mimetics (Andrä et al. 2011; Hammer et al. 2010) as well as at PC/PS membranes (Jörg Andrä, personal communication).

It should be noted that the permeabilization processes did apparently not involve or promote extensive membrane disruption as typically only insignificant amounts of cellular debris were observed. Nonetheless, as it has been demonstrated before with other cancerous mammalian cell lines (Gross et al. 2013; Drechsler and Andrä 2011; Schröder-Borm et al. 2005), here, also patient-derived CRC cells responded to NK-2-related peptide attacks by partially drastic changes in the morphologic appearance involving rounding and membrane blebbing. Interestingly, Wang and co-workers (2009b) noticed comparable cellular responses of human leukemia cells upon treatment with polybia-MPI, an HDP from the venom of the social wasp.

Basic information on both location and orientation of peptide NK-2 molecules upon membrane intercalation could be inferred from the calculated physicochemical peptide properties as well as from tryptophan fluorescence spectroscopy.

At first, considering the low average hydrophobicity of the selected active peptides in conjunction with their quite equally distributed amphipathicity (see tables 5.1 and 5.2), an activity exhibition through the formation of regular transmembrane-spanning pores, like suggested for the barrel-stave mode of action, is highly improbable. In close resemblance to peptide NK-2, both cecropin A and B (Holak et al. 1988; Steiner et al. 1981), antimicrobial peptides of the cell-free immunity of insects, adopt a secondary structure of two hinged  $\alpha$ -helices in lipid bilayer vicinity. Interestingly, both cecropin subtypes were found to directly disrupt the membrane of bladder cancer cells (Suttman et al. 2008) and were proposed to act against bacteria by a mechanism that includes the formation of transient transmembrane pores (Hung et al. 1999; Steiner et al. 1988). According to Eisenberg and co-workers (1984), the helices of cecropin A and B feature consecutive 11-residue segments with mean hydrophobicities of

−0.22 and −0.41 and concomitant hydrophobic moment values of 0.80 and 0.89, respectively. This combination characterized at least the corresponding segments as clearly surface-prone according to the hydrophobic moment plot introduced by the authors. These parameters match remarkably well with those determined here for (the full lengths of) peptide NK-2 and its most improved variants (with  $H = -0.26 \dots -0.29$ , and  $\mu H_{\text{mean}} = 0.79 \dots 0.81$ ), strongly suggesting a similar membrane surface propensity as well as interaction mechanism.

Secondly, it was demonstrated by tryptophan fluorescence blue shift analysis that both the amino-terminal and the mid-sequence segment of NK-2 intercalated deeply and to similar extents into PS-bearing lipid vesicle membranes, even slightly favoring the mid-part at furtherly increased PS contents. Instead, the peptide's carboxy-terminus resided in a shorter-range distance to the membrane-aqueous interface. This outcome underlined that the mid-part of NK-2 apparently conserved the flexible hinge region (around residues Thr-13 to Leu-15) located in between of helices 3 and 4 of the originating NK-lysin protein (see also figure 2.4). It is suggested that NK-2's predominantly  $\alpha$ -helical secondary structure adopts a non-linear but wedge-shaped conformation with a tilted orientation relative to the membrane normal, while – at least in parts – upholding proximity to the bilayer surface. These results are in very good correlation with findings from NK-2-related orientational investigations using molecular dynamics simulations (Pimthon et al. 2009), as well as with experimental data from X-ray scattering (Olak 2008) and solid-state NMR spectroscopy (Udupi Seetharamacharya 2005).

Finally, several of the here-applied experimental approaches furthermore provided insights into the kinetics underlying the interactions of the investigated peptides with cellular membranes as well as biomembrane-mimetic systems. Fluorescence microscopic experiments revealed that peptide accumulation at the membranes of low-PS HROC107 and high-PS HROC24 cells was in all cases quickly succeeded by permeabilization and cell death, with first killing events typically registered within the range of a few minutes from treatment initiation. However, two major tendencies evolved as (i) the survival of low-PS HROC107 cells was markedly prolonged as compared to the high-PS CRC cell variant, and (ii) derivative C7A-D21K exerted cancer cell killing activity at substantially accelerated kinetics as compared to the parent peptide NK-2. In general, the rapidness of the killing process itself strongly supports the cytoplasmic membrane to be the principle peptide target (Gaspar et al. 2013; Huang et al. 2011; Boman 2003), because intracellular targeting usually requires longer interaction timespans (Nicolas 2009). In line with this, the kinetics of calcein leakage from dye-

encapsulating PC/PS liposomes were considerably quicker with peptides NK-2 and C7A-D21K as compared to melittin (yet, the final degree of leakage was higher with the latter). For the reference peptide, membrane permeabilization via the formation of regular pores from previously self-associated melittin dimers is described (Hristova et al. 2001). Instead, the clearly different mechanism exerted by NK-2 and C7A-D21K featured an apparently faster kinetic.

### 6.2.3 Concatenated Mechanistic Information

Altogether, the ensemble of (mechanistic) findings made in the course of this work could serve as individual signposts characterizing peptide NK-2 as well as its structurally enhanced derivatives regarding their putative mode of action against the here-involved cancerous cells. The schematic model given in figure 6.1 outlines key stages in the peptides' interactions with (idealized) cancer cell membranes.

- Initially, the presence and accessibility of anionic PS on the membrane surface of a cancerous cell triggers the recruitment of peptide NK-2, which holds true also for its structurally improved derivatives. At this stage, the peptide molecules are anticipated to be randomly coiled or at least predominantly unstructured (see figure 6.1, ❶). A certain degree of electrostatic attraction between the polycationic peptide molecules and the negatively net-charged membrane surface favors the spatial approximation between both and increases the interaction probability. However, the selective accumulation of peptides at the cancer cell membrane is correlated to the outer leaflet's PS content, and is explicitly independent from its overall net charge. This implies PS-specific interactions to play a crucial role for the selective targeting of cancerous as opposed to normal cells.
- In vicinity to the bilayer interface, NK-2 and its enhanced derivatives adopt an  $\alpha$ -helical secondary structure. The now highly amphipathic peptides align in parallel to the lipid bilayer normal in the first place, orienting with their hydrophilic helical face to the exoplasmic surface and with the hydrophobic face striving towards the bilayer hydrocarbon core. This results in a putatively carpet-like coverage of the membrane surface (see ❷).
- Upon reaching or exceeding a peptide-specific local threshold concentration, hydrophobic interactions between the peptide and the lipid bilayer core are main driving forces triggering the subsequent step of membrane insertion (see ❸). Membrane-intercalated NK-2 molecules appear in a bent shape probably angled resembling the natural conformation

in the originating NK-lysin protein. The carboxy-terminus has a higher tendency to locate in surficial proximity while a deeper integration is observed for the mid-part to amino-terminal sequence moiety.

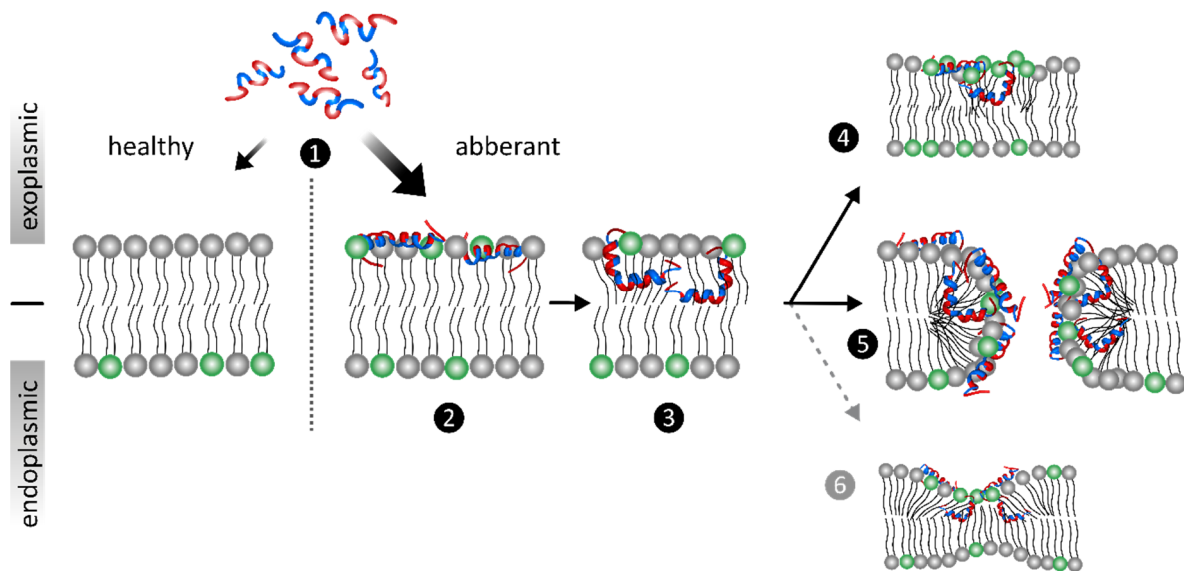


**Figure 6.1: Proposed mechanism of action of peptide NK-2 against cancer cells.** Predominantly hydrophobic and hydrophilic segments of the peptide's amino acid sequence are represented in blue and red, respectively. Choline lipid head-groups of PC are depicted in grey, negatively charged PS head-groups in red. After selective attraction of peptides to PS-exposing cancer cells (①), the peptide conformation shifts from a previously unstructured state to a predominantly  $\alpha$ -helical fold. Carpet-like membrane surface coverage (②) is succeeded by the insertion of peptide molecules into the bilayer (③). NK-2 intercalated into PS-bearing membranes possesses an angled shape bent at a mid-sequence flexible hinge region. The C-terminus remains in proximity to the bilayer surface while the mid-to-N-terminal moiety inserts deeper. Finally, peptide-induced impairment e.g. by transient pore formation (④), lipid packing perturbation (⑤) and/or membrane thinning (⑥), not yet experimentally proven), can lead to lethal permeabilization of the membrane barrier within a few minutes.

- With ongoing accumulation and insertion of peptide molecules, also the chance for membrane impairment events increases. Most likely such mechanisms lead to a transient permeabilization and may include, but might not be limited to, the reversible formation of (toroidal) transmembrane pores (see ④) and/or the disturbance of the lipid packing, e.g. by the induction of PS-enriched domains (see ⑤). Speculatively, another probable impairment route is membrane thinning (see ⑥), which has not been explicitly proven for the here-described NK-2 peptides so far but is a very common membrane disintegration mechanism induced by  $\alpha$ -helical, amphipathic HDPs (Sato and Feix 2006; Mecke et al. 2005; Ludtke et al. 1995).
- Rapid peptide-membrane interaction kinetics enable the total process from binding to (lethal) permeabilization to be completed within the range of just a few minutes.

### 6.3 Conclusion and Outlook

In the scope of this thesis, peptide NK-2 successfully demonstrated potency against a human prostate cancer model cell line as well as, of special relevance, against two patient-derived colorectal carcinoma cells. Yet, the peptide's basically considerable anticancer performance was limited by a pronounced activity inhibition in serum-supplemented cell culture medium implying a most probably restricted applicability of NK-2 under physiological conditions.

Structure-function analyses enclosing an ensemble of more than 30 rationally designed derivatives of the lead peptide NK-2 revealed a group of peptides with concomitantly elevated potency, stability, as well as selectivity for cancerous over healthy human cells. Substituting NK-2's non-functional cysteine residue at position 7 by either alanine or leucine turned out to be the key modification to render the peptide functional under complete medium conditions. The additional exchange or omission of the sole negatively charged aspartate at position 21 yielded derivatives C7A-D21K and C7A- $\Delta$  (shortened by residues 18 to 21), respectively, which emerged as outstandingly enhanced NK-2 variants. Peptide-induced target membrane binding, intercalation as well as effective cell killing by membrane permeabilization occurred extremely quickly, making the best-performing NK-2 analogs highly promising candidates for future anticancer medication development in principle.

Apart from an activity and stability optimization of the peptide's lead structure itself, an effective anti-cancer cell performance is likewise dependent on the target preference, thus on the cancer cell selectivity. Concluding from a range of *in vitro* tests, involving human (cancerous) cell lines as well as artificial membranes as targets, it is proposed that the magnitude of the accessible membrane surface charge is not a primarily decisive factor for selective interactions with membrane-active NK-2-derived peptides. Instead of the cumulative parameter of a target membrane's net charge, experimental data suggest that the level of surface-exposed PS is of crucial importance for the activity of peptide NK-2 and structurally improved anticancer variants thereof in terms of their cancer cell selectivity, the overall efficacy, as well as the underlying mode of action and kinetics.

Generally speaking, these findings underpin the significance of PS as a cancer cell-specific surface factor being a promising target candidate for selective tumor treatment. Currently, PS-directed anticancer therapy approaches are typically based on the use of annexin A5 (Qiu et al. 2013; Frey et al. 2009) or monoclonal antibodies such as bavituximab (Mahoney et al. 2015).

Both attempts aim at shielding externalized PS on cancer cells in order to surmount its immunosuppressive effects in the tumor microenvironment. Here, enhanced NK-2 peptide variants acted by a direct physical membrane attack mechanism against PS-exposing cancer cells. In conjunction with the rapid underlying kinetics, this is thought to provide a most adequate armory to overcome existing resistances as well as to forestall the emergence of new resistance mechanisms.

At present, the systemic application of HDPs in general is to be considered rather unlikely due to stability and bioavailability constraints *in vivo*. Nonetheless, structural peptide optimization as well as drug formulation approaches strive towards coping these limitations. Most probably, local or topical administration seem to offer the opportunities with best prospects for success. In line with this, peptides C7A-D21K as well as C7A- $\Delta$  were shown to considerably curb the progression of human colon cancer xenografts in mice after repetitive intratumoral injections (Maletzki et al. 2014). The concomitant anticancer and antibacterial effectiveness of such peptides could also provide a combined benefit, e.g. after surgical removal of a solid tumor, as the peptides ideally target residual cancer cells as well as prevent microbial infections.

Finally, in recent years, the presence of surface-exposed PS evolved more and more as a universal cancer cell hallmark. Yet, the abundance of this putative target structure can be variable, just like it was observed here in direct comparison of a high- versus a low-PS CRC cell line of otherwise striking congruence. Thus, it seems reasonable to assume that any PS-targeted therapy (e.g. using NK-2-derived peptides) cannot be expected to be equally effective in all patients – not even in those diagnosed with the same type of cancer.

This should be perceived as an advocacy for the principles of personalized medicine. Presuming that information about the surface PS levels on cancerous cells of a particular patient's tumor were available, tailoring of a targeted peptide-based cancer treatment could be realized. For malignancies displaying elevated amounts of PS, optimized derivatives of peptide NK-2 could putatively provide an effective as well as molecularly targeted, thus, selective therapy option.

## BIBLIOGRAPHY

- Agyei D, Danquah MK (2011) Industrial-scale manufacturing of pharmaceutical-grade bioactive peptides. *Biotechnol Adv* 29, 3: 272-277
- Alves ID, Carre M, Lavielle S (2015) A Pathway Toward Tumor Cell-Selective CPPs? *Methods Mol Biol* 1324: 279-301
- Al-Wasaby S, de Miguel D, Aporta A, Naval J, Conde B, Martínez-Lostao L, Anel A (2015) In vivopotential of recombinant granulysin against human tumors. *OncoImmunology* 4, 9: e1036213
- An Y, Li L, Yang D, Jia N, Xu C, Wang Q, Wang S, Yuan S (2014) Anticancer activity of tuftsin-derived T peptide in postoperative residual tumors. *Anticancer Drugs* 25, 8: 857-867
- Andersson M, Gunne H, Agerberth B, Boman A, Bergman T, Olsson B, Dagerlind A, Wigzell H, Boman HG, Gudmundsson GH (1996) NK-lysin, structure and function of a novel effector molecule of porcine T and NK cells. *Vet Immunol Immunopathol* 54, 1-4: 123-126
- Andersson M, Gunne H, Agerberth B, Boman A, Bergman T, Sillard R, Jornvall H, Mutt V, Olsson B, Wigzell H (1995) NK-lysin, a novel effector peptide of cytotoxic T and NK cells. Structure and cDNA cloning of the porcine form, induction by interleukin 2, antibacterial and antitumour activity. *EMBO J* 14, 8: 1615-1625
- Andrä J, Böhling A, Gronewold TM, Schlecht U, Perpeet M, Gutschmann T (2008) Surface acoustic wave biosensor as a tool to study the interaction of antimicrobial peptides with phospholipid and lipopolysaccharide model membranes. *Langmuir* 24, 16: 9148-9153
- Andrä J, Goldmann T, Ernst CM, Peschel A, Gutschmann T (2011) Multiple peptide resistance factor (MprF)-mediated Resistance of *Staphylococcus aureus* against antimicrobial peptides coincides with a modulated peptide interaction with artificial membranes comprising lysyl-phosphatidylglycerol. *J Biol Chem* 286, 21: 18692-18700
- Andrä J, Koch MH, Bartels R, Brandenburg K (2004) Biophysical characterization of endotoxin inactivation by NK-2, an antimicrobial peptide derived from mammalian NK-lysin. *Antimicrob Agents Chemother* 48, 5: 1593-1599
- Andrä J, Leippe M (1999) Candidacidal activity of shortened synthetic analogs of amoebapores and NK-lysin. *Med Microbiol Immunol* 188, 3: 117-124
- Andrä J, Monreal D, Martinez de Tejada G, Olak C, Brezesinski G, Gomez SS, Goldmann T, Bartels R, Brandenburg K, Moriyon I (2007) Rationale for the design of shortened derivatives of the NK-lysin-derived antimicrobial peptide NK-2 with improved activity against Gram-negative pathogens. *J Biol Chem* 282, 20: 14719-14728
- Armstrong D, Zidovetzki R Helical Wheel Projections, version: Id: wheel.pl, v 1.4 2009-10-20 21:23:36 don Exp. (2016) <http://rzlab.ucr.edu/scripts/wheel/wheel.cgi> , accessed on 28.01.2016
- Avanti Polar Lipids Inc. (2015) <http://www.avantilipids.com/>, accessed on 10.12.2015

- Bae S, Oh K, Kim H, Kim Y, Kim H, Hwang Y, Lee D, Kang JS, Lee WJ (2013) The effect of alloferon on the enhancement of NK cell cytotoxicity against cancer via the up-regulation of perforin/granzyme B secretion. *Immunobiology* 218, 8: 1026-1033
- Bahar AA, Ren D (2013) Antimicrobial peptides. *Pharmaceuticals (Basel)* 6, 12: 1543-1575
- Bankovic J, Andrić J, Todorovic N, Podolski-Renic A, Milošević Z, Miljković Đ, Krause J, Ruždijic S, Tanić N, Pešić M (2013) The elimination of P-glycoprotein over-expressing cancer cells by antimicrobial cationic peptide NK-2: The unique way of multi-drug resistance modulation. *Exp Cell Res* 319, 7: 1013-1027
- Bechinger B, Lohner K (2006) Detergent-like actions of linear amphipathic cationic antimicrobial peptides. *Biochim Biophys Acta* 1758, 9: 1529-1539
- Beven L, Helluin O, Molle G, Duclouier H, Wroblewski H (1999) Correlation between anti-bacterial activity and pore sizes of two classes of voltage-dependent channel-forming peptides. *Biochim Biophys Acta* 1421, 1: 53-63
- Bevens E, Comfurius P, Zwaal R (1996) Regulatory Mechanisms in Maintenance and Modulation of Transmembrane Lipid Asymmetry: Pathophysiological Implications. *Lupus* 5, 5: 480-487
- Birge RB, Boeltz S, Kumar S, Carlson J, Wanderley J, Calianese D, Barcinski M, Brekken RA, Huang X, Hutchins JT, Freimark B, Empig C, Mercer J, Schroit AJ, Schett G, Herrmann M (2016) Phosphatidylserine is a global immunosuppressive signal in efferocytosis, infectious disease, and cancer. *Cell Death Differ* 23, 6: 962-978
- Björn C, Håkansson J, Myhrman E, Sjöstrand V, Haug T, Lindgren K, Blencke H, Stensvåg K, Mahlapuu M (2012) Anti-infectious and anti-inflammatory effects of peptide fragments sequentially derived from the antimicrobial peptide centrocin 1 isolated from the green sea urchin, *Strongylocentrotus droebachiensis*. *AMB Express* 2, 1: 67
- Boman HG (1995) Peptide antibiotics and their role in innate immunity. *Annu Rev Immunol* 13: 61-92
- Boman HG (2003) Antibacterial peptides: basic facts and emerging concepts. *J Intern Med* 254, 3: 197-215
- Bommarius B, Jenssen H, Elliott M, Kindrachuk J, Pasupuleti M, Gieren H, Jaeger KE, Hancock RE, Kalman D (2010) Cost-effective expression and purification of antimicrobial and host defense peptides in *Escherichia coli*. *Peptides* 31, 11: 1957-1965
- Boo HJ, Hong JY, Kim SC, Kang JI, Kim MK, Kim EJ, Hyun JW, Koh YS, Yoo ES, Kwon JM, Kang HK (2013) The anticancer effect of fucoidan in PC-3 prostate cancer cells. *Mar Drugs* 11, 8: 2982-2999
- Boukamp P, Petrussevska RT, Breitkreutz D, Hornung J, Markham A, Fusenig NE (1988) Normal keratinization in a spontaneously immortalized aneuploid human keratinocyte cell line. *J Cell Biol* 106, 3: 761-771

- Brandenburg K, Garidel P, Fukuoka S, Howe J, Koch MH, Gutschmann T, Andrä J (2010) Molecular basis for endotoxin neutralization by amphipathic peptides derived from the alpha-helical cationic core-region of NK-lysin. *Biophys Chem* 150, 1-3: 80-87
- Brattain MG, Fine WD, Khaled FM, Thompson J, Brattain DE (1981) Heterogeneity of malignant cells from a human colonic carcinoma. *Cancer Res* 41, 5: 1751-1756
- Bray BL (2003) Large-scale manufacture of peptide therapeutics by chemical synthesis. *Nat Rev Drug Discov* 2, 7: 587-593
- Bretscher MS (1972) Asymmetrical lipid bilayer structure for biological membranes. *Nat New Biol* 236, 61: 11-12
- Brewer D, Lajoie G (2000) Evaluation of the metal binding properties of the histidine-rich antimicrobial peptides histatin 3 and 5 by electrospray ionization mass spectrometry. *Rapid Commun Mass Spectrom* 14, 19: 1736-1745
- Brogden KA (2005) Antimicrobial peptides: pore formers or metabolic inhibitors in bacteria? *Nat Rev Microbiol* 3, 3: 238-250
- Bruckheimer EM, Schroit AJ (1996) Membrane phospholipid asymmetry: host response to the externalization of phosphatidylserine. *J Leukoc Biol* 59, 6: 784-788
- Bu JH, Zheng QY, Chen CF, Huang ZT (2004) New fluorescence-quenching process through resumption of PET process induced by complexation of alkali metal ion. *Org Lett* 6, 19: 3301-3303
- Bucki R, Namiot DB, Namiot Z, Savage PB, Janmey PA (2008) Salivary mucins inhibit antibacterial activity of the cathelicidin-derived LL-37 peptide but not the cationic steroid CSA-13. *J Antimicrob Chemother* 62, 2: 329-335
- Chen J, Xu XM, Underhill CB, Yang S, Wang L, Chen Y, Hong S, Creswell K, Zhang L (2005) Tachyplesin activates the classic complement pathway to kill tumor cells. *Cancer Res* 65, 11: 4614-4622
- Chen KG, Sikic BI (2012) Molecular pathways: regulation and therapeutic implications of multidrug resistance. *Clin Cancer Res* 18, 7: 1863-1869
- Chen Y, Tsai T, Ye X, Lin T (2015) Anti-proliferative effect on a colon adenocarcinoma cell line exerted by a membrane disrupting antimicrobial peptide KL15. *Cancer Biology & Therapy* 16, 8: 1172-1183
- Chernysh S, Irina K, Irina A (2012) Anti-tumor activity of immunomodulatory peptide alloferon-1 in mouse tumor transplantation model. *Int Immunopharmacol* 12, 1: 312-314
- Chu HL, Yip BS, Chen KH, Yu HY, Chih YH, Cheng HT, Chou YT, Cheng JW (2015) Novel antimicrobial peptides with high anticancer activity and selectivity. *PLoS One* 10, 5: e0126390
- Cichorek M, Kozłowska K, Witkowski JM, Zarzeczna M (2000) Flow cytometric estimation of the plasma membrane diversity of transplantable melanomas, using annexin V. *Folia Histochem Cytobiol* 38, 1: 41-43

- Ciobanasu C, Rzeszutek A, Kubitscheck U, Willumeit R (2015) NKCS, a Mutant of the NK-2 Peptide, Causes Severe Distortions and Perforations in Bacterial, But Not Human Model Lipid Membranes. *Molecules* 20, 4: 6941-6958
- Claudia Olak. (2008) Biophysikalische Studien zur Wechselwirkung des antimikrobiellen Peptides NK-2 mit membran-mimetischen Systemen. Universität Potsdam
- Cleland JL, Powell MF, Shire SJ (1993) The development of stable protein formulations: a close look at protein aggregation, deamidation, and oxidation. *Crit Rev Ther Drug Carrier Syst* 10, 4: 307-377
- Colombo G, Curnis F, De Mori GM, Gasparri A, Longoni C, Sacchi A, Longhi R, Corti A (2002) Structure-activity relationships of linear and cyclic peptides containing the NGR tumor-homing motif. *J Biol Chem* 277, 49: 47891-47897
- Cruciani RA, Barker JL, Zasloff M, Chen HC, Colamonici O (1991) Antibiotic magainins exert cytolytic activity against transformed cell lines through channel formation. *Proc Natl Acad Sci U S A* 88, 9: 3792-3796
- Dempsey CE (1990) The actions of melittin on membranes. *Biochim Biophys Acta* 1031, 2: 143-161
- Dennis JW, Granovsky M, Warren CE (1999) Glycoprotein glycosylation and cancer progression. *Biochim Biophys Acta* 1473, 1: 21-34
- Dennison S, Whittaker M, Harris F, Phoenix D (2006) Anticancer  $\alpha$ -Helical Peptides and Structure / Function Relationships Underpinning Their Interactions with Tumour Cell Membranes. *Curr Protein Peptide Sci* 7, 6: 487-499
- Desai TJ, Toombs JE, Minna JD, Brekken RA, Udugamasooriya DG (2016) Identification of lipid-phosphatidylserine (PS) as the target of unbiasedly selected cancer specific peptide-peptoid hybrid PPS1. *Oncotarget*, published online Apr. 22, doi: 10.18632/oncotarget.8929
- Desgranges S, Ruddle CC, Burke LP, McFadden TM, O'Brien JE, Fitzgerald-Hughes D, Humphreys H, Smyth TP, Devocelle M (2012)  $\beta$ -Lactam-host defence peptide conjugates as antibiotic prodrug candidates targeting resistant bacteria. *RSC Advances* 2, 6: 2480
- Deyrieux AF, Wilson VG (2007) In vitro culture conditions to study keratinocyte differentiation using the HaCaT cell line. *Cytotechnology* 54, 2: 77-83
- Dobrzynska I, Szachowicz-Petelska B, Sulkowski S, Figaszewski Z (2005) Changes in electric charge and phospholipids composition in human colorectal cancer cells. *Mol Cell Biochem* 276, 1-2: 113-119
- Dong HP, Holth A, Kleinberg L, Ruud MG, Elstrand MB, Trope CG, Davidson B, Risberg B (2009) Evaluation of cell surface expression of phosphatidylserine in ovarian carcinoma effusions using the annexin-V/7-AAD assay: clinical relevance and comparison with other apoptosis parameters. *Am J Clin Pathol* 132, 5: 756-762
- Douglas S, Hoskin D, Hilchie A (2014) Assessment of Antimicrobial (Host Defense) Peptides as Anti-Cancer Agents. In: Nixon AE (ed) . Humana Press, pp 159-170

- Drechsler S, Andrä J (2011) Online monitoring of metabolism and morphology of peptide-treated neuroblastoma cancer cells and keratinocytes. *J Bioenerg Biomembr* 43, 3: 275-285
- Du Q, Hou X, Ge L, Li R, Zhou M, Wang H, Wang L, Wei M, Chen T, Shaw C (2014) Cationicity-enhanced analogues of the antimicrobial peptides, AcrAP1 and AcrAP2, from the venom of the scorpion, *Androctonus crassicauda*, display potent growth modulation effects on human cancer cell lines. *Int J Biol Sci* 10, 10: 1097-1107
- Ebenhan T, Gheysens O, Kruger HG, Zeevaart JR, Sathekge MM (2014) Antimicrobial Peptides: Their Role as Infection-Selective Tracers for Molecular Imaging. *BioMed Research International* 2014: 1-15
- Eisenberg D, Schwarz E, Komaromy M, Wall R (1984) Analysis of membrane and surface protein sequences with the hydrophobic moment plot. *J Mol Biol* 179, 1: 125-142
- Eisenberg D, Weiss RM, Terwilliger TC (1982) The helical hydrophobic moment: a measure of the amphiphilicity of a helix. *Nature* 299, 5881: 371-374
- Fadnes B, Rekdal O, Uhlin-Hansen L (2009) The anticancer activity of lytic peptides is inhibited by heparan sulfate on the surface of the tumor cells. *BMC Cancer* 9: 183
- Fadnes B, Uhlin-Hansen L, Lindin I, Rekdal O (2011) Small lytic peptides escape the inhibitory effect of heparan sulfate on the surface of cancer cells. *BMC Cancer* 11: 116-2407-11-116
- Fan K, Li H, Wang Z, Du W, Yin W, Sun Y, Jiang J (2014) Expression and Purification of the Recombinant Porcine NK-lysin in *Pichia pastoris* and Observation of Anticancer Activity in Vitro. *Prep Biochem Biotechnol* 46, 1: 65-70
- Fernandez-Vega I, Garcia-Suarez O, Garcia B, Crespo A, Astudillo A, Quiros LM (2015) Heparan sulfate proteoglycans undergo differential expression alterations in right sided colorectal cancer, depending on their metastatic character. *BMC Cancer* 15: 742
- Forde E, Devocelle M (2015) Pro-moieties of antimicrobial peptide prodrugs. *Molecules* 20, 1: 1210-1227
- Förster T (1948) Zwischenmolekulare Energiewanderung und Fluoreszenz. *Annalen der Physik* 437, 1-2: 55-75
- Fox CH, Johnson FB, Whiting J, Roller PP (1985) Formaldehyde fixation. *J Histochem Cytochem* 33, 8: 845-853
- Frey B, Schildkopf P, Rodel F, Weiss EM, Munoz LE, Herrmann M, Fietkau R, Gaipf US (2009) AnnexinA5 renders dead tumor cells immunogenic--implications for multimodal cancer therapies. *J Immunotoxicol* 6, 4: 209-216
- Fuster MM, Esko JD (2005) The sweet and sour of cancer: glycans as novel therapeutic targets. *Nat Rev Cancer* 5, 7: 526-542
- Garcia-Suarez O, Garcia B, Fernandez-Vega I, Astudillo A, Quiros LM (2014) Neuroendocrine tumors show altered expression of chondroitin sulfate, glypican 1, glypican 5, and syndecan 2 depending on their differentiation grade. *Front Oncol* 4: 15

- Gaspar D, Veiga AS, Castanho MA (2013) From antimicrobial to anticancer peptides. A review. *Front Microbiol* 4: 294
- Gelhaus C, Jacobs T, Andrä J, Leippe M (2008) The antimicrobial peptide NK-2, the core region of mammalian NK-lysin, kills intraerythrocytic *Plasmodium falciparum*. *Antimicrob Agents Chemother* 52, 5: 1713-1720
- Giuliani A, Pirri G, Nicoletto S (2007) Antimicrobial peptides: an overview of a promising class of therapeutics. *Open Life Sciences* 2, 1: 1-33
- Gofman Y, Linser S, Rzeszutek A, Shental-Bechor D, Funari SS, Ben-Tal N, Willumeit R (2010) Interaction of an antimicrobial peptide with membranes: experiments and simulations with NKCS. *J Phys Chem B* 114, 12: 4230-4237
- Gross S, Andrä J (2012) Anticancer peptide NK-2 targets cell surface sulphated glycans rather than sialic acids. *Biol Chem* 393, 8: 817-827
- Gross S, Wilms D, Krause J, Brezesinski G, Andrä J (2013) Design of NK-2-derived peptides with improved activity against equine sarcoid cells. *J Pept Sci* 19, 10: 619-628
- Guani-Guerra E, Santos-Mendoza T, Lugo-Reyes SO, Teran LM (2010) Antimicrobial peptides: general overview and clinical implications in human health and disease. *Clin Immunol* 135, 1: 1-11
- Haag AF, Kerscher B, Dall'Angelo S, Sani M, Longhi R, Baloban M, Wilson HM, Mergaert P, Zanda M, Ferguson GP (2012) Role of cysteine residues and disulfide bonds in the activity of a legume root nodule-specific, cysteine-rich peptide. *J Biol Chem* 287, 14: 10791-10798
- Habermann E (1954) Zur Pharmakologie des Melittin. *Naunyn-Schmiedeberg's Archiv für experimentelle Pathologie und Pharmakologie* 222, 1-2: 173-175
- Habermann E (1972) Bee and Wasp Venoms. *Science* 177, 4046: 314-322
- Hallock KJ, Lee D, Ramamoorthy A (2003) MSI-78, an Analogue of the Magainin Antimicrobial Peptides, Disrupts Lipid Bilayer Structure via Positive Curvature Strain. *Biophys J* 84, 5: 3052-3060
- Hammer MU, Brauser A, Olak C, Brezesinski G, Goldmann T, Gutschmann T, Andrä J (2010) Lipopolysaccharide interaction is decisive for the activity of the antimicrobial peptide NK-2 against *Escherichia coli* and *Proteus mirabilis*. *Biochem J* 427, 3: 477-488
- Han YY, Liu HY, Han DJ, Zong XC, Zhang SQ, Chen YQ (2013) Role of glycosylation in the anticancer activity of antibacterial peptides against breast cancer cells. *Biochem Pharmacol* 86, 9: 1254-1262
- Hanahan D, Weinberg RA (2011) Hallmarks of cancer: the next generation. *Cell* 144, 5: 646-674
- Hancock RE, Haney EF, Gill EE (2016) The immunology of host defence peptides: beyond antimicrobial activity. *Nat Rev Immunol* 16, 5: 321-334
- Hancock REW, Sahl H (2006) Antimicrobial and host-defense peptides as new anti-infective therapeutic strategies. *Nat Biotechnol* 24, 12: 1551-1557

- Hanulova M, Andrä J, Garidel P, Olak C, Howe J, Funari S, Gutschmann T, Brandenburg K (2009) Interaction of Melittin with Phospholipid- and Lipopolysaccharide-Containing Model Membranes. *Anti-Infective Agents in Medicinal Chemistry* 8, 1: 17-27
- Harris F, Dennison SR, Singh J, Phoenix DA (2011) On the selectivity and efficacy of defense peptides with respect to cancer cells. *Med Res Rev* 33, 1: 190-234
- He K, Ludtke SJ, Worcester DL, Huang HW (1996) Neutron scattering in the plane of membranes: structure of alamethicin pores. *Biophys J* 70, 6: 2659-2666
- He Z, Mangala LS, Theriot CA, Rohde LH, Wu H, Zhang Y (2012) Cell killing and radiosensitizing effects of atorvastatin in PC3 prostate cancer cells. *J Radiat Res* 53, 2: 225-233
- Hofmann K, Stoffel W (1992) PROFILEGRAPH: an interactive graphical tool for protein sequence analysis. *Comput Appl Biosci* 8, 4: 331-337
- Hol WGJ (1985) The role of the  $\alpha$ -helix dipole in protein function and structure. *Prog Biophys Mol Biol* 45, 3: 149-195
- Holak TA, Engstroem A, Kraulis PJ, Lindeberg G, Bennich H, Jones TA, Gronenborn AM, Clore GM (1988) The solution conformation of the antibacterial peptide cecropin A: a nuclear magnetic resonance and dynamical simulated annealing study. *Biochemistry* 27, 20: 7620-7629
- Horobin RW (2002) Amino di- and triarylmethane dyes. In: Horobin RW, Kiernan JA (eds) *Conn's Biological Stains: A Handbook of Dyes, Stains and Fluorochromes for Use in Biology and Medicine*, 10th edition edn. Taylor & Francis, pp 249
- Hoskin DW, Ramamoorthy A (2008) Studies on anticancer activities of antimicrobial peptides. *Biochim Biophys Acta* 1778, 2: 357-375
- Hou L, Zhao X, Wang P, Ning Q, Meng M, Liu C (2013) Antitumor activity of antimicrobial peptides containing CisoDGRC in CD13 negative breast cancer cells. *PLoS One* 8, 1: e53491
- Hristova K, Dempsey CE, White SH (2001) Structure, Location, and Lipid Perturbations of Melittin at the Membrane Interface. *Biophys J* 80, 2: 801-811
- Hu J, Chen C, Zhang S, Zhao X, Xu H, Zhao X, Lu JR (2011) Designed antimicrobial and antitumor peptides with high selectivity. *Biomacromolecules* 12, 11: 3839-3843
- Huang J, Xu Y, Hao D, Huang Y, Liu Y, Chen Y (2010) Structure-guided de novo design of  $\alpha$ -helical antimicrobial peptide with enhanced specificity. *Pure Appl Chem* 82, 1
- Huang Y, Feng Q, Yan Q, Hao X, Chen Y (2015) Alpha-Helical Cationic Anticancer Peptides: A Promising Candidate for Novel Anticancer Drugs. *Mini Reviews in Medicinal Chemistry* 15, 1: 73-81
- Huang Y, He L, Li G, Zhai N, Jiang H, Chen Y (2014) Role of helicity of  $\alpha$ -helical antimicrobial peptides to improve specificity. *Protein Cell* 5, 8: 631-642

- Huang Y-, Wang X-, Wang H-, Liu Y, Chen Y (2011) Studies on Mechanism of Action of Anticancer Peptides by Modulation of Hydrophobicity Within a Defined Structural Framework. *Molecular Cancer Therapeutics* 10, 3: 416-426
- Hui L, Leung K, Chen HM (2002) The combined effects of antibacterial peptide cecropin A and anti-cancer agents on leukemia cells. *Anticancer Res* 22, 5: 2811-2816
- Hung S, Wang W, Chan SI, Chen HM (1999) Membrane Lysis by the Antibacterial Peptides Cecropins B1 and B3: A Spin-Label Electron Spin Resonance Study on Phospholipid Bilayers. *Biophys J* 77, 6: 3120-3133
- Ince TA, Sousa AD, Jones MA, Harrell JC, Agoston ES, Krohn M, Selfors LM, Liu W, Chen K, Yong M, Buchwald P, Wang B, Hale KS, Cohick E, Sergeant P, Witt A, Kozhekbaeva Z, Gao S, Agoston AT, Merritt MA, Foster R, Rueda BR, Crum CP, Brugge JS, Mills GB (2015) Characterization of twenty-five ovarian tumour cell lines that phenocopy primary tumours. *Nat Commun* 6: 7419
- Iwasaki T, Ishibashi J, Tanaka H, Sato M, Asaoka A, Taylor D, Yamakawa M (2009) Selective cancer cell cytotoxicity of enantiomeric 9-mer peptides derived from beetle defensins depends on negatively charged phosphatidylserine on the cell surface. *Peptides* 30, 4: 660-668
- Jacobs T, Bruhn H, Gaworski I, Fleischer B, Leippe M (2003) NK-lysin and its shortened analog NK-2 exhibit potent activities against *Trypanosoma cruzi*. *Antimicrob Agents Chemother* 47, 2: 607-613
- James S, Gibbs BF, Toney K, Bennett HP (1994) Purification of antimicrobial peptides from an extract of the skin of *Xenopus laevis* using heparin-affinity HPLC: characterization by ion-spray mass spectrometry. *Anal Biochem* 217, 1: 84-90
- Jenssen H, Hamill P, Hancock RE (2006) Peptide antimicrobial agents. *Clin Microbiol Rev* 19, 3: 491-511
- John E, Jähnig F (1988) Dynamics of melittin in water and membranes as determined by fluorescence anisotropy decay. *Biophys J* 54, 5: 817-827
- Kaconis Y, Kowalski I, Howe J, Brauser A, Richter W, Razquin-Olazarán I, Inigo-Pestana M, Garidel P, Rossle M, Martinez de Tejada G, Gutschmann T, Brandenburg K (2011) Biophysical mechanisms of endotoxin neutralization by cationic amphiphilic peptides. *Biophys J* 100, 11: 2652-2661
- Kaighn ME, Narayan KS, Ohnuki Y, Lechner JF, Jones LW (1979) Establishment and characterization of a human prostatic carcinoma cell line (PC-3). *Invest Urol* 17, 1: 16-23
- Kannagi R, Yin J, Miyazaki K, Izawa M (2008) Current relevance of incomplete synthesis and neo-synthesis for cancer-associated alteration of carbohydrate determinants--Hakomori's concepts revisited. *Biochim Biophys Acta* 1780, 3: 525-531
- Kay JG, Koivusalo M, Ma X, Wohland T, Grinstein S (2012) Phosphatidylserine dynamics in cellular membranes. *Mol Biol Cell* 23, 11: 2198-2212

- Kenis H, Reutelingsperger C (2009) Targeting phosphatidylserine in anti-cancer therapy. *Curr Pharm Des* 15, 23: 2719-2723
- Khoo K, Yu S (2010) Mass Spectrometric Analysis of Sulfated N- and O-Glycans. In: Fukuda M (ed) *Glycomics*, pp 3-26
- Kim JM, Lee YH, Ku CR, Lee EJ (2011) The cyclic pentapeptide d-Arg<sup>3</sup>FC131, a CXCR4 antagonist, induces apoptosis of somatotrope tumor and inhibits tumor growth in nude mice. *Endocrinology* 152, 2: 536-544
- Kim YJ, Varki A (1997) Perspectives on the significance of altered glycosylation of glycoproteins in cancer. *Glycoconj J* 14, 5: 569-576
- Kirby BJ, Hasselbrink EF (2004) Zeta potential of microfluidic substrates: 1. Theory, experimental techniques, and effects on separations. *Electrophoresis* 25, 2: 187-202
- Kirszberg C, Lima LG, Da Silva de Oliveira A, Pickering W, Gray E, Barrowcliffe TW, Rumjanek VM, Monteiro RQ (2009) Simultaneous tissue factor expression and phosphatidylserine exposure account for the highly procoagulant pattern of melanoma cell lines. *Melanoma Res* 19, 5: 301-308
- Kleeff J, Ishiwata T, Kumbasar A, Friess H, Buchler MW, Lander AD, Korc M (1998) The cell-surface heparan sulfate proteoglycan glypican-1 regulates growth factor action in pancreatic carcinoma cells and is overexpressed in human pancreatic cancer. *J Clin Invest* 102, 9: 1662-1673
- Kolata GB (1975) Microvilli: A Major Difference Between Normal and Cancer Cells? *Science* 188, 4190: 819-820
- Kondo E, Saito K, Tashiro Y, Kamide K, Uno S, Furuya T, Mashita M, Nakajima K, Tsumuraya T, Kobayashi N, Nishibori M, Tanimoto M, Matsushita M (2012) Tumour lineage-homing cell-penetrating peptides as anticancer molecular delivery systems. *Nat Commun* 3: 951
- Kuroda K, Fukuda T, Isogai H, Okumura K, Krstic-Demonacos M, Isogai E (2015) Antimicrobial peptide FF/CAP18 induces apoptotic cell death in HCT116 colon cancer cells via changes in the metabolic profile. *Int J Oncol* 46, 4: 1516-1526
- Lakowicz JR (ed) (2006) *Principles of Fluorescence Spectroscopy*. Springer Science+Business Media, LLC, New York
- Lee SH, Meng XW, Flatten KS, Loegering DA, Kaufmann SH (2013) Phosphatidylserine exposure during apoptosis reflects bidirectional trafficking between plasma membrane and cytoplasm. *Cell Death Differ* 20, 1: 64-76
- Lehrer RI, Ganz T (1999) Antimicrobial peptides in mammalian and insect host defence. *Curr Opin Immunol* 11, 1: 23-27
- Lemeshko VV (2013) Electrical potentiation of the membrane permeabilization by new peptides with anticancer properties. *Biochimica et Biophysica Acta (BBA) - Biomembranes* 1828, 3: 1047-1056

- Li S, Schoneich C, Borchardt RT (1995) Chemical instability of protein pharmaceuticals: Mechanisms of oxidation and strategies for stabilization. *Biotechnol Bioeng* 48, 5: 490-500
- Liang X, Kaya A, Zhang Y, Le DT, Hua D, Gladyshev VN (2012) Characterization of methionine oxidation and methionine sulfoxide reduction using methionine-rich cysteine-free proteins. *BMC Biochem* 13: 21-2091-13-21
- Liberio MS, Joanitti GA, Fontes W, Castro MS (2013) Anticancer peptides and proteins: a panoramic view. *Protein Pept Lett* 20, 4: 380-391
- Liepinsh E, Andersson M, Ruyschaert JM, Otting G (1997) Saposin fold revealed by the NMR structure of NK-lysin. *Nat Struct Biol* 4, 10: 793-795
- Linnebacher M, Maletzki C, Ostwald C, Klier U, Krohn M, Klar E, Prall F (2010) Cryopreservation of human colorectal carcinomas prior to xenografting. *BMC Cancer* 10: 362-2407-10-362
- Liu X, Li Y, Li Z, Lan X, Leung PH, Li J, Yang M, Ko F, Qin L (2015) Mechanism of Anticancer Effects of Antimicrobial Peptides. *J Fiber Bioeng Inform* 8, 1: 25-36
- Lohner K, Blondelle S (2005) Molecular Mechanisms of Membrane Perturbation by Antimicrobial Peptides and the Use of Biophysical Studies in the Design of Novel Peptide Antibiotics. *Comb Chem High Throughput Screen* 8, 3: 241-256
- Ludtke S, He K, Huang H (1995) Membrane thinning caused by magainin 2. *Biochemistry* 34, 51: 16764-16769
- M.D. Anderson Cancer Center, National Cancer Institute (NCI) Intratumoral Injections of LL37 for Melanoma. (2016) <https://clinicaltrials.gov/show/NCT02225366> , accessed on 07.01.2016
- Mader JS, Hoskin DW (2006) Cationic antimicrobial peptides as novel cytotoxic agents for cancer treatment. *Expert Opin Investig Drugs* 15, 8: 933-946
- Mader JS, Smyth D, Marshall J, Hoskin DW (2006) Bovine Lactoferricin Inhibits Basic Fibroblast Growth Factor- and Vascular Endothelial Growth Factor165-Induced Angiogenesis by Competing for Heparin-Like Binding Sites on Endothelial Cells. *Am J Pathol* 169, 5: 1753-1766
- Maher S, McClean S (2008) Melittin exhibits necrotic cytotoxicity in gastrointestinal cells which is attenuated by cholesterol. *Biochem Pharmacol* 75, 5: 1104-1114
- Mahoney KM, Rennert PD, Freeman GJ (2015) Combination cancer immunotherapy and new immunomodulatory targets. *Nat Rev Drug Discov* 14, 8: 561-584
- Maisetta G, Di Luca M, Esin S, Florio W, Brancatisano FL, Bottai D, Campa M, Batoni G (2008) Evaluation of the inhibitory effects of human serum components on bactericidal activity of human beta defensin 3. *Peptides* 29, 1: 1-6
- Maletzki C, Gock M, Randow M, Klar E, Huehns M, Prall F, Linnebacher M (2015) Establishment and characterization of cell lines from chromosomal unstable colorectal cancer. *World J Gastroenterol* 21, 1: 164-176

- Maletzki C, Klier U, Marinkovic S, Klar E, Andrä J, Linnebacher M (2014) Host defense peptides for treatment of colorectal carcinoma - a comparative in vitro and in vivo analysis. *Oncotarget* 5, 12: 4467-4479
- Maletzki C, Stier S, Gruenert U, Gock M, Ostwald C, Prall F, Linnebacher M (2012) Establishment, characterization and chemosensitivity of three mismatch repair deficient cell lines from sporadic and inherited colorectal carcinomas. *PLoS One* 7, 12: e52485
- Marr AK, Gooderham WJ, Hancock RE (2006) Antibacterial peptides for therapeutic use: obstacles and realistic outlook. *Curr Opin Pharmacol* 6, 5: 468-472
- Marshall NJ, Goodwin CJ, Holt SJ (1995) A critical assessment of the use of microculture tetrazolium assays to measure cell growth and function. *Growth Regul* 5, 2: 69-84
- Martinez-Lostao L, Miguel D, Al-Wasaby S, Gallego-Lleyda A, Anel A (2015) Death ligands and granulysin: mechanisms of tumor cell death induction and therapeutic opportunities. *Immunotherapy* 7, 8: 883-882
- Matsuzaki K, Murase O, Fujii N, Miyajima K (1996) An antimicrobial peptide, magainin 2, induced rapid flip-flop of phospholipids coupled with pore formation and peptide translocation. *Biochemistry* 35, 35: 11361-11368
- Matsuzaki K, Sugishita K, Fujii N, Miyajima K (1995) Molecular Basis for Membrane Selectivity of an Antimicrobial Peptide, Magainin 2. *Biochemistry* 34, 10: 3423-3429
- Mecke A, Lee D, Ramamoorthy A, Orr BG, Banaszak Holl MM (2005) Membrane Thinning Due to Antimicrobial Peptide Binding: An Atomic Force Microscopy Study of MSI-78 in Lipid Bilayers. *Biophys J* 89, 6: 4043-4050
- Medeiros KA, Joanitti GA, Silva LP (2014) Chitosan nanoparticles for dermaseptin peptide delivery toward tumor cells in vitro. *Anticancer Drugs* 25, 3: 323-331
- Melo MN, Ferre R, Castanho MA (2009) Antimicrobial peptides: linking partition, activity and high membrane-bound concentrations. *Nat Rev Microbiol* 7, 3: 245-250
- Minahk CJ, Morero RD (2003) Inhibition of enterocin CRL35 antibiotic activity by mono- and divalent ions. *Lett Appl Microbiol* 37, 5: 374-379
- Mookherjee N, Hancock RE (2007) Cationic host defence peptides: innate immune regulatory peptides as a novel approach for treating infections. *Cell Mol Life Sci* 64, 7-8: 922-933
- Moreland JL, Gramada A, Buzko OV, Zhang Q, Bourne PE (2005) The Molecular Biology Toolkit (MBT): a modular platform for developing molecular visualization applications. *BMC Bioinformatics* 6, 1: 1-7
- Morshed RA, Muroski ME, Dai Q, Wegscheid ML, Auffinger B, Yu D, Han Y, Zhang L, Wu M, Cheng Y, Lesniak MS (2016) Cell-Penetrating Peptide-Modified Gold Nanoparticles for the Delivery of Doxorubicin to Brain Metastatic Breast Cancer. *Mol Pharm* 13, 6: 1843-1854
- Mosmann T (1983) Rapid colorimetric assay for cellular growth and survival: Application to proliferation and cytotoxicity assays. *J Immunol Methods* 65, 1-2: 55-63

- Nicolas P (2009) Multifunctional host defense peptides: intracellular-targeting antimicrobial peptides. *FEBS J* 276, 22: 6483-6496
- Nie D, Ren SX, Shen J, Cheng ASL, Lu L, Chan RLY, Li ZJ, Wang XJ, Wong CCM, Zhang L, Ng SSM, Chan FL, Chan FKL, Yu J, Sung JJY, Wu WKK, Cho CH (2013) FK-16 Derived from the Anticancer Peptide LL-37 Induces Caspase-Independent Apoptosis and Autophagic Cell Death in Colon Cancer Cells. *PLoS One* 8, 5: e63641
- Niemirowicz K, Prokop I, Wilczewska AZ, Wnorowska U, Piktel E, Watek M, Savage PB, Bucki R (2015) Magnetic nanoparticles enhance the anticancer activity of cathelicidin LL-37 peptide against colon cancer cells. *Int J Nanomedicine* 10: 3843-3853
- Nitzsche R, Simon F (1997) Bestimmung des Zetapotentials aus Messungen der elektroforetischen Mobilität. *tm - Technisches Messen* 64: 106-113
- Nozaki Y, Tanford C (1967) Examination of titration behavior. In: *Anonymous Enzyme Structure*. Academic Press, pp 715-734
- Olak C, Muentner A, Andrä J, Brezesinski G (2008) Interfacial properties and structural analysis of the antimicrobial peptide NK-2. *J Pept Sci* 14, 4: 510-517
- Pace CN, Scholtz JM (1998) A helix propensity scale based on experimental studies of peptides and proteins. *Biophys J* 75, 1: 422-427
- Papo N, Seger D, Makovitzki A, Kalchenko V, Eshhar Z, Degani H, Shai Y (2006) Inhibition of Tumor Growth and Elimination of Multiple Metastases in Human Prostate and Breast Xenografts by Systemic Inoculation of a Host Defense-Like Lytic Peptide. *Cancer Research* 66, 10: 5371-5378
- Papo N, Shahar M, Eisenbach L, Shai Y (2003) A novel lytic peptide composed of DL-amino acids selectively kills cancer cells in culture and in mice. *J Biol Chem* 278, 23: 21018-21023
- Papo N, Shai Y (2005) Host defense peptides as new weapons in cancer treatment. *Cell Mol Life Sci* 62, 7-8: 784-790
- Pearce OMT, Läubli H (2015) Sialic acids in cancer biology and immunity. *Glycobiology* 26, 2: 111-128
- Peck-Miller KA, Darveau RP, Fell HP (1993) Identification of serum components that inhibit the tumoricidal activity of amphiphilic alpha helical peptides. *Cancer Chemother Pharmacol* 32, 2: 109-115
- Pimthon J, Willumeit R, Lendlein A, Hofmann D (2009) Membrane association and selectivity of the antimicrobial peptide NK-2: a molecular dynamics simulation study. *J Pept Sci* 15, 10: 654-667
- Pink DA, Truelstrup Hansen L, Gill TA, Quinn BE, Jericho MH, Beveridge TJ (2003) Divalent Calcium Ions Inhibit the Penetration of Protamine through the Polysaccharide Brush of the Outer Membrane of Gram-Negative Bacteria. *Langmuir* 19, 21: 8852-8858

- Pohl A, Lage H, Muller P, Pomorski T, Herrmann A (2002) Transport of phosphatidylserine via MDR1 (multidrug resistance 1)P-glycoprotein in a human gastric carcinoma cell line. *Biochem J* 365, Pt 1: 259-268
- Pouny Y, Rapaport D, Mor A, Nicolas P, Shai Y (1992) Interaction of antimicrobial dermaseptin and its fluorescently labeled analogs with phospholipid membranes. *Biochemistry* 31, 49: 12416-12423
- Qiu F, Hu M, Tang B, Liu X, Zhuang H, Yang J, Hua Z (2013) Annexin V-TRAIL fusion protein is a more sensitive and potent apoptotic inducer for cancer therapy. *Sci Rep* 3: 3565
- Ran S, Downes A, Thorpe PE (2002) Increased exposure of anionic phospholipids on the surface of tumor blood vessels. *Cancer Res* 62, 21: 6132-6140
- Rao LVM, Tait JF, Hoang AD (1992) Binding of annexin V to a human ovarian carcinoma cell line (OC-2008). Contrasting effects on cell surface factor VIIa/tissue factor activity and prothrombinase activity. *Thromb Res* 67, 5: 517-531
- Raucher D, Ryu JS (2015) Cell-penetrating peptides: strategies for anticancer treatment. *Trends Mol Med* 21, 9: 560-570
- Ren J, Hamada J, Okada F, Takeichi N, Morikawa K, Hosokawa M, Kobayashi H (1990) Correlation between the presence of microvilli and the growth or metastatic potential of tumor cells. *Jpn J Cancer Res* 81, 9: 920-926
- Ren SX, Shen J, Cheng AS, Lu L, Chan RL, Li ZJ, Wang XJ, Wong CC, Zhang L, Ng SS, Chan FL, Chan FK, Yu J, Sung JJ, Wu WK, Cho CH (2015) Correction: FK-16 Derived from the Anticancer Peptide LL-37 Induces Caspase-Independent Apoptosis and Autophagic Cell Death in Colon Cancer Cells. *PLoS One* 10, 6: e0131750
- Riedl S, Leber R, Rinner B, Schaidler H, Lohner K, Zweytick D (2015) Human lactoferricin derived di-peptides deploying loop structures induce apoptosis specifically in cancer cells through targeting membranous phosphatidylserine. *Biochimica et Biophysica Acta (BBA) - Biomembranes* 1848, 11, Part A: 2918-2931
- Riedl S, Rinner B, Asslaber M, Schaidler H, Walzer S, Novak A, Lohner K, Zweytick D (2011b) In search of a novel target - phosphatidylserine exposed by non-apoptotic tumor cells and metastases of malignancies with poor treatment efficacy. *Biochim Biophys Acta* 1808, 11: 2638-2645
- Riedl S, Zweytick D, Lohner K (2011a) Membrane-active host defense peptides – Challenges and perspectives for the development of novel anticancer drugs. *Chem Phys Lipids* 164, 8: 766-781
- Risso A, Zanetti M, Gennaro R (1998) Cytotoxicity and apoptosis mediated by two peptides of innate immunity. *Cell Immunol* 189, 2: 107-115
- Rodrigues EG, Dobroff AS, Cavarsan CF, Paschoalin T, Nimrichter L, Mortara RA, Santos EL, Fazio MA, Miranda A, Daffre S, Travassos LR (2008) Effective topical treatment of subcutaneous murine B16F10-Nex2 melanoma by the antimicrobial peptide gomesin. *Neoplasia* 10, 1: 61-68

- Sanderson RD, Yang Y, Suva LJ, Kelly T (2004) Heparan sulfate proteoglycans and heparanase-partners in osteolytic tumor growth and metastasis. *Matrix Biol* 23, 6: 341-352
- Sansom MS (1991) The biophysics of peptide models of ion channels. *Prog Biophys Mol Biol* 55, 3: 139-235
- Sato H, Feix JB (2006) Peptide-membrane interactions and mechanisms of membrane destruction by amphipathic  $\alpha$ -helical antimicrobial peptides. *Biochimica et Biophysica Acta (BBA) - Biomembranes* 1758, 9: 1245-1256
- Savitzky A, Golay MJE (1964) Smoothing and Differentiation of Data by Simplified Least Squares Procedures. *Anal Chem* 36, 8: 1627-1639
- Scane TM, Hawkins DF (1986) Antibacterial activity in human amniotic fluid: dependence on divalent cations. *Br J Obstet Gynaecol* 93, 6: 577-581
- Schadich E, Mason D, Cole AL (2013) Neutralization of bacterial endotoxins by frog antimicrobial peptides. *Microbiol Immunol* 57, 2: 159-161
- Schmidtchen A, Frick IM, Andersson E, Tapper H, Bjorck L (2002) Proteinases of common pathogenic bacteria degrade and inactivate the antibacterial peptide LL-37. *Mol Microbiol* 46, 1: 157-168
- Schmidtchen A, Frick IM, Bjorck L (2001) Dermatan sulphate is released by proteinases of common pathogenic bacteria and inactivates antibacterial alpha-defensin. *Mol Microbiol* 39, 3: 708-713
- Schmidtchen A, Pasupuleti M, Malmsten M (2014) Effect of hydrophobic modifications in antimicrobial peptides. *Adv Colloid Interface Sci* 205: 265-274
- Schröder-Borm H, Bakalova R, Andrä J (2005) The NK-lysin derived peptide NK-2 preferentially kills cancer cells with increased surface levels of negatively charged phosphatidylserine. *FEBS Lett* 579, 27: 6128-6134
- Schröder-Borm H, Willumeit R, Brandenburg K, Andrä J (2003) Molecular basis for membrane selectivity of NK-2, a potent peptide antibiotic derived from NK-lysin. *Biochim Biophys Acta* 1612, 2: 164-171
- Schutters K, Reutelingsperger C (2010) Phosphatidylserine targeting for diagnosis and treatment of human diseases. *Apoptosis* 15, 9: 1072-1082
- Schweizer F (2009) Cationic amphiphilic peptides with cancer-selective toxicity. *Eur J Pharmacol* 625, 1-3: 190-194
- Seo MD, Kang TJ, Lee CH, Lee AY, Noh M (2012) HaCaT Keratinocytes and Primary Epidermal Keratinocytes Have Different Transcriptional Profiles of Cornified Envelope-Associated Genes to T Helper Cell Cytokines. *Biomol Ther (Seoul)* 20, 2: 171-176
- Shai Y (2002) Mode of action of membrane active antimicrobial peptides. *Biopolymers* 66, 4: 236-248
- Sharma A, Kapoor P, Gautam A, Chaudhary K, Kumar R, Chauhan JS, Tyagi A, Raghava GP (2013) Computational approach for designing tumor homing peptides. *Sci Rep* 3: 1607

- Sharma SV (1993) Melittin-induced hyperactivation of phospholipase A2 activity and calcium influx in ras-transformed cells. *Oncogene* 8, 4: 939-947
- Shim JH, Kim KH, Cho YS, Choi HS, Song EY, Myung PK, Kang JS, Suh SK, Park SN, Yoon DY (2008) Protective effect of oxidative stress in HaCaT keratinocytes expressing E7 oncogene. *Amino Acids* 34, 1: 135-141
- Siegel R, Ma J, Zou Z, Jemal A (2014) Cancer statistics, 2014. *CA: A Cancer Journal for Clinicians* 64, 1: 9-29
- Simmons TL, Andrianasolo E, McPhail K, Flatt P, Gerwick WH (2005) Marine natural products as anticancer drugs. *Mol Cancer Ther* 4, 2: 333-342
- Sinthuvanich C, Veiga AS, Gupta K, Gaspar D, Blumenthal R, Schneider JP (2012) Anticancer beta-hairpin peptides: membrane-induced folding triggers activity. *J Am Chem Soc* 134, 14: 6210-6217
- Sivertsen A, Isaksson J, Leiros HS, Svenson J, Svendsen J, Brandsdal B (2014) Synthetic cationic antimicrobial peptides bind with their hydrophobic parts to drug site II of human serum albumin. *BMC Structural Biology* 14, 1: 4
- Sok M, Sentjurc M, Schara M (1999) Membrane fluidity characteristics of human lung cancer. *Cancer Lett* 139, 2: 215-220
- Sommer A, Fries A, Cornelsen I, Speck N, Koch-Nolte F, Gimpl G, Andrä J, Bhakdi S, Reiss K (2012) Melittin Modulates Keratinocyte Function. *J Biol Chem* 287, 28: 23678-23689
- Son DJ, Lee JW, Lee YH, Song HS, Lee CK, Hong JT (2007) Therapeutic application of anti-arthritis, pain-releasing, and anti-cancer effects of bee venom and its constituent compounds. *Pharmacol Ther* 115, 2: 246-270
- Sood R, Kinnunen PKJ (2008) Cholesterol, lanosterol, and ergosterol attenuate the membrane association of LL-37(W27F) and temporin L. *Biochimica et Biophysica Acta (BBA) - Biomembranes* 1778, 6: 1460-1466
- Stadtman ER, Van Remmen H, Richardson A, Wehr NB, Levine RL (2005) Methionine oxidation and aging. *Biochim Biophys Acta* 1703, 2: 135-140
- Steiner H, Andreu D, Merrifield RB (1988) Binding and action of cecropin and cecropin analogues: Antibacterial peptides from insects. *Biochimica et Biophysica Acta (BBA) - Biomembranes* 939, 2: 260-266
- Steiner H, Hultmark D, Engstrom A, Bennich H, Boman HG (1981) Sequence and specificity of two antibacterial proteins involved in insect immunity. *Nature* 292, 5820: 246-248
- Steinstraesser L, Schubert C, Hauk J, Becerikli M, Stricker I, Koeller M, Hatt H, von Duering M, Shai Y, Steinau HU, Jacobsen F (2011) Oncolytic designer host defense peptide suppresses growth of human liposarcoma. *Int J Cancer* 128, 12: 2994-3004
- Stenger S, Rosat J, Bloom BR, Krensky AM, Modlin RL (1999) Granulysin: a lethal weapon of cytolytic T cells. *Immunol Today* 20, 9: 390-394

- Sudheendra Udipi Seetharamacharya. (2005) Etudes structurales par Résonance Magnétique Nucléaire du solide de polypeptides membranaires dans des bicouches lipidiques. Applications aux peptides et aux protéins formants des canaux ioniques. Université Louis Pasteur de Strasbourg
- Suttman H, Retz M, Paulsen F, Harder J, Zwergel U, Kamradt J, Wullich B, Unteregger G, Stöckle M, Lehmann J (2008) Antimicrobial peptides of the Cecropin-family show potent antitumor activity against bladder cancer cells. *BMC Urol* 8: 5
- Suzuki T, Fujikura K, Higashiyama T, Takata K (1997) DNA Staining for Fluorescence and Laser Confocal Microscopy. *J Histochem Cytochem* 45, 1: 49-53
- Svenson J, Brandsdal BO, Stensen W, Svendsen JS (2007) Albumin binding of short cationic antimicrobial micropeptides and its influence on the in vitro bactericidal effect. *J Med Chem* 50, 14: 3334-3339
- Tait JF, Gibson D (1992) Phospholipid binding of annexin V: Effects of calcium and membrane phosphatidylserine content. *Arch Biochem Biophys* 298, 1: 187-191
- Thun MJ, DeLancey JO, Center MM, Jemal A, Ward EM (2010) The global burden of cancer: priorities for prevention. *Carcinogenesis* 31, 1: 100-110
- Torre LA, Bray F, Siegel RL, Ferlay J, Lortet-Tieulent J, Jemal A (2015) Global cancer statistics, 2012. *CA: A Cancer Journal for Clinicians* 65, 2: 87-108
- Tossi A (2005) Host defense peptides: roles and applications. *Curr Protein Pept Sci* 6, 1: 1-3
- Tosteson MT, Holmes SJ, Razin M, Tosteson DC (1985) Melittin lysis of red cells. *J Membr Biol* 87, 1: 35-44
- Tyagi A, Kapoor P, Kumar R, Chaudhary K, Gautam A, Raghava GP (2013) In silico models for designing and discovering novel anticancer peptides. *Sci Rep* 3: 2984
- Urban P, Valle-Delgado JJ, Moles E, Marques J, Diez C, Fernandez-Busquets X (2012) Nanotools for the delivery of antimicrobial peptides. *Curr Drug Targets* 13, 9: 1158-1172
- Utsugi T, Schroit AJ, Connor J, Bucana CD, Fidler IJ (1991) Elevated expression of phosphatidylserine in the outer membrane leaflet of human tumor cells and recognition by activated human blood monocytes. *Cancer Res* 51, 11: 3062-3066
- van Meerloo J, Kaspers GJ, Cloos J (2011) Cell sensitivity assays: the MTT assay. *Methods Mol Biol* 731: 237-245
- Vance JE, Steenbergen R (2005) Metabolism and functions of phosphatidylserine. *Prog Lipid Res* 44, 4: 207-234
- Vance JE, Tasseva G (2013) Formation and function of phosphatidylserine and phosphatidylethanolamine in mammalian cells. *Biochim Biophys Acta* 1831, 3: 543-554
- Verkleij AJ, Zwaal RF, Roelofsen B, Comfurius P, Kastelijn D, van Deenen LL (1973) The asymmetric distribution of phospholipids in the human red cell membrane. A combined study using phospholipases and freeze-etch electron microscopy. *Biochim Biophys Acta* 323, 2: 178-193

- Vij N, Nguyen LT, Chau JK, Perry NA, de Boer L, Zaat SAJ, Vogel HJ (2010) Serum Stabilities of Short Tryptophan- and Arginine-Rich Antimicrobial Peptide Analogs. *PLoS One* 5, 9: e12684
- Wang G, Li X, Wang Z (2009a) APD2: the updated antimicrobial peptide database and its application in peptide design. *Nucleic Acids Res* 37, Database: D933-D937
- Wang G, Li X, Wang Z (2015b) APD3: the antimicrobial peptide database as a tool for research and education. *Nucleic Acids Res* 44, D1: D1087-D1093
- Wang G, Mishra B, Lau K, Lushnikova T, Golla R, Wang X (2015a) Antimicrobial peptides in 2014. *Pharmaceuticals* 8, 1: 123-150
- Wang KR, Yan JX, Zhang BZ, Song JJ, Jia PF, Wang R (2009b) Novel mode of action of polybia-MPI, a novel antimicrobial peptide, in multi-drug resistant leukemic cells. *Cancer Lett* 278, 1: 65-72
- Wang XJ, Wang XM, Teng D, Zhang Y, Mao RY, Wang JH (2014) Recombinant production of the antimicrobial peptide NZ17074 in *Pichia pastoris* using SUMO3 as a fusion partner. *Lett Appl Microbiol* 59, 1: 71-78
- Watson GW, Wickramasekara S, Palomera-Sanchez Z, Black C, Maier CS, Williams DE, Dashwood RH, Ho E (2014) SUV39H1/H3K9me3 attenuates sulforaphane-induced apoptotic signaling in PC3 prostate cancer cells. *Oncogenesis* 3: e131
- Weghuber J, Aichinger MC, Brameshuber M, Wieser S, Ruprecht V, Plochberger B, Madl J, Horner A, Reipert S, Lohner K, Henics T, Schutz GJ (2011) Cationic amphipathic peptides accumulate sialylated proteins and lipids in the plasma membrane of eukaryotic host cells. *Biochim Biophys Acta* 1808, 10: 2581-2590
- Wei G, Campagna AN, Bobek LA (2007) Factors affecting antimicrobial activity of MUC7 12-mer, a human salivary mucin-derived peptide. *Ann Clin Microbiol Antimicrob* 6, 1: 14
- Wei L, Huang C, Yang H, Li M, Yang J, Qiao X, Mu L, Xiong F, Wu J, Xu W (2015) A potent anti-inflammatory peptide from the salivary glands of horsefly. *Parasites & Vectors* 8, 1: 1-13
- White SH, Wimley WC (1999) Membrane protein folding and stability: physical principles. *Annu Rev Biophys Biomol Struct* 28: 319-365
- Whittle JR, Lewis MT, Lindeman GJ, Visvader JE (2015) Patient-derived xenograft models of breast cancer and their predictive power. *Breast Cancer Res* 17: 17
- Willumeit R, Kumpugdee M, Funari SS, Lohner K, Navas BP, Brandenburg K, Linser S, Andrä J (2005) Structural rearrangement of model membranes by the peptide antibiotic NK-2. *Biochim Biophys Acta* 1669, 2: 125-134
- Wimley WC, White SH (1996) Experimentally determined hydrophobicity scale for proteins at membrane interfaces. *Nat Struct Biol* 3, 10: 842-848

- Yamaguchi S, Huster D, Waring A, Lehrer RI, Kearney W, Tack BF, Hong M (2001) Orientation and Dynamics of an Antimicrobial Peptide in the Lipid Bilayer by Solid-State NMR Spectroscopy. *Biophys J* 81, 4: 2203-2214
- Yang L, Harroun TA, Weiss TM, Ding L, Huang HW (2001) Barrel-Stave Model or Toroidal Model? A Case Study on Melittin Pores. *Biophys J* 81, 3: 1475-1485
- Yasemin Manavbasi. (2012) NKCS derived peptides as novel cancer therapeutics. Technische Universität Graz
- Ye J, Zheng X, Leung KW, Chen HM, Sheu F (2004) Induction of Transient Ion Channel-Like Pores in a Cancer Cell by Antibiotic Peptide. *J Biochem* 136, 2: 255-259
- Yeaman MR, Yount NY (2003) Mechanisms of antimicrobial peptide action and resistance. *Pharmacol Rev* 55, 1: 27-55
- Yeung A, Gellatly S, Hancock R (2011) Multifunctional cationic host defence peptides and their clinical applications. *Cellular and Molecular Life Sciences* 68, 13: 2161-2176
- Yin LM, Edwards MA, Li J, Yip CM, Deber CM (2012) Roles of hydrophobicity and charge distribution of cationic antimicrobial peptides in peptide-membrane interactions. *J Biol Chem* 287, 10: 7738-7745
- Yount NY, Yeaman MR (2012) Emerging themes and therapeutic prospects for anti-infective peptides. *Annu Rev Pharmacol Toxicol* 52: 337-360
- Zaslhoff M (2002) Antimicrobial peptides of multicellular organisms. *Nature* 415, 6870: 389-395
- Zelezetsky I, Tossi A (2006) Alpha-helical antimicrobial peptides - using a sequence template to guide structure-activity relationship studies. *Biochim Biophys Acta* 1758, 9: 1436-1449
- Zhu X, Dong N, Wang Z, Ma Z, Zhang L, Ma Q, Shan A (2014) Design of imperfectly amphipathic alpha-helical antimicrobial peptides with enhanced cell selectivity. *Acta Biomater* 10, 1: 244-257
- Zwaal RF, Comfurius P, Bevers EM (2005) Surface exposure of phosphatidylserine in pathological cells. *Cell Mol Life Sci* 62, 9: 971-988

## APPENDIX

**Table A.1: Hydrophobicity scales.** The Normalized Consensus (NC) scale and the Whole-Residue Interface (WIF) scale have been introduced by Eisenberg et al. (1984) and Wimley and White (1996), respectively. The NC scale combines multiple previously proposed scales and assigns each amino acid residue ( $i$ ) a particular hydrophobicity value ( $H_i$ ). It ranks the individual contribution of each residue based on its particular physicochemical properties in such a way that the mean over all contributive factors equals 0 with a standard deviation of  $\pm 1$ . In despite, the WIF scale additionally takes influences of peptide bonds into account and ranks individual amino acids based on transfer free energies ( $\Delta G_{WIF}$ ) resulting from experimentally determined for lipid bilayer partitioning. "n.d." means not determined.

Index $i$	Amino acid (3-, 1-letter-code)	$H_i$ according to NC / -	$H_i$ as $\Delta G_{WIF}$ according to WIF / kcal/mol
1	Alanine (Ala, A)	0.62	0.17
2	Arginine (Arg, R)	-2.53	0.81
3	Asparagine (Asn, N)	-0.78	0.42
4	Aspartic acid (Asp, D)	-0.90	1.23
5	Cysteine (Cys, C)	0.29	-0.24
6	Glutamine (Gln, Q)	-0.85	0.58
7	Glutamic acid (Glu, E)	-0.74	2.02
8	Glycine (Gly, G)	0.48	0.01
9	Histidine (His, H)	-0.40	0.17
10	Isoleucine (Ile, I)	1.38	-0.31
11	Leucine (Leu, L)	1.06	-0.56
12	Lysine (Lys, K)	-1.50	0.99
13	Methionine (Met, M)	0.64	-0.23
14	Phenylalanine (Phe, F)	1.19	-1.13
15	Proline (Pro, P)	0.12	0.45
16	Serine (Ser, S)	-0.18	0.13
17	Threonine (Thr, T)	-0.05	0.14
18	Tryptophan (Trp, W)	0.81	-1.85
19	Tyrosine (Tyr, Y)	0.26	-0.94
20	Valine (Val, V)	1.08	0.07
	Mean	0.00	n.d.
	Standard deviation	1.00	n.d.

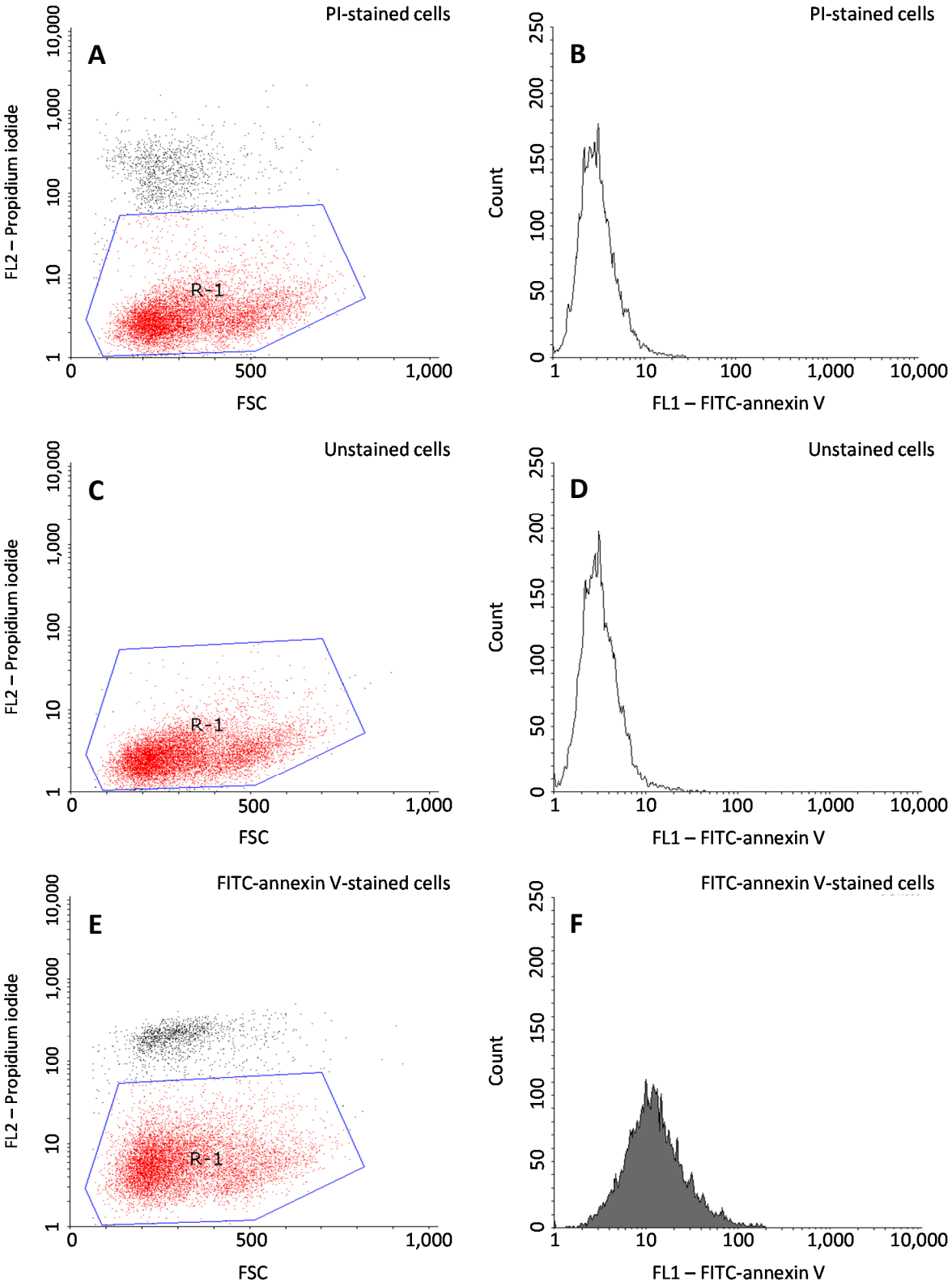


**Figure A.1: Pre-evaluation processing of flow cytometry data.** Initially, for the sake of dead cell exclusion, gating (R-1, red dots) was done manually in dot plots of the FL2 (propidium iodide; PI) versus forward scatter (FSC) signals (A). Pre-gated populations of unstained (C) and FITC-annexin V-stained cells (E) were then individually analyzed based on histogram intensity plots of their FL1 (FITC) signals (D and F, respectively). The ratio of the geometric mean fluorescence intensities from (F) over (D) represents a measure of the cellular PS exposure.

Appendix

**Table A.2: Sequences and structure-related peptide properties as assessed separately for N- and C-terminal segments.** Expanding the set of calculated physicochemical peptide features presented in table 5.1, the same parameters were additionally determined for peptide segments notionally separating N-terminal (index *N*) and C-terminal (index *C*) sequence moieties. The split point of each sequence is indicated by a tilde symbol (~). Peptides are sorted in the order of decreasing sequence length (*n*), and accordingly assigned a numerical identifier (ID). Referring to the sequence of NK-2, residue changes are indicated by bold type letters, while hyphens represent omissions. All peptides, except C7S-OH, were synthesized with amidated C-termini. Determined parameters enclosed each peptide's net charge (*Q*) and average charge per residue (*Q/n*) at physiological pH, the mean hydrophobicity (*H*), as well as the proportions of hydrophobicity to net (*H/Q*) and average residual charge (*H/(Q/n)*). Background grey-scale coding delineates single-substitution (IDs 2-13), multiple-substitution (IDs 14-16), and deletion (IDs 17-34) variants of parent peptide NK-2 (ID 1). An asterisk (\*) indicates the non-NK-2-related reference peptide melittin.

ID	Peptide	<i>n<sub>N</sub></i>	<i>n<sub>C</sub></i>	<i>Q<sub>N</sub></i>	<i>Q<sub>C</sub></i>	$(Q/n)_N$	$(Q/n)_C$	<i>H<sub>N</sub></i>	<i>H<sub>C</sub></i>	$(H/Q)_N$	$(H/Q)_C$	$(H/(Q/n))_N$	$(H/(Q/n))_C$	
1	NK-2	KILRGV <b>C</b> CKIMRT~FLRRISKDIL <b>TG</b> KK	13	14	+5	+5	+0.38	+0.36	-0.25	-0.20	-0.051	-0.041	-0.66	-0.57
2	I2W	KWLRGV <b>C</b> CKIMRT~FLRRISKDIL <b>TG</b> KK	13	14	+5	+5	+0.38	+0.36	-0.30	-0.20	-0.060	-0.041	-0.77	-0.57
3	R4L	KIL <b>L</b> GV <b>C</b> CKIMRT~FLRRISKDIL <b>TG</b> KK	13	14	+4	+5	+0.31	+0.36	+0.02	-0.20	+0.006	-0.041	+0.07	-0.57
4	C7A	KILRGV <b>A</b> CKIMRT~FLRRISKDIL <b>TG</b> KK	13	14	+5	+5	+0.38	+0.36	-0.23	-0.20	-0.046	-0.041	-0.59	-0.57
5	C7L	KILRGV <b>L</b> CKIMRT~FLRRISKDIL <b>TG</b> KK	13	14	+5	+5	+0.38	+0.36	-0.19	-0.20	-0.039	-0.041	-0.51	-0.57
6	C7S	KILRGV <b>S</b> CKIMRT~FLRRISKDIL <b>TG</b> KK	13	14	+5	+5	+0.38	+0.36	-0.29	-0.20	-0.058	-0.041	-0.75	-0.57
7	C7S-OH	KILRGV <b>S</b> CKIMRT~FLRRISKDIL <b>TG</b> KK- <b>OH</b>	13	14	+5	+4	+0.38	+0.29	-0.29	-0.20	-0.058	-0.051	-0.75	-0.71
8	M11L	KILRGV <b>C</b> CKI <b>L</b> RT~FLRRISKDIL <b>TG</b> KK	13	14	+5	+5	+0.38	+0.36	-0.22	-0.20	-0.044	-0.041	-0.58	-0.57
9	F14W	KILRGV <b>C</b> CKIMRT~ <b>W</b> LRRISKDIL <b>TG</b> KK	13	14	+5	+5	+0.38	+0.36	-0.25	-0.23	-0.051	-0.046	-0.66	-0.65
10	R17L	KILRGV <b>C</b> CKIMRT~FL <b>L</b> ISKDIL <b>TG</b> KK	13	14	+5	+4	+0.38	+0.29	-0.25	+0.07	-0.051	0.018	-0.66	+0.26
11	D21K	KILRGV <b>C</b> CKIMRT~FLRRISK <b>I</b> L <b>TG</b> KK	13	14	+5	+7	+0.38	+0.50	-0.25	-0.25	-0.051	-0.036	-0.66	-0.50
12	D21L	KILRGV <b>C</b> CKIMRT~FLRRISK <b>L</b> I <b>L</b> TGKK	13	14	+5	+6	+0.38	+0.43	-0.25	-0.05	-0.051	-0.009	-0.66	-0.12
13	G25W	KILRGV <b>C</b> CKIMRT~FLRRISKDIL <b>TW</b> KK	13	14	+5	+5	+0.38	+0.36	-0.25	-0.18	-0.051	-0.036	-0.66	-0.50
14	C7A-D21K	KILRGV <b>A</b> CKIMRT~FLRRISK <b>K</b> I <b>L</b> TGKK	13	14	+5	+7	+0.38	+0.50	-0.23	-0.25	-0.046	-0.036	-0.59	-0.50
15	C7A-K8L-D21K	KILRGV <b>A</b> L <b>K</b> IMRT~FLRRISK <b>K</b> I <b>L</b> TGKK	13	14	+4	+7	+0.31	+0.50	-0.03	-0.25	-0.008	-0.036	-0.10	-0.50
16	C7A-M11L-D21K	KILRGV <b>A</b> CKI <b>L</b> RT~FLRRISK <b>K</b> I <b>L</b> TGKK	13	14	+5	+7	+0.38	+0.50	-0.20	-0.25	-0.039	-0.036	-0.51	-0.50
17	NK-2-K	-ILRGV <b>C</b> CKIMRT <b>F</b> ~LRRISKDIL <b>TG</b> KK	13	13	+4	+5	+0.31	+0.38	-0.05	-0.41	-0.012	-0.082	-0.15	-1.07
18	NK-2-KK	KILRGV <b>C</b> CKIMR~TFLRRISKDIL <b>TG</b> --	12	13	+5	+3	+0.42	+0.23	-0.27	-0.09	-0.054	-0.031	-0.65	-0.40
19	NK-2-KKK	-ILRGV <b>C</b> CKIMRT~FLRRISKDIL <b>TG</b> --	12	12	+4	+3	+0.33	+0.25	-0.15	-0.10	-0.038	-0.032	-0.45	-0.38
20	C7A-Δ	KILRGV <b>A</b> CKIM~RTFLRR---IL <b>TG</b> KK	11	12	+4	+6	+0.36	+0.50	-0.04	-0.46	-0.009	-0.077	-0.10	-0.92
21	L3K-C7A-F14K-Δ	KI <b>K</b> RGV <b>A</b> CKIM~RT <b>K</b> LRR---IL <b>TG</b> KK	11	12	+5	+7	+0.45	+0.58	-0.27	-0.68	-0.054	-0.098	-0.59	-1.17
22	NK23a	KI--- <b>S</b> CKIMRT <b>F</b> L~RRISKDIL <b>TG</b> KK	11	12	+4	+5	+0.36	+0.42	-0.15	-0.53	-0.037	-0.107	-0.40	-1.28
23	NK23b	KILRGV <b>S</b> CKIM---~RRISKDIL <b>TG</b> KK	11	12	+4	+5	+0.36	+0.42	-0.11	-0.53	-0.027	-0.107	-0.30	-1.28
24	NK23c (C7S-Δ)	KILRGV <b>S</b> CKIM~RTFLRR---IL <b>TG</b> KK	11	12	+4	+6	+0.36	+0.50	-0.11	-0.46	-0.027	-0.077	-0.30	-0.92
25	C20	--- <b>K</b> IMRTFLRR~ISKDIL <b>TG</b> KK	10	10	+5	+3	+0.50	+0.30	-0.64	-0.13	-0.127	-0.044	-1.27	-0.44
26	C20-DK	--- <b>K</b> IMRTFLRR~ISK <b>K</b> I <b>L</b> TGKK	10	10	+5	+5	+0.50	+0.50	-0.64	-0.19	-0.127	-0.039	-1.27	-0.39
27	NK19a	KI--- <b>S</b> CKIMRT~FLRR---IL <b>TG</b> KK	9	10	+4	+5	+0.44	+0.50	-0.43	-0.29	-0.107	-0.059	-0.97	-0.59
28	NK19b	KILRGV <b>S</b> CK~IM---RR---IL <b>TG</b> KK	9	10	+4	+5	+0.44	+0.50	-0.36	-0.32	-0.089	-0.063	-0.80	-0.63
29	NK19b-KR	<b>R</b> ILRGV <b>S</b> RR~IM---RR---IL <b>TG</b> RR	9	10	+4	+5	+0.44	+0.50	-0.70	-0.52	-0.175	-0.105	-1.58	-1.05
30	N17	KILRGV <b>S</b> ~KIMRTFLRR-----	8	9	+3	+5	+0.38	+0.56	-0.21	-0.54	-0.071	-0.108	-0.57	-0.97
31	NK15	KILRGV <b>S</b> ~K-----R---IL <b>TG</b> KK	7	8	+2	+5	+0.29	+0.63	-0.03	-0.52	-0.015	-0.104	-0.11	-0.83
32	NK13	KI--- <b>S</b> CKI~MRTFLRR-----	6	7	+3	+4	+0.50	+0.57	-0.32	-0.68	-0.107	-0.170	-0.64	-1.19
33	NK11	KI--- <b>S</b> K-----R---~IL <b>TG</b> KK	5	6	+3	+3	+0.60	+0.50	-0.87	-0.02	-0.289	-0.007	-1.44	-0.04
34	I10	--- <b>K</b> IMR~TFLRR-----	5	5	+3	+3	+0.60	+0.60	-0.70	-0.57	-0.234	-0.191	-1.17	-0.95
35	Melittin*	GIGAVL <b>K</b> VLT <b>T</b> GL~PALIS <b>W</b> IKR <b>K</b> RQ	13	13	+1	+5.0	+0.08	+0.38	+0.55	-0.35	+0.552	-0.070	+7.18	-0.91

## Appendix

---

```
% -----
% Author:      Dominik Wilms
% Date:        16.10.2014
% Version:     1.1 (TRP Assay Evaluation)
% Last change: 23.10.2014
% -----

clc, clear, close all;

%% Denote name of Excel file to work with
filename = 'XYZ.xlsx';

%% Create raw data matrix for Excel readout
[nums,txt]=xlsread(filename);           % read from Excel file

%% Create matrices for intensity data (RFU) and wavelengths (Lambda)
RFU      = nums(:,2:end);
Lambda(:, :) = nums(:,1);

%% VARIABLE PARAMETERS: Check before running the script!
p3 = length(RFU(1,:));                 % # of wells
p4 = 1;                                % scanning interval [nm]
p5 = 310;                               % start wavelength [nm]
p6 = 400;                               % end wavelength [nm]
p7 = ((p6-p5)/p4)+1;                   % # of rows in matrix "RFU"

%% Savitzky-Golay Smoothing Filter (column by column)
% Input for separately declared function savitzkyGolayFilt()
x = RFU;
N = 2;                                  % polynomial order of savitzkyGolayFilt
DN = 0;                                 % differentiation order (0 := smoothing)
F = 21;                                 % frame size

Results = savitzkyGolayFilt(x,N,DN,F);  % write smoothed data point into analogous
                                        % row/column of output matrix "Results"

[p,q] = size(Results);
x1 = zeros(p+1,q+1);                   % Preallocation of a all-zeros matrix

x1(2:end,1) = Lambda(:,1);             % first row of „x1“ contains wavelengths in nm
x1(2:end,2:end) = Results(:,:);       % write output to "x1", start at row_2, col_2

%% Search column by column for RFU_max and Lambda_max and add to end of smoothed data columns
for l = 2:q+1;

x1(p+3,l) = max(x1(:,l));              % search intensity max column-by-column, write
                                        % to RFU_max

[maxwerte, maxzeilen] = max(x1(:,l));
[maxwert, maxspalte] = max(maxwerte);
maxzeile = maxzeilen(maxspalte);
x1(p+4,l) = x1(maxzeile,l);           % search and add corresponding Lambda_max
value
end

%% Write smoothed spectra into new workbook of the original Excel file
%% Name of the new Excel worksheet contains smoothing factor (F = frame)
F1 = num2str(F);                       % convert F into string
SN = {'Savitzky-Golay F =',F1};        % create cell array
sheetname = strjoin(SN);
xlswrite(filename,x1,sheetname,'A1');  % Write numerics to new worksheet
xlswrite(filename,txt,sheetname,'A1'); % Override first row
```

**Figure A.2: Matlab code for the determination of blue shifts from tryptophan fluorescence spectrum data.** The given code exemplarily depicts the Matlab code to deduce the resulting blue shift from spectrum data of peptide I2W in the presence and absence of PC:PS (50:50) liposomes. Smoothing of raw data, recorded by Tecan infinite M200pro, was realized by the application of a Savitzky-Golay filter at a smoothing frame size of 21 nm. Search tasks for fluorescence intensity maxima and corresponding wavelength positions were automated, and results were exported to Microsoft Excel files together with the smoothed spectrum data to enable subsequent blue shift calculations.

## ACKNOWLEDGEMENTS

First and foremost, I would like to express my sincere gratitude to my supervisor, Prof. Dr. Jörg Andrä from the Hamburg University of Applied Sciences (HAW Hamburg), for giving me the opportunity to carry out my research and conclude this thesis under his guidance, for countless constructive discussions, for his invaluable advice and support.

Moreover, I would also like to thank Prof. Dr. Thomas Gutschmann from the Leibniz Research Center Borstel as well as Prof. Dr. Christian Hübner from the University of Lübeck for agreeing to examine this thesis as first and second referee, respectively.

For financial support, I am grateful to the German Science Foundation (DFG, grant AN301/5-1 to J.A.) as well as to the Faculty of Life Sciences of the HAW Hamburg.

I am deeply thankful to the members of the HAW's Department of Biotechnology and the working group "Arbeitskreis Chemie", and, especially, to the Faculty's former Dean, Prof. Dr. Claus-Dieter Wacker, for their open-mindedness regarding my research, their constant willingness to help, and, especially, for the ever-positive atmosphere. I would also like to sincerely thank Prof. Dr. Oliver Ullrich from the molecular biology and cell culture techniques lab as well the lab's "good-hearted soul", Elisabeth Schäfer, for their cooperativeness, trust, and hospitality.

I would like to show my gratitude to Christine Hamann and Irina von Cube from the Research Center Borstel for advice and assistance regarding FRET and FACS experiments, respectively. I am also grateful to Sabrina Groth, who performed KI-quenching experiments. Nonetheless, I am thankful to all members of the FZ Borstel working groups 'Biophysics' and 'Immunobiophysics' for their everlasting readiness to discuss data and share experiences – and for making every visit at Borstel a fruitful and worthwhile journey.

I am also obliged to Drs. Michael Linnebacher and Claudia Maletzki for the uncomplicated collaboration and the warm welcome during my short-term research stay at the University of Rostock, and for providing the valuable patient-derived HROC cell lines.

Worthy of note, I would like to thank all of the students working under my supervision during lab projects and practical courses – for doing so without complaining.

My dear friends and colleagues, Jessi and Björn, I would like to thank for many inspiring discussions – on- or off-topic – and for providing welcome distractions from tedious lab routines or writer’s blocks.

I owe genuine and utmost gratitude to my life companion, Sarah, for her unshakable trust in me, her remarkable patience and understanding over weeks, months, years. I cannot overestimate her enduring support – may this be by encouraging me to continue while concomitantly bearing with my moods, or by supplying me (and my colleagues) with most delicious cakes and pastries.

Last but not least, a years-long effort like this would not have been possible without the continuous support and encouragement from my family. Thank you for being a steady source of motivation!

Finally, I feel dedicated to offer my apologies to all those who have not been mentioned personally but supported me in any respect in the successful completion of this thesis.